To the Graduate Council:

I am submitting herewith a dissertation written by Nagamanickam Ganesan entitled "A Dynamic Finite Element Modeling Techinique For Frame Structures." I have examined the final copy of this dissertation for form and content and recommend that it be accepted in partial fulfillment of the requirements for the degree of Doctor of Philosophy, with a major in Engineering Science and Mechanics.

R. Engels

Remi C. Engels, Major Professor

We have read this dissertation and recommend its acceptance:

VC Reddy

Basil W. Antar

[illegible]

John E. Caruthers

Accepted for the Council:

C W Minkel

Vice Provost
and Dean of the Graduate School

A DYNAMIC FINITE ELEMENT MODELING TECHNIQUE FOR FRAME STRUCTURES

A Dissertation
Presented for the
Doctor of Philosophy
Degree
The University of Tennessee, Knoxville

Nagamanickam Ganesan

May 1991

DEDICATION

For Our Next Generation:

Abhirami, Narmadha and Niranjan.

My lord
  who swept me away forever
   into joy that day,

made me over into himself

and sang in Tamil
his own songs
through me:

what shall I say
  to the first of things,
   flame
   standing there,

where can I find the right words
   to say my thanks ?

... Nammalvar.

ACKNOWLEDGEMENTS

The author is deeply indebted to Dr. Remi C. Engels who defined this topic of study and guided its progress at every stage. Without his conscientious supervision, it would have been impossible to bring this work to completion.

The author also wishes to express his gratitude to the other committee members: Dr. Kapaluru C. Reddy, Dr. Trevor H. Moulden, Dr. Basil N. Antar and Dr. John E. Caruthers for their valuable suggestions.

The work described herein was partially supported by Kirtland Air Force Base, New Mexico under Contract F29601–85–K–0054.

Finally, the author expresses his sincere thanks to the library staff at the University of Tennessee Space Institute for their help in procuring the necessary literature and to Mrs. Linda Williams for her excellent help in the typesetting of the manuscript.

ABSTRACT

A dynamic analysis technique for generic structural elements is presented. The modeling approach combines many aspects of the standard finite element method with a broader interpretation of the Craig/Bampton substructuring technique. The deterioration of the modal content of standard finite element models can be linked to the neglect of interface restrained assumed modes. Restoration of a few of these modes leads to higher accuracy with fewer generalized coordinates compared to the regular consistent mass matrix approach. Furthermore, since the proposed models possess the hierarchical property, no need exists for subdivision of basic elements such as rods, shafts and beams thereby simplifying the input data and allowing for different levels of approximation with little additional effort.

The dynamic finite elements for the axial rod, the torsional shaft, the Bernoulli–Euler beam and the Timoshenko beam are derived in terms of static constraint modes and interface restrained normal modes. In addition, the equations for the Bernoulli–Euler beam and the Timoshenko beam elements are simplified using several types of interface restrained assumed modes. These dynamic finite element models can be easily incorporated into existing structual analysis software. Next, an element assembly process is presented, in which at each stage, the resulting component can be considered as a single larger element. A special algorithm, with good convergence properties, to solve the eigenvalue problem at each stage is developed. The manner in which the elements are modeled and assembled leads to a cost–effective solution of the structural eigenvalue problem. Various demonstration examples, including a large spatial truss, are implemented in order to evaluate the performance of the different dynamic finite element models.

TABLE OF CONTENTS

LIST OF FIGURES

LIST OF TABLES

LIST OF SYMBOLS

A	Area of Cross Section
I	Area Moment of Inertia
I_z	Area Polar Moment of Inertia
E	Young's Modulus of Elasticity
G	Shear Modulus
J	Mass Polar Moment of Inertia
ρ	Mass Density
g	Acceleration due to Gravity
k	Shear Coefficient
ν	Poisson's Ratio
f	Natural Frequency
ω	Circular Natural Frequency
ω_c	Cut–off Frequency
u	Axial Displacement
v	Transverse Displacement
θ	Rotation Angle of Cross Section
ψ	Shear Angle
U	Element Potential Energy
T	Element Kinetic Energy
M	Mass Matrix
K	Stiffness Matrix
$\boldsymbol{F}$	Generalized Force Vector
$\boldsymbol{q}_I$	Interface Displacement Vector
$\boldsymbol{q}$	Generalized Displacement Vector

CHAPTER 1

INTRODUCTION

1.1 Background

Because of their low mass to stiffness ratios, frames are frequently used to build space antennas, communication platforms and other orbiting structures. The design of such structures often requires the determination of the dynamic displacement response and the corresponding internal stresses. To this end, analytical models of these structures need to be developed. Due to geometric complexities, material variations and irregular boundary conditions, some form of discretization or lumping of the structure becomes necessary in order to obtain a meaningful model. The finite element method is one discretization technique which together with Lagrange's equations allows for the derivation of a useful discrete mass and stiffness matrix for the system.

In order to obtain the displacement response, it is customary to first perform a modal analysis and then write the displacement vector as a linear combination of the computed modeshapes. Large flexible structures generally possess many closely spaced low frequency modes. Therefore, finite element models for such structures tend to be of large size. The computational effort to obtain the natural frequencies and mode shapes is approximately proportional to the cube of the model order. There are basically two ways to reduce the cost of the eigenvalue problem solution. The first consists of model order reduction and the second involves the development of faster and more cost-effective algorithms.

There are essentially three different approaches to model order reduction which are often applied simultaneously. The first approach is aimed at the element level. The idea here is to develop element models which have superior convergence characteristics. As a consequence, a given accuracy can be obtained with fewer degrees of freedom thereby reducing the overall number of degrees of freedom at the system level. Zienkiewicz, Gago and Kelly [1] introduced the p–version of the finite element method for static problems. During successive refinement stages, higher degree polynomial shape functions are used involving new nodes on the element while the element size remains fixed. Peano [2] and Babuska [3] discuss the advantages of the p–version over the conventional finite element method called the h–version where the element size is successively reduced while the order of the shape functions remains fixed. In the dynamic case, Bennighof and Meirovitch [4] have shown that the p–version of the finite element method combines the modeling flexibility of the standard finite element method with the excellent convergence properties of the classical Rayleigh–Ritz method.

The second class of order reduction techniques consists of truncating modes at the component level. The origin of such component mode synthesis techniques can be traced to Hurty [5]. Complex structures are often subdivided into a number of smaller components or substructures. Each substructure can then be modeled independently and a set of component modes computed. A model for the overall structure is obtained by enforcing interface displacement compatibility between the various components. In the process, component modes are usually truncated according to a preset cut-off frequency. The resulting order reduction is generally quite significant. In order to facilitate the assembly process, Hurty introduced the concept of static constraint modes. Substructure modes are in fact measured relative to a linear combination of rigid body modes and static constraint modes. In reality, there is no need to distinguish between rigid body and constraint modes, an observation made by Craig and Bampton [6]. In their component mode synthesis technique, Craig and Bampton use a combination of static constraint modes and interface restrained normal modes to model the system. The method yields results identical to Hurty's but is far less cumbersome to use. Because of its simplicity and excellent convergence properties, this method is very popular and widely used.

Since the publication of the original work by Hurty, there have been many suggestions for improvement. For the most part, the main differences lie in the types of component modes used. One method makes use of free–free substructure modes, which are the natural modes of an unconstrained substructure. Because discrete interface displacements do not appear explicitly in the retained displacement vector, special techniques are needed to couple the substructures. Benfield and Hruda [7] advocate improved substructure modes which are mass and stiffness loaded at the interface, thereby partially accounting for the dynamic effects of neighboring components. Kuhar and Stahle [8] introduce a method to use free–free substructure modes that are interconnected by flexible links so that there are no common attachment points between substructures. Hintz [9] extended the concept of attachment modes, initially developed for a constrained substructure by Bamford [10], to free–free modes which are capable of producing the exact static response of a substructure to static loading at the interface points. The displacement transformation leaves the interface displacements in tact, enabling simple substructure coupling via the conditions of interface displacement continuity. MacNeal [11] introduced a method which accounts for the stiffness contribution of the discarded higher modes. This results in the addition of the so called residual flexibility. The extension of MacNeal's work to a second order approximation is discussed by Rubin [12].

Finally, a third opportunity for order reduction presents itself at the system level. Guyan [13] developed a transformation based on the standard static condensation technique which relates a set of slave degrees of freedom to a set of master degrees of freedom. The underlying assumption is that the slaves are related to the masters in an essentially static manner. The Guyan reduction method then, removes the slave degrees of freedom from the problem resulting in a substantially smaller model size. This however is done at the expense of a redistribution of the mass of the system. Error bounds for this technique are given by Geradin [14] and Thomas [15]. Several authors suggested improvements of the method. Kidder [16] shows that the standard Guyan reduction only represents the first order term in the series expansion of the exact transformation between slaves and masters. He therefore suggests retention of higher order terms in the series which unfortunately involve the unknown eigenvalues. In a comment on Kidder's work, Flax [17] states that the eigenvalues of the system obtained after constraining all the masters must be larger than the frequency spectrum of interest for the Guyan reduction to be valid. One major problem is the choice of masters and slaves. Henshell and Ong [18] proposed an a priori choice of the number of masters and the elimination of one slave degree of freedom at a time, based on the magnitude of the corresponding stiffness to mass ratio. Shah and Raymond [19] note that this automatic procedure must also satisfy the condition mentioned in Flax's work.

Several cost-effective algorithms pertinent to the present study can be identified. Generally, these algorithms should take advantage of the sparseness and/or the special form of the stiffness and mass matrices. In addition, suitable algorithms should also exploit the physical properties associated with a structural eigenvalue problem. The relative merits of different algorithms are discussed in Jennings [20]. The determinant search method is effective when the matrices are highly banded and no trial vectors are available. Coordinate relaxation techniques, while preserving sparsity, are suitable when only a few eigenvalues are needed. Because of the loss of orthogonality among the vectors, computer implementation of the Lanczos method must be done with care. Nour-Omid, Parlett and Taylor [21] state that a correctly implemented Lanczos method competes well with methods such as the subspace iteration. Because of its simplicity and excellent convergence properties, the use of subspace iteration is well established. Jennings [22] proves that there is a correspondence between the Guyan reduction technique and the first round of iterations in the subspace iteration method. Although the Guyan reduction yields good approximate solutions for the lower frequencies and mode shapes of the structural system, higher accuracy is often desired. To this end, Cheu, Johnson and Craig [23] proposed to use the subspace iteration technique in conjunction with the Guyan reduction method. The columns of the Guyan reduction transformation are used as starting vectors for a series of subspace iterations. Because these starting vectors form a subspace which is close to the desired dominant subspace, it is expected that only a few iterations will lead to complete convergence.

1.2 Overview of the Present Study

This dissertation is devoted to the development of order reduction methods for large structural models. These techniques will be applied at the element, component and system level as indicated in Section 1.1. In addition, techniques to improve the convergence rate of the system eigenvalue problem will be derived.

In the next chapter, the assumed modes method with static constraint modes and interface restrained assumed modes is described and the relationship of the static constraint modes with the standard finite element shape functions is established. It will be shown that the Craig–Bampton component mode synthesis technique can be used to obtain a complete representation of the element displacement vector. The standard finite element method is then shown to be an approximation whereby all the interface restrained assumed modes are neglected. Ignoring the interface restrained assumed modes leads to an inaccurate mass distribution over the element. This in turn necessitates a finer discretization of the element domain resulting into larger order models. Instead of relying on mesh refinement it is proposed to retain a few of the interface restrained assumed modes at the element level. This yields superior convergence at the system level with far fewer retained generalized displacement coordinates. As an added benefit, the use of interface restrained assumed modes dramatically reduces the need for further element subdivisions so that an adaptive modeling capability can be easily implemented. Finally, the mass and stiffness matrices for a generic structure in terms of static constraint modes and interface restrained assumed modes are derived.

Chapter 3 deals with the development of dynamic finite elements for the axial bar, the torsional bar, the Bernoulli–Euler beam and the Timoshenko beam in terms of static constraint modes and interface restrained normal modes. In order to simplify the dynamic finite element equations of motion for the Bernoulli–Euler beam, trigonometric functions are chosen as interface restrained assumed modes and in the case of the Timoshenko beam, two types of interface restrained assumed modes are used i.e., trigonometric and ploynomial functions. Only a limited number of interface restrained assumed modes are retained at this level thereby reducing the ultimate order of the system. Computer subroutines are derived for each of the dynamic finite elements.

The truncation of interface restrained assumed modes can be continued at the component level in a natural manner. Elements are assembled by enforcing the interface displacement compatibility conditions. When a reasonable number of elements are assembled, a component eigenvalue problem of modest order is solved and interface restrained assumed modes are truncated according to a given cutoff frequency which is based on a desired system fidelity. A special algorithm with excellent convergence characteristics is developed to solve the intermediate component eigenvalue problems. The development of these component level order reduction techniques is detailed in Chapter 4. This new algorithm can also be used for the solution of the final eigenvalue problem. By now, the order of the problem should already be drastically reduced. Ordinarily, component level techniques will suffice to solve this eigenvalue problem, thereby preserving the continuity of the solution process. However, in case the final interface becomes large,special remedies may be required.

In Chapter 5 several demonstration problems are considered. Comparisons of the different dynamic finite elements are made with the standard finite element method and estimates of computational efficiency are given. In addition, the developed techniques are applied to the realistic example of a large space truss.

Finally in Chapter 6, general conclusions and recommendations are offered with regard to the use of dynamic finite elements in structural dynamics applications and with regard to the developed order reduction techniques.

CHAPTER 2

EQUATIONS OF MOTION FOR A GENERIC STRUCTURE

2.1 Assumed Modes Method

The structural element E in Figure 1 is shown in a deformed state. This element is assumed to undergo small displacements about its equilibrium position.The inertial position vector $\boldsymbol{R}$ of point P is

$$\boldsymbol{R} = \boldsymbol{R}_0 + \boldsymbol{r} + \boldsymbol{e} \tag{2.1.1}$$

where $\boldsymbol{r}$ is the position vector of point A relative to the local reference frame. The point P coincides with A in the undeformed state. The vector $\boldsymbol{e}$ is the Lagrangian elastic displacement vector which is measured in the local reference frame.

2.1.1 Assumed Modes

The assumed modes method consists of several orderly steps [24]. The first step is to approximate the elastic displacement vector $\boldsymbol{e}\ (x, y, z, t) = \lfloor u\ v\ w \rfloor^T$ by a linear combination of assumed modes $\boldsymbol{\phi}_i(x, y, z)$,

$$\boldsymbol{e} \cong \sum_{i=1}^{n} \boldsymbol{\phi}_i(x, y, z) q_i(t) \stackrel{\text{def}}{=} \phi\ \boldsymbol{q} \tag{2.1.2}$$

The time dependent coefficients $q_i(t)$ are called generalized coordinates.

The assumed modes must be admissible functions, *i.e.*, they must be i) complete ii) linearly independent iii) sufficiently differentiable i.e., at least to an order equal to that of the highest derivative in the element strain energy and iv) satisfy at least the geometric boundary conditions of the element E.

The choice of the assumed modes constitutes the second step in the assumed modes method.

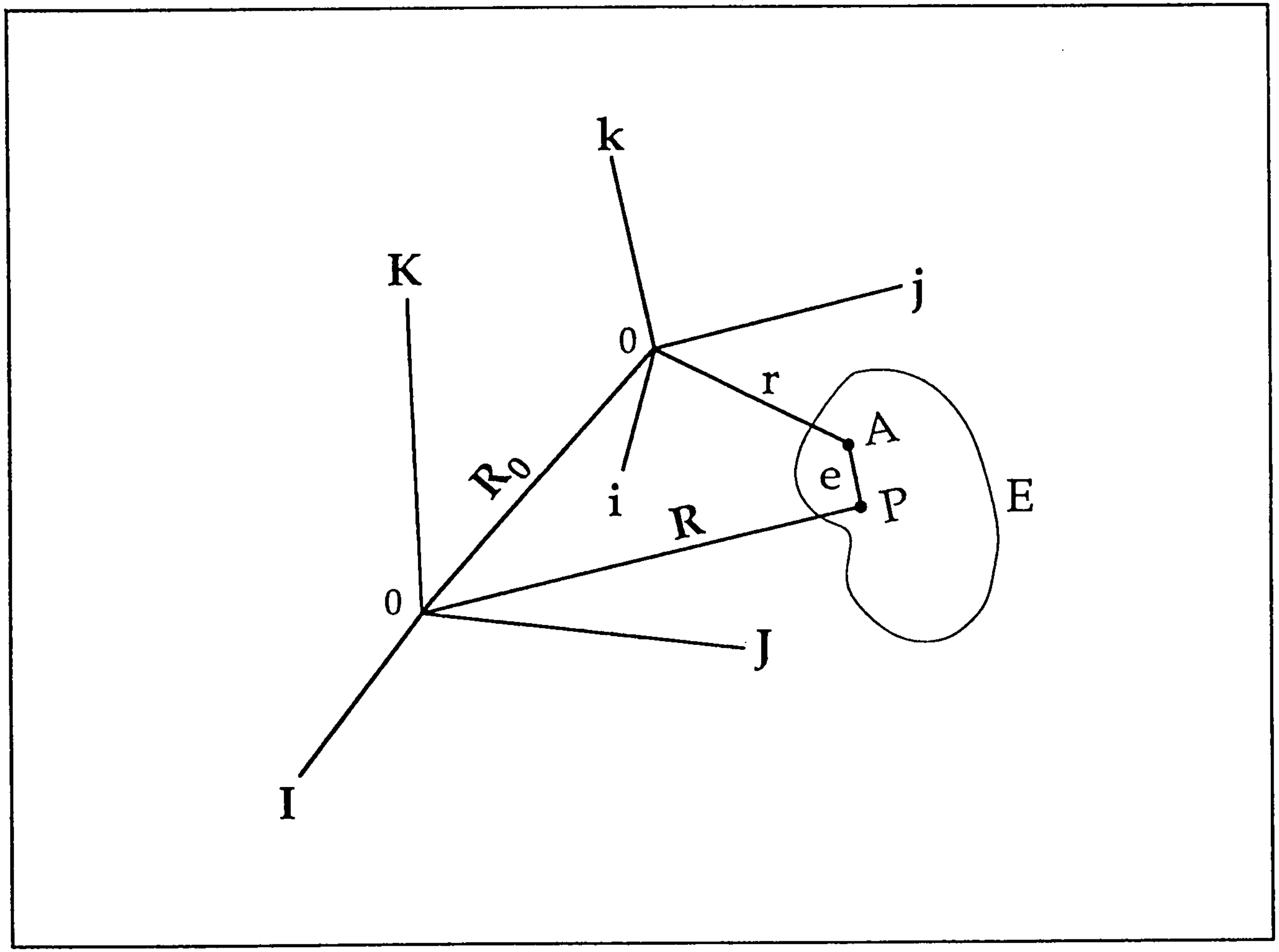

Figure 1. Structural Element and Reference Frames

2.1.2 Static Constraint Modes and Interface Restrained Assumed Modes

The physical interface of the element E is defined as the collection of all points, curves, and surfaces the element has in common with its neighbors. If this interface can be suitably modeled, all interface displacement coordinates can be collected into a single interface displacement vector $\boldsymbol{q}_I(t)$. This vector $\boldsymbol{q}_I$ is chosen as a partition of $\boldsymbol{q}$.

$$\boldsymbol{q} = \begin{Bmatrix} \boldsymbol{q}_I \\ \overline{\boldsymbol{q}} \end{Bmatrix} \tag{2.1.3}$$

where $\overline{\boldsymbol{q}}$ represents the remaining $(n - I)$ generalized coordinates.

Following the continuous version of the assumed modes method by Engels [25], the Lagrangian elastic displacement vector $\boldsymbol{e}(x, y, x, t)$ for the generic element E is written as the sum of two separate vectors $\boldsymbol{e}_I$ and $\overline{\boldsymbol{e}}$.

$$\boldsymbol{e} = \boldsymbol{e}_I + \overline{\boldsymbol{e}} \tag{2.1.4}$$

where $\boldsymbol{e}_I$ is a quasi-static displacement due to the nodal displacement $\boldsymbol{q}_I$ and is expressed as a linear combination of the assumed modes ϕ_I.

$$\boldsymbol{e}_I = \phi_I \, \boldsymbol{q}_I \tag{2.1.5}$$

The assumed modes ϕ_I are chosen as the so called static constraint modes. Static constraint modes are designed to accurately capture the static deformation of the element E caused by the physical displacements q_{Ij}.

The static constraint mode $\boldsymbol{\phi}_j$ (i.e., the j-th column in ϕ_I) corresponding to the displacement coordinate q_{Ij} is defined as the static deformation of the element E for $q_{Ij} = 1$ and $q_{Ii} = 0$ for all $i \neq j$.

The second part $\overline{\boldsymbol{e}}$ in Eq. (2.1.4) represents the remainder of the total displacement vector $\boldsymbol{e}$. It is that part of $\boldsymbol{e}$ which is measured relative to $\boldsymbol{e}_I$ by an absolute observer. Clearly, $\overline{\boldsymbol{e}}$ vanishes at the interface and therefore can be expressed as a linear combination of assumed modes $\overline{\boldsymbol{\phi}}_i$ which are restrained at the $\boldsymbol{q}_I$ coordinates. The interface restrained assumed mode $\overline{\boldsymbol{\phi}}_i$ corresponding to the displacement coordinate $\overline{q}_i$ is defined as an admissible deformation pattern of the element E with $\boldsymbol{q}_I = 0$. Collecting all $\overline{\boldsymbol{\phi}}_i$ as the columns of the matrix $\overline{\phi}$ leads to

$$\overline{\boldsymbol{e}} = \overline{\phi}\, \overline{\boldsymbol{q}} \tag{2.1.6}$$

The vector $\overline{\boldsymbol{q}}$ represents a set of generalized coordinates to be determined as part of the solution. One example of $\overline{\boldsymbol{\phi}}_i$ modes are the normal modes of E restrained at the $\boldsymbol{q}_I$ coordinates. It should be stressed that although restrained normal modes have unique advantages, they are only one of many possible sets. In fact, $\overline{\phi}$ modes need only be restricted to admissible functions that vanish at the $\boldsymbol{q}_I$ coordinates.

Substituting Eqs. (2.1.5) and (2.1.6) into Eq. (2.1.4), the displacement vector $\boldsymbol{e}$ becomes

$$\boldsymbol{e} = [\phi_I\ \overline{\phi}] \begin{Bmatrix} \boldsymbol{q}_I \\ \overline{\boldsymbol{q}} \end{Bmatrix} \tag{2.1.7}$$

It should be noted that the representation of $\boldsymbol{e}$ in Eq. (2.1.7) is complete in the sense that any degree of accuracy is theoretically possible as long as enough $\overline{\phi}$ modes are retained.

2.1.3 Shape Functions

In the standard finite element method, the variation of the elastic displacement vector $\boldsymbol{e}$ over the element is represented by interpolation or shape functions. These shape functions are identical to the static constraint modes $\boldsymbol{\phi}_I$ [25]. The finite element method neglects $\overline{\boldsymbol{e}}$ completely. Also, the entire element mass is redistributed over the interface degrees of freedom. This redistribution via the shape functions is known as the consistent mass matrix approach to finite element modeling. The resulting error in the response vector is negligible only when the displacement vector $\bar{\boldsymbol{e}}$ is small. This condition is fulfilled when the element deforms in a nearly static manner. This is accomplished by refining the finite element mesh thereby producing stiffer elements which leads to a smaller $\bar{\boldsymbol{e}}$ displacement.

Another way to ensure convergence to a desired model fidelity is suggested by Eq. (2.1.7) and leads to the so called dynamic finite element modeling technique. Instead of neglecting the displacement vector $\bar{\boldsymbol{e}}$, one can retain a limited number of $\bar{\boldsymbol{q}}_j$ coordinates thereby improving the mass distribution of the element E.

2.2 Element Mass and Stiffness Matrices

In this section the mass and stiffness matrix for the generic element E will be derived in terms of the generalized displacement vector $\boldsymbol{q}$ given by Eq. (2.1.3). This is the third step in the assumed modes method.

The inertial position vector $\boldsymbol{R}$ can be expressed as

$$\boldsymbol{R} = \boldsymbol{R}_0 + \boldsymbol{r} + \phi\, \boldsymbol{q} \tag{2.2.1}$$

where Eq. (2.1.2) was substituted into Eq. (2.1.1). Because in this application the vector $\boldsymbol{r}$ and the matrix ϕ are time independent, the inertial velocity vector $\dot{\boldsymbol{R}}$ is

$$\dot{\boldsymbol{R}} = \phi\, \dot{\boldsymbol{q}} \tag{2.2.2}$$

and the kinetic energy T becomes

$$T = \frac{1}{2} \int_E \dot{\boldsymbol{R}}^T \dot{\boldsymbol{R}}\, dm = \frac{1}{2} \dot{\boldsymbol{q}}^T \left(\int_E \phi^T \phi\, dm \right) \dot{\boldsymbol{q}} \tag{2.2.3}$$

Therefore, the element mass matrix takes on the form

$$M = \int_E \phi^T \phi\, dm \tag{2.2.4}$$

The final form of M is obtained by substituting $\phi = [\phi_I \; \overline{\phi}]$ from Eq. (2.1.7) into Eq. (2.2.4) and writing

$$M = \begin{bmatrix} M_{II} & M_{IN} \\ M_{IN}^T & M_{NN} \end{bmatrix} \tag{2.2.5}$$

where

$$\begin{aligned} M_{II} &= \int\limits_E \phi_I^T \phi_I \, dm \\ M_{IN} &= \int\limits_E \phi_I^T \overline{\phi} \, dm \\ M_{NN} &= \int\limits_E \overline{\phi}^T \overline{\phi} \, dm \end{aligned} \tag{2.2.6}$$

Note that if the interface restrained assumed modes are taken to be orthogonal to the mass distribution, then M_{NN} becomes diagonal.

The element potential energy U is by definition

$$U = \frac{1}{2} \int\limits_E \boldsymbol{\epsilon}^T \boldsymbol{\tau} dV \tag{2.2.7}$$

where $\boldsymbol{\epsilon}$ and $\boldsymbol{\tau}$ are the 6×1 strain and stress vectors for the element E respectively. For a linear material,

$$\boldsymbol{\tau} = C\boldsymbol{\epsilon} \tag{2.2.8}$$

in which C is termed the material stiffness matrix. Also, $\boldsymbol{\epsilon}$ is related to $\boldsymbol{e}$ as follows,

$$\boldsymbol{\epsilon} = B\boldsymbol{e} \tag{2.2.9}$$

where the elements of B are the appropriate partial derivatives $\partial/\partial x, \partial/\partial y$ and $\partial/\partial z$. Combining Eqs. (2.2.7),(2.2.8),(2.2.9) and Eq. (2.1.2) yields

$$U = \frac{1}{2}\boldsymbol{q}^T K \boldsymbol{q} \tag{2.2.10}$$

with

$$K = \int\limits_E (B\phi)^T C (B\phi) dV \tag{2.2.11}$$

substituting $\phi = [\phi_I \; \overline{\phi}]$ from Eq. (2.1.7) into Eq. (2.2.11) leads to the following expression for stiffness matrix,

$$K = \begin{bmatrix} K_{II} & 0 \\ 0 & K_{NN} \end{bmatrix} \tag{2.2.12}$$

with

$$\begin{aligned} K_{II} &= \int_E (B\phi_I)^T C (B\phi_I) dV \\ K_{NN} &= \int_E (B\overline{\phi})^T C (B\overline{\phi}) dV \end{aligned} \tag{2.2.13}$$

If $\overline{\phi}$ is chosen to be orthogonal to the stiffness distribution, then K_{NN} becomes diagonal. It is important to note that the IN–partition K_{IN} in K vanishes, *i.e.*,

$$K_{IN} = \int_E (B\phi_I)^T C (B\overline{\phi}) dV = 0 \tag{2.2.14}$$

Physically, this means that no stiffness coupling exists between $\boldsymbol{q}_I$ and $\overline{\boldsymbol{q}}$, and mathematically, it indicates stiffness orthogonality between the static constraint modes and interface restrained assumed modes. To prove Eq. (2.2.14) consider the following series of static problems,

$$\begin{bmatrix} K_{II} & K_{IN} \\ K_{IN}^T & K_{NN} \end{bmatrix} \begin{Bmatrix} \boldsymbol{q}_I^j \\ \overline{\boldsymbol{q}}^j \end{Bmatrix} = \begin{Bmatrix} \boldsymbol{P}_I^j \\ \boldsymbol{0} \end{Bmatrix}, \; j = 1, 2, \ldots, I \tag{2.2.15}$$

where the applied interface force vectors $\boldsymbol{P}_I^j$ ($j = 1, 2, \ldots, I$) are chosen such that

$$\boldsymbol{q}_I^j = \lfloor 0 \; 0 \; \ldots \; 0 \; \overset{j}{1} \; 0 \; \ldots \; 0 \rfloor^T \tag{2.2.16}$$

Due to the definition of $\overline{\boldsymbol{\varepsilon}}$, the vector $\overline{\boldsymbol{\varepsilon}}$ is zero since no noninterface forces are applied. Therefore from Eq. (2.1.6), $\overline{\boldsymbol{q}}^j = \boldsymbol{0}$ ($j = 1, 2, \ldots, I$) for such static problems. The second partition in Eq. (2.2.15) then yields

$$K_{IN}^T \, \boldsymbol{q}_I^j = \boldsymbol{0} \tag{2.2.17}$$

Combining Eqs. (2.2.17) and (2.2.18) shows that the jth row of the matrix K_{IN} is zero. This is true for all $j = 1, 2, \ldots, I$ and therefore $K_{IN} = 0$. Note that the elements of K_{IN} are independent of the dynamic state of the element so that $K_{IN} = 0$ in both the static and the dynamic case.

Lagrange's equations of motion for an undamped generic element can finally be written as

$$M\ddot{\boldsymbol{q}} + K\boldsymbol{q} = \boldsymbol{F} \tag{2.2.18}$$

where M and K are given by Eqs. (2.2.5) and (2.2.12).

The load vector $\boldsymbol{F}$ corresponding to the distributed force $\boldsymbol{f}(x, y, z, t)$ can be obtained from the virtual work expression,

$$\delta W = \int\limits_{E} \boldsymbol{f}^T \delta \boldsymbol{e}\; dV \stackrel{\text{def}}{=} \boldsymbol{F}\delta\boldsymbol{q} \tag{2.2.19}$$

Substituting Eq. (2.1.2) into Eq. (2.2.19) yields

$$\boldsymbol{F} = \int\limits_{E} \phi^T \boldsymbol{f} dV \tag{2.2.20}$$

Furthermore using Eq. (2.1.7) in Eq. (2.2.20) leads to

$$\boldsymbol{F} \stackrel{\text{def}}{=} \left\{ \begin{matrix} \boldsymbol{F}_I \\ \overline{\boldsymbol{F}} \end{matrix} \right\} = \int\limits_{E} \begin{bmatrix} \phi_I^T \\ \overline{\phi}^T \end{bmatrix} \boldsymbol{f} dV \tag{2.2.21}$$

Note that in the case where only interface forces are applied, $\overline{\boldsymbol{F}} = \boldsymbol{0}$ because $\overline{\phi}$ vanishes at the interface.

CHAPTER 3

DYNAMIC FINITE ELEMENTS

3.1 Axial Bar

3.1.1 Line Element

Consider the axial bar as illustrated in Figure 2. The bar is assumed to undergo vibrations along its own axis and as a rigid body can only move along that same axis.

Following Reference [25], the interface displacements are defined as the end displacements. i.e.,

$$q_I = \lfloor q_1 \; q_2 \rfloor^T = \lfloor u(0,t) \; u(L,t) \rfloor^T \tag{3.1.1}$$

The noninterface degrees of freedom are $u(x,t)$ with $x \neq 0, L$.

The static constraint modes are computed from the following static equilibrium equation

$$EA \, \frac{\partial^2 u}{\partial x^2} = 0 \tag{3.1.2}$$

where E is Young's modulus and A is the cross-sectional area. The appropriate boundary conditions for the static constraint modes are $u(0,t) = 1$, $u(0,t) = 0$ and $u(L,t) = 0$, $u(L,t) = 1$ respectively. The ϕ_I matrix then becomes

$$\phi_I = \left[1 - \frac{x}{L} \;\; \frac{x}{L} \right] \tag{3.1.3}$$

where L is the length of the bar.

The interface restrained normal modes and the corresponding natural frequencies are found by solving the eigenvalue problem given by the partial differential equation,

$$\rho A \, \frac{\partial^2 u}{\partial t^2} - EA \, \frac{\partial^2 u}{\partial x^2} = 0 \tag{3.1.4}$$

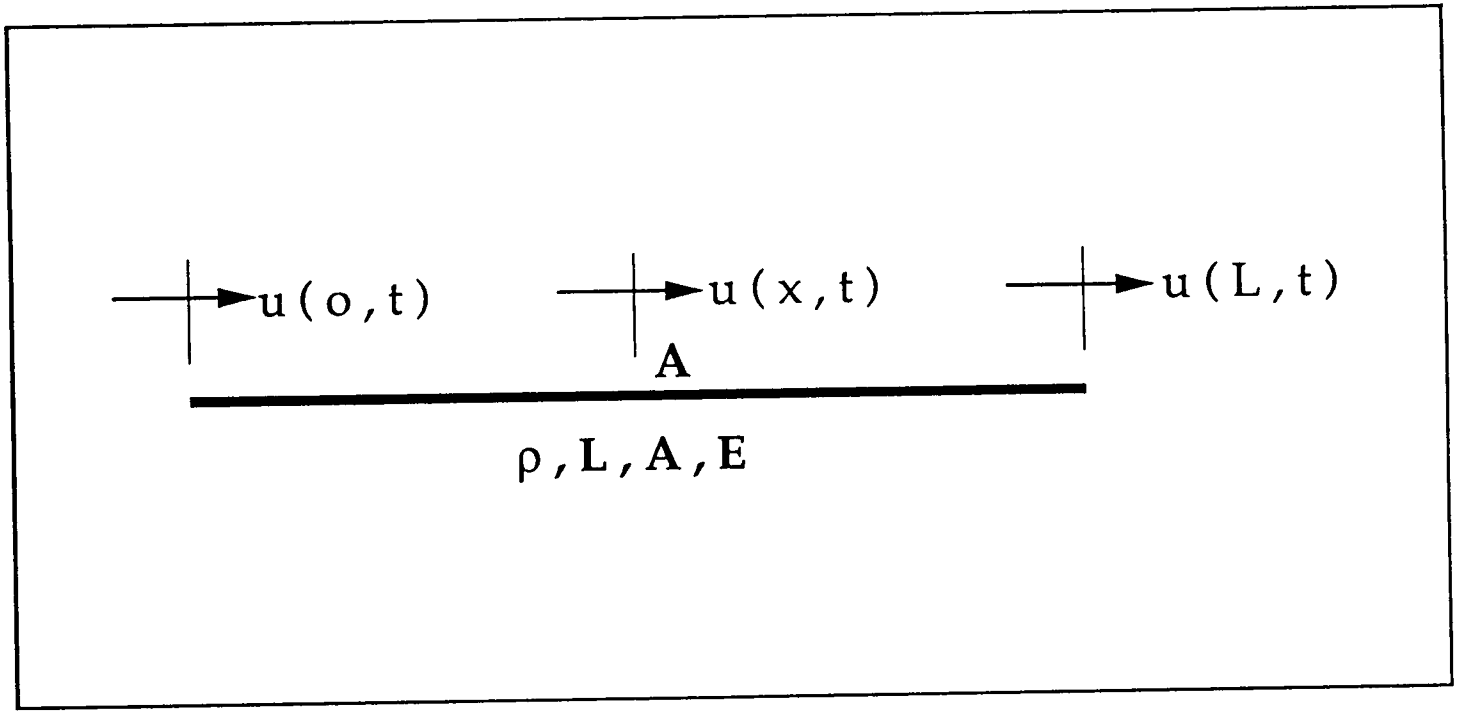

Figure 2. Axial Bar (Line Element)

subject to the clamped–clamped boundary conditions. i.e., $u(0,t)=0$ and $u(L,t)=0$ and where ρ represents the mass density of the bar. The interface restrained normal modes are found as

$$\overline{\phi}_j(x)=\sqrt{\frac{2}{\rho AL}}\sin j\frac{\pi x}{L}, \quad j=1,2,\ldots,\infty \tag{3.1.5}$$

According to Eq. (2.1.7), the displacement vector, $\boldsymbol{u}$ can be written as

$$\boldsymbol{u}=[\phi_I\ \overline{\phi}]\begin{Bmatrix} q_I \\ \overline{q} \end{Bmatrix} \tag{3.1.6}$$

The kinetic energy T of the axial bar element is

$$T=\frac{1}{2}\int_0^L \rho A\dot{u}^2 dx \tag{3.1.7}$$

where the dot $(\dot{\ })$ denotes the partial derivative with respect to time t. Substituting Eq. (3.1.3), (3.1.5) and (3.1.6) into Eq. (3.1.7) yields

$$T=\frac{1}{2}\begin{Bmatrix} \dot{q}_I \\ \dot{\overline{q}} \end{Bmatrix}^T \begin{bmatrix} M_{II} & M_{IN} \\ M_{IN}^T & M_{NN} \end{bmatrix} \begin{Bmatrix} \dot{q}_I \\ \dot{\overline{q}} \end{Bmatrix} \tag{3.1.8}$$

where the mass matrix partitions are evaluated as

$$\begin{aligned}
M_{II} &= \int_0^L \rho A\phi_I^T\ \phi_I dx = \frac{\rho AL}{6}\begin{bmatrix} 2 & 1 \\ 1 & 2 \end{bmatrix} \\
M_{NN} &= \int_0^L \rho A\overline{\phi}^T\overline{\phi} dx = I \\
M_{IN} &= \int_0^L \rho A\phi_I^T\overline{\phi} dx \\
&= \frac{\sqrt{2\rho AL}}{\pi}\begin{bmatrix} 1 & \frac{1}{2} & \cdots & \frac{1}{j} & \cdots \\ 1 & -\frac{1}{2} & \cdots & \frac{(-1)^{j+1}}{j} & \cdots \end{bmatrix}
\end{aligned} \tag{3.1.9}$$

Note that M_{II} is the standard consistent finite element mass matrix for an axial bar. The matrix M_{IN} in Eq. (3.1.9) represents the mass coupling between $\boldsymbol{q}_I$ and $\overline{\boldsymbol{q}}$ which is neglected in the standard finite element method. Because of the orthonormality of the interface restrained normal modes, M_{NN} becomes a unit matrix.

The element strain energy is

$$U = \frac{1}{2} \int_0^L EAu'^2 \, dx \tag{3.1.10}$$

where the prime $(\ )'$ indicates the partial derivative with respect to x. This time, from Eq. (3.1.6) it follows that

$$\boldsymbol{u}' = \left[\phi_I' \ \overline{\phi}\,'\right] \begin{Bmatrix} \boldsymbol{q}_I \\ \boldsymbol{q} \end{Bmatrix} \tag{3.1.11}$$

Substituting Eq. (3.1.11) into Eq. (3.1.10), the stiffness matrix K becomes

$$K = \begin{bmatrix} K_{II} & 0 \\ 0 & K_{NN} \end{bmatrix} \tag{3.1.12}$$

where

$$K_{II} = \int_0^L EA\phi_I'^T \phi_I' dx = \frac{EA}{L} \begin{bmatrix} 1 & -1 \\ -1 & 1 \end{bmatrix}$$

$$K_{NN} = \int_0^L EA\overline{\phi}\,'^T \, \overline{\phi}\,' dx = \text{Diag.}\ [\omega_1^2,\ \omega_2^2\ \cdots] \tag{3.1.13}$$

$$\omega_j^2 = j^2\pi^2 \frac{E}{\rho L^2}, \quad j = 1, 2, \ldots, \infty$$

Here ω_j are the clamped–clamped circular natural frequencies of the bar. Note that K_{II} in Eq. (3.1.13) is the standard finite element stiffness matrix for the axial bar and that as expected

$$K_{IN} = \int_0^L EA\phi_I'^T \, \overline{\phi}\,' dx = 0 \tag{3.1.14}$$

3.1.2 Planar Element

The planar bar element shown in Figure 3 is assumed to execute small elastic motions along its axis and small planar rigid body motions. Infinite rigidity is assumed in the transverse direction. The only difference with the line element is that the transverse inertia must be accounted for.

In Reference [25], the displacement vector is written as,

$$\begin{Bmatrix} u \\ v \end{Bmatrix} = \begin{bmatrix} 1-\frac{x}{L} & \frac{x}{L} & 0 & 0 \\ 0 & 0 & 1-\frac{x}{L} & \frac{x}{L} \end{bmatrix} \begin{Bmatrix} u_1 \\ u_2 \\ v_1 \\ v_2 \end{Bmatrix} + \begin{bmatrix} \overline{\phi} \\ 0 \end{bmatrix} \overline{q} \tag{3.1.15}$$

where

$$q_I = \lfloor u_1 \; u_2 \; v_1 \; v_2 \rfloor^T = \lfloor u(0,t) \; u(L,t) \; v(0,t) \; v(L,t) \rfloor^T \tag{3.1.16}$$

The matrix $\overline{\phi}$ in Eq. (3.1.15) is given by Eq. (3.1.5) and the third and fourth columns in the first matrix of Eq. (3.1.15) represent the static constraint modes for v_1 and v_2. Because of the infinite rigidity in the transverse direction, the lower partition in the second matrix of Eq. (3.1.15) must be taken to be zero. The kinetic and potential energies for the planar bar element are

$$T = \frac{1}{2} \int_0^L \rho A(\dot{u}^2 + \dot{v}^2) dx \tag{3.1.17}$$

$$U = \frac{1}{2} \int_0^L EA u'^2 dx \tag{3.1.18}$$

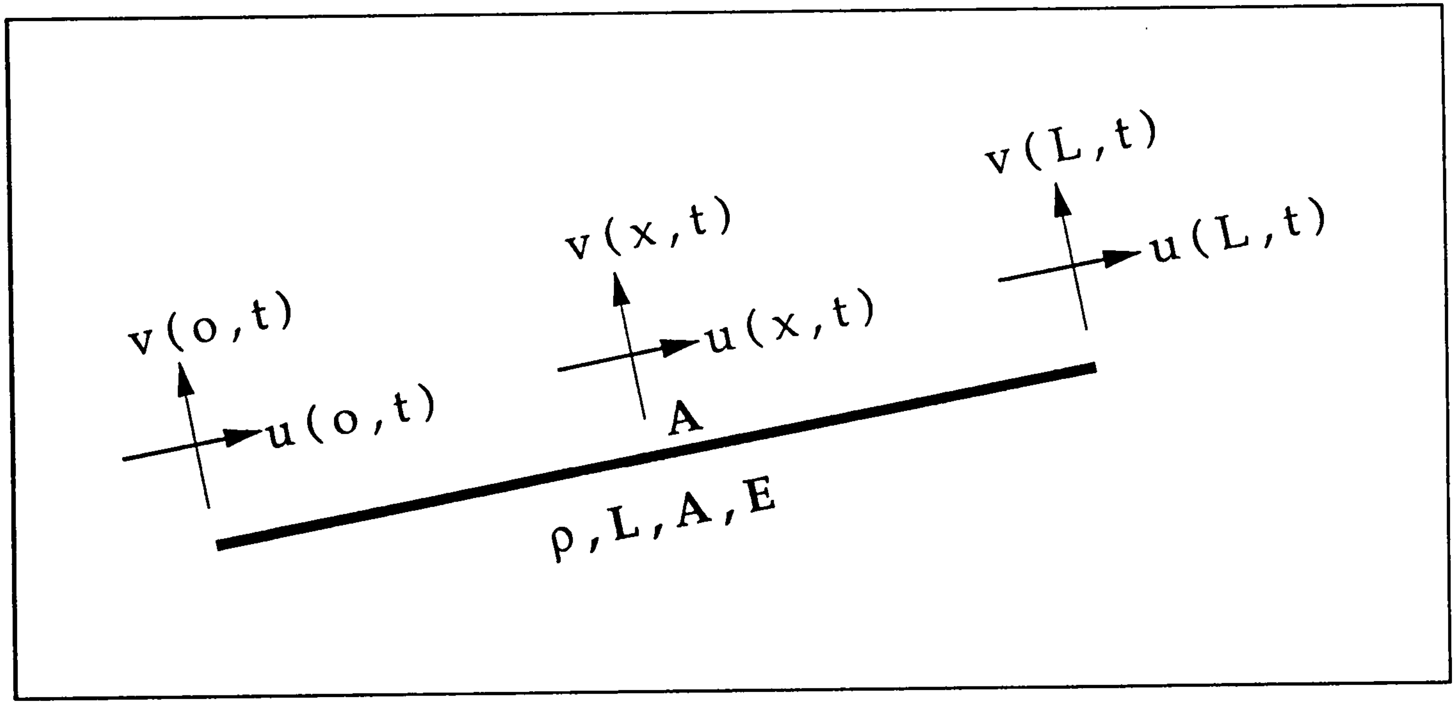

Figure 3. Axial Bar (Planar Element)

Substituting Eq. (3.1.15) in Eqs. (3.1.17) and (3.1.18) leads to

$$M_{II} = \frac{\rho AL}{6}\begin{bmatrix} 2 & 1 & 0 & 0 \\ 1 & 2 & 0 & 0 \\ 0 & 0 & 2 & 1 \\ 0 & 0 & 1 & 2 \end{bmatrix}$$

$$M_{IN} = \frac{\sqrt{2}\rho AL}{\pi}\begin{bmatrix} 1 & \frac{1}{2} & \cdots & \frac{1}{j} & \cdots \\ 1 & -\frac{1}{2} & \cdots & \frac{(-1)^{j+1}}{j} & \cdots \\ 0 & 0 & \cdots & 0 & \cdots \\ 0 & 0 & \cdots & 0 & \cdots \end{bmatrix}$$

$$M_{NN} = I$$

$$K_{II} = \frac{EA}{L}\begin{bmatrix} 1 & -1 & 0 & 0 \\ -1 & 1 & 0 & 0 \\ 0 & 0 & 0 & 0 \\ 0 & 0 & 0 & 0 \end{bmatrix} \tag{3.1.19}$$

$$K_{IN} = 0$$

$$K_{NN} = \text{Diag.}\ (\omega_1^2, \omega_2^2, \ldots), \qquad \omega_j^2 = j^2\pi^2\frac{E}{\rho L^2}$$

Note that the planar element equations can be obtained from the line element equations by expanding the interface vector to include v_1 and v_2 and by adding the appropriate consistent mass matrix. The stiffness matrix and the $\overline{q}$ partitions are not affected.

3.1.3 Spatial Element

The spatial bar element to be used for three dimensional truss analysis is obtained by adding the third displacement w. The displacement vector can be written as,

$$\begin{Bmatrix} u \\ v \\ w \end{Bmatrix} = \begin{bmatrix} 1-\frac{x}{L} & \frac{x}{L} & 0 & 0 & 0 & 0 \\ 0 & 0 & 1-\frac{x}{L} & \frac{x}{L} & 0 & 0 \\ 0 & 0 & 0 & 0 & 1-\frac{x}{L} & \frac{x}{L} \end{bmatrix} \begin{Bmatrix} u(0,t) \\ u(L,t) \\ v(0,t) \\ v(L,t) \\ w(0,t) \\ w(L,t) \end{Bmatrix} + \begin{bmatrix} \overline{\phi} \\ 0 \\ 0 \end{bmatrix} \overline{q} \quad (3.1.20)$$

The kinetic and potential energies for the spatial bar element are

$$T = \frac{1}{2}\int_0^L \rho A(\dot{u}^2 + \dot{v}^2 + \dot{w}^2)dx \qquad (3.1.21)$$

$$U = \frac{1}{2}\int_0^L EAu'^2 dx \qquad (3.1.22)$$

Substituting Eq. (3.1.20) in Eqs. (3.1.21) and (3.1.22) again leads to

$$M_{II} = \frac{\rho AL}{6}\begin{bmatrix} 2 & 1 & 0 & 0 & 0 & 0 \\ 1 & 2 & 0 & 0 & 0 & 0 \\ 0 & 0 & 2 & 1 & 0 & 0 \\ 0 & 0 & 1 & 2 & 0 & 0 \\ 0 & 0 & 0 & 0 & 2 & 1 \\ 0 & 0 & 0 & 0 & 1 & 2 \end{bmatrix}$$

$$M_{IN} = \frac{\sqrt{2\rho AL}}{\pi}\begin{bmatrix} 1 & \frac{1}{2} & \cdots & \frac{1}{j} & \cdots \\ 1 & -\frac{1}{2} & \cdots & \frac{(-1)^{j+1}}{j} & \cdots \\ 0 & 0 & \cdots & 0 & \cdots \\ 0 & 0 & \cdots & 0 & \cdots \\ 0 & 0 & \cdots & 0 & \cdots \\ 0 & 0 & \cdots & 0 & \cdots \end{bmatrix}$$

$$M_{NN} = I$$

$$K_{II} = \frac{EA}{L} \begin{bmatrix} 1 & -1 & 0 & 0 & 0 & 0 \\ -1 & 1 & 0 & 0 & 0 & 0 \\ 0 & 0 & 0 & 0 & 0 & 0 \\ 0 & 0 & 0 & 0 & 0 & 0 \\ 0 & 0 & 0 & 0 & 0 & 0 \\ 0 & 0 & 0 & 0 & 0 & 0 \end{bmatrix} \tag{3.1.23}$$

$$K_{IN} = 0$$

$$K_{NN} = \text{Diag. } (\omega_1^2, \omega_2^2, \ldots), \qquad \omega_j^2 = j^2 \pi^2 \frac{E}{\rho L^2}, \quad j = 1, 2, \ldots$$

In conclusion, it can be said that the spatial bar element equations can be obtained from the line element equations by adding the appropriate consistent mass matrices for v and w.

3.2 Torsional Bar

Consider the torsional bar element as illustrated in Figure 4. The material and geometric properties are given by I_z the area polar moment of inertia, J the mass polar moment of inertia per unit length of the bar, G the shear modulus of elasticity and L the length of the torsional element.

Because the differential equation of motion for the torsional bar is formally identical to the one for the axial bar, the derivation of the element mass and stiffness matrices is also identical. The appropriate substitutions are

$$\boldsymbol{u} \Longrightarrow \boldsymbol{\theta}$$

$$\rho A \Longrightarrow J$$

$$EA \Longrightarrow GI_z$$

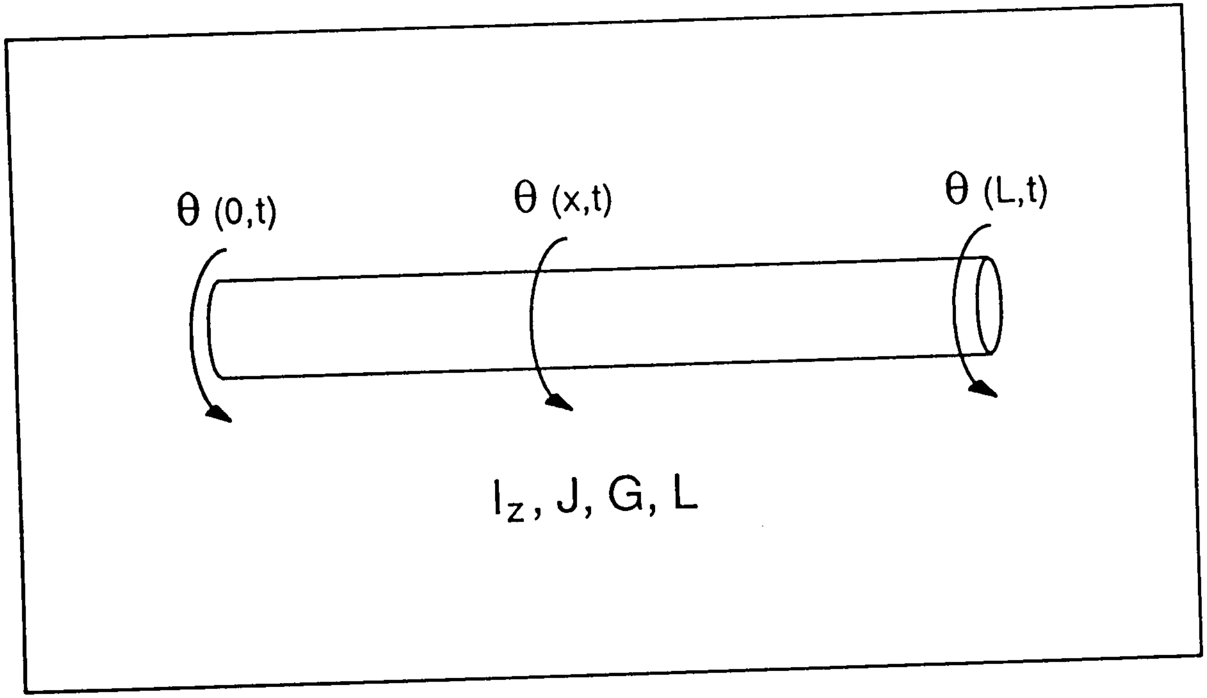

Figure 4. Torsional Bar (Line Element)

Therefore, Eq. (3.1.9) yields

$$M_{II} = \frac{JL}{6}\begin{bmatrix} 2 & 1 \\ 1 & 2 \end{bmatrix}$$

$$M_{NN} = I$$

$$M_{IN} = \frac{\sqrt{2JL}}{\pi}\begin{bmatrix} 1 & \frac{1}{2} & \cdots & \frac{1}{j} & \cdots \\ 1 & -\frac{1}{2} & \cdots & \frac{(-1)^{j+1}}{j} & \cdots \end{bmatrix} \tag{3.2.1}$$

$$K_{II} = \frac{I_z G}{L}\begin{bmatrix} 1 & -1 \\ -1 & 1 \end{bmatrix}$$

$$K_{NN} = \text{Diag. } [\omega_1^2,\ \omega_2^2\ \cdots], \quad \omega_j^2 = j^2\pi^2\frac{I_z G}{JL^2},\ j = 1, 2, \ldots, \infty$$

3.3 Bernoulli–Euler Beam

3.3.1 Normal Modes As Interface Restrained Assumed Modes

A beam in transverse vibration is shown in Figure 5. In the classical theory of a beam in pure bending, cross sections perpendicular to the neutral axis remain plane and perpendicular to the neutral axis after undergoing deformation, i.e., transverse shear deformation is neglected. For dynamic analysis, rotary inertia is also ignored. The relevent parameters are ρ the mass density, E Young's modulus of elasticity, A the cross sectional area , I the area moment of inertia of the cross section about the neutral axis and L the beam length.

Following Reference [25], the interface displacement vector $\boldsymbol{q}_I$ is defined as

$$\boldsymbol{q}_I = \lfloor v(0,t)\ \theta(0,t)\ v(L,t)\ \theta(L,t) \rfloor^T \tag{3.3.1}$$

Note that the rotation $\theta(x,t)$ is given by

$$\theta(x,t) = \frac{\partial v(x,t)}{\partial x} \tag{3.3.2}$$

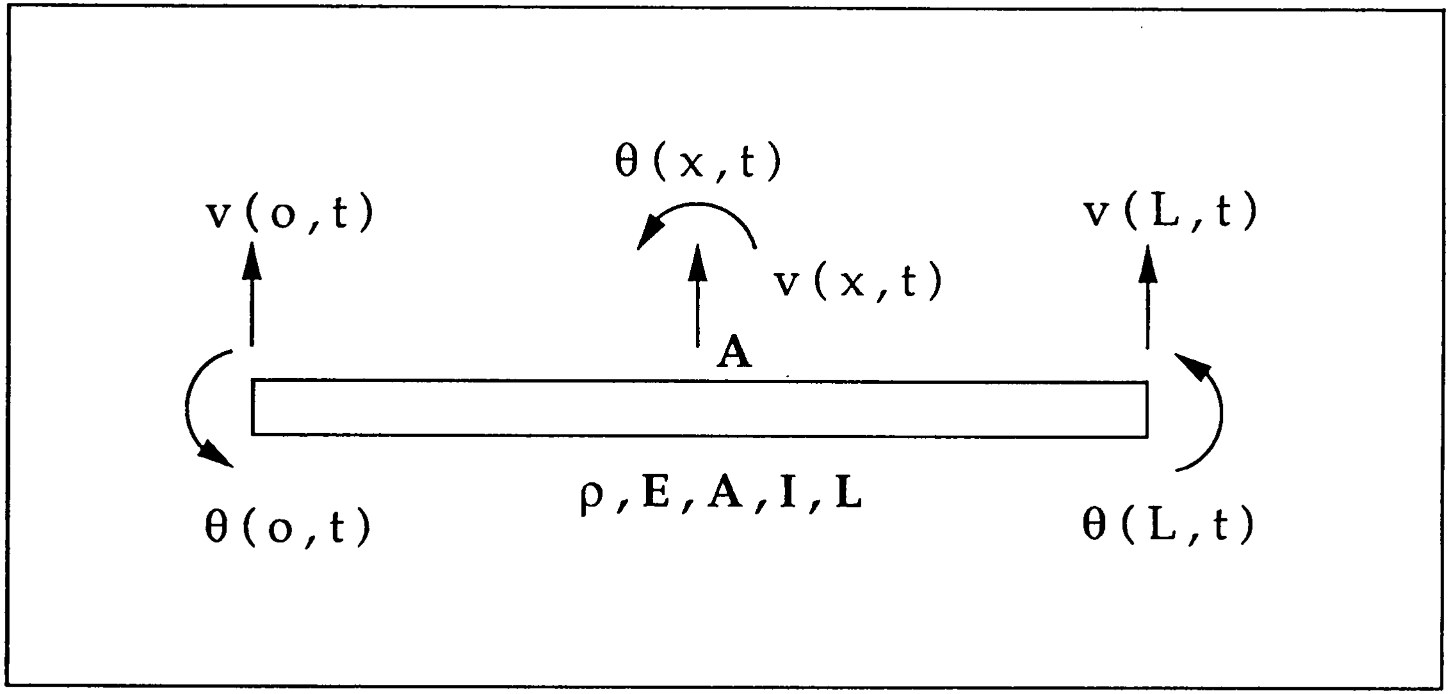

Figure 5. Bernoulli–Euler Beam Element

The displacement vector $\boldsymbol{e}$ is considered to have only one component, i.e., v. Eq. (2.1.7) is therefore written as

$$v = \lfloor \phi_1 \ \phi_2 \ \phi_3 \ \phi_4 \ \rfloor q_I + \overline{\phi}\,\overline{q} \tag{3.3.3}$$

The static constraint modes, ϕ_j are computed from the static equilibrium equation $(EIv'')'' = 0$ subjected to the following boundary conditions

$$\begin{aligned} &v_1 = 1,\ \theta_1 = v_2 = \theta_2 = 0 \\ &v_1 = 0,\ \theta_1 = 1,\ v_2 = \theta_2 = 0 \\ &v_1 = \theta_1 = 0,\ v_2 = 1,\ \theta_2 = 0 \\ &v_1 = \theta_1 = v_2 = 0,\ \theta_2 = 1 \end{aligned} \tag{3.3.4}$$

The resulting static constraint modes are

$$\begin{aligned} \phi_1 &= 1 - 3\xi^2 + 2\xi^3 \\ \phi_2 &= L\left[\xi - 2\xi^2 + \xi^3\right] \\ \phi_3 &= 3\xi^2 - 2\xi^3 \\ \phi_4 &= L\left[-\xi^2 + \xi^3\right] \end{aligned} \tag{3.3.5}$$

in which $\xi = \dfrac{x}{L}$. Note that these constraint modes are in fact the standard finite element shape functions for the Bernoulli–Euler beam.

Next, the interface restrained normal modes and the corresponding natural frequencies are obtained from solving the eigenvalue problem associated with the differential equation

$$EI\,\frac{\partial^4 v}{\partial x^4} + \rho A\,\frac{\partial^2 v}{\partial t^2} = 0 \tag{3.3.6}$$

subjected to the clamped–clamped boundary conditions

$$\begin{aligned} v(x,t) &= 0 \text{ for } x = 0 \text{ and } L \\ \theta(x,t) &= 0 \text{ for } x = 0 \text{ and } L \end{aligned} \tag{3.3.7}$$

The characteristic equation is found to be

$$\cos\beta\ \cosh\beta - 1 = 0 \tag{3.3.8}$$

with

$$\beta = \lambda L, \quad \lambda^4 = \frac{\rho A \omega^2}{EI} \tag{3.3.9}$$

Solving the transcendental equation (3.3.8) yields

$$\beta_i = 4.7300, 7.8532, 10.9956, \ldots \tag{3.3.10}$$

Note that these values of β are independent of the structural and geometric parameters of the beam and represent a one time computation. The mode shapes are given by

$$\overline{\phi}_i = C_i \left\{(\sinh\beta_i\xi - \sin\beta_i\xi) - \alpha_i(\cosh\beta_i\xi - \cos\beta_i\xi)\right\}, \ i = 1, 2, \cdots, \infty \tag{3.3.11}$$

where C_i is the mass normalization constant for the i–th mode and

$$\xi = \frac{x}{L}, \quad \alpha_i = \frac{\sinh\beta_i - \sin\beta_i}{\cosh\beta_i - \cos\beta_i} \tag{3.3.12}$$

The normalization constant C_i must satisfy

$$\rho A \int_0^L \overline{\phi}_i^2 dx = 1 \tag{3.3.13}$$

Using Eq. (3.3.11) in Eq. (3.3.13) yields

$$C_i = \frac{1}{\sqrt{\rho A L f(\beta_i)}} \tag{3.3.14}$$

with

$$f(\beta_i) = \int_0^1 \left\{(\sinh\beta_i\xi - \sin\beta_i\xi) - \alpha_i(\cosh\beta_i\xi - \cos\beta_i\xi)\right\}^2 d\xi \tag{3.3.15}$$

In explicit terms and omitting the i index for simplicity,

$$f(\beta) = \frac{1}{4\beta}[\sinh 2\beta - \sin 2\beta + 4\cos\beta\sinh\beta - 4\sin\beta\cosh\beta]$$
$$+\frac{\alpha^2}{4\beta}[4\beta + \sinh 2\beta + \sin 2\beta - 4\cos\beta\sinh\beta - 4\sin\beta\cosh\beta]$$
$$-\frac{\alpha}{2\beta}[\cosh 2\beta - 1 + 2\sin^2\beta - 4\sin\beta\sinh\beta] = \alpha^2 \tag{3.3.16}$$

The kinetic energy for the Bernoulli-Euler beam is

$$T = \frac{1}{2}\int_0^L \rho A\dot{v}^2 dx \tag{3.3.17}$$

Using Eq. (3.3.3) in Eq. (3.3.17) leads to the mass matrix partitions

$$M_{II} = \frac{\rho AL}{420}\begin{bmatrix} 156 & 22L & 54 & -13L \\ 22L & 4L^2 & 13L & -3L^2 \\ 54 & 13L & 156 & -22L \\ -13L & -3L^2 & -22L & 4L^2 \end{bmatrix} \tag{3.3.18}$$

$$M_{NN} = I$$

$$M_{IN} = [m_{ji}],\ m_{ji} = \rho A\int_0^L \phi_j\overline{\phi}_i dx \tag{3.3.19}$$

$$i = 1, 2, \cdots, \infty,\ j = 1, 2, 3, 4$$

with

$$\begin{aligned} m_{1i} &= \rho ALC_i\{c_{17} - 3c_{19} + 2c_{20}\}_i \\ m_{2i} &= \rho AL^2C_i\{c_{18} - 2c_{19} + c_{20}\}_i \\ m_{3i} &= \rho ALC_i\{3c_{19} - 2c_{20}\}_i \\ m_{4i} &= \rho AL^2C_i\{-c_{19} + c_{20}\}_i \end{aligned} \tag{3.3.20}$$

where

$$c_1 = \frac{\cosh\beta - 1}{\beta},\ c_2 = \frac{\beta\cosh\beta - \sinh\beta}{\beta^2}$$

$$c_3 = \left(\frac{1}{\beta} + \frac{2}{\beta^3}\right)\cosh\beta - \frac{2}{\beta^2}\sinh\beta - \frac{2}{\beta^3}$$

$$c_4 = \left(\frac{1}{\beta} + \frac{6}{\beta^3}\right)\cosh\beta - \left(\frac{3}{\beta^2} + \frac{6}{\beta^4}\right)\sinh\beta$$

$$c_5 = \frac{\sinh\beta}{\beta},\ c_6 = \frac{\beta\sinh\beta - \cosh\beta + 1}{\beta^2}$$

$$c_7 = \left(\frac{1}{\beta} + \frac{2}{\beta^3}\right)\sinh\beta - \frac{2}{\beta^2}\cosh\beta$$

$$c_8 = \left(\frac{1}{\beta} + \frac{6}{\beta^3}\right)\sinh\beta - \left(\frac{3}{\beta^2} + \frac{6}{\beta^4}\right)\cosh\beta + \frac{6}{\beta^4}$$

$$c_9 = \frac{1-\cos\beta}{\beta}, \; c_{10} = \frac{\sin\beta - \beta\cos\beta}{\beta^2}$$

$$c_{11} = \frac{2}{\beta^2}\sin\beta - \frac{\beta^2-2}{\beta^3}\cos\beta - \frac{2}{\beta^3}$$

$$c_{12} = \frac{3\beta^2-6}{\beta^4}\sin\beta - \frac{\beta^2-6}{\beta^3}\cos\beta$$

$$c_{13} = \frac{\sin\beta}{\beta}, \; c_{14} = \frac{\cos\beta + \beta\sin\beta - 1}{\beta^2}$$

$$c_{15} = \frac{2}{\beta^2}\cos\beta + \frac{\beta^2-2}{\beta^3}\sin\beta \tag{3.3.21}$$

$$c_{16} = \frac{3\beta^2-6}{\beta^4}\cos\beta + \frac{\beta^2-6}{\beta^3}\sin\beta + \frac{6}{\beta^4}$$

$$\begin{aligned} c_{17} &= c_1 - c_9 - \alpha c_5 + \alpha c_{13} \\ c_{18} &= c_2 - c_{10} - \alpha c_6 + \alpha c_{14} \\ c_{19} &= c_3 - c_{11} - \alpha c_7 + \alpha c_{15} \\ c_{20} &= c_4 - c_{12} - \alpha c_8 + \alpha c_{16} \end{aligned} \tag{3.3.22}$$

Note that M_{II} is the standard consistent mass matrix for the Bernoulli–Euler beam.

Next, the potential energy of the Bernoulli–Euler beam element is

$$U = \frac{1}{2}\int_0^L EIv''^2\,dx \tag{3.3.23}$$

Application of Eq. (3.3.3) in Eq. (3.3.23) yields

$$
\begin{aligned}
&K_{II} = \frac{EI}{L^3}\begin{bmatrix} 12 & 6L & -12 & 6L \\ 6L & 4L^2 & -6L & 2L^2 \\ -12 & -6L & 12 & -6L \\ 6L & 2L^2 & -6L & 4L^2 \end{bmatrix} \\
&K_{IN} = 0 \\
&K_{NN} = \text{Diag}\ [\omega_1^2\ \omega_2^2\ \cdots], \qquad \omega_i^2 = \beta_i^4 \frac{EI}{\rho A L^4}, \quad i = 1, 2, \cdots
\end{aligned}
\tag{3.3.24}
$$

Because interface restrained normal modes are employed, the M_{NN} matrix becomes unity and the K_{IN} matrix vanishes. Due to the rapid increase of ω_i^2 with i, convergence is actually faster than in the case of the axial bar elements.

While the use of normal modes as interface restrained assumed modes yields the highest convergence rate, numerical difficulties may be encountered [26-28]. Indeed, while working in single precision numerical instabilities are encountered when $i > 5$ due to the computation of differences of large numbers. In double precision and quadruple precision ill–conditioning occurs for $i > 15$ and $i > 27$, respectively. In the case of the Bernoulli–Euler beam this is not a serious handicap because the number of normal modes needed is rarely larger than five. In addition, most of the computations involved are one time computations only. If need be however, Chang and Craig [26] suggested a remedy which allows for retaining up to thirty normal modes in double precision without computational degradation. The Chang and Craig remedy was in fact implemented as part of the Bernoulli–Euler element subroutine. Another option is to use a different set of interface restrained assumed modes which provide numerical stability for all i. As indicated before, interface restrained modes need only be admissable. When a set of interface restrained assumed modes are used different from the normal modes set, a decrease in convergence rate can be expected. In the next section a set of trigonometric modes will be considered. It will be shown that trigonometric modes produce very stable and cost–effective elements, while sacrificing only marginally in terms of convergence rate.

3.3.2 Trigonometric Functions As Interface Restrained Assumed Modes

In this section, trigonometric functions are introduced as an alternative to normal modes. The resulting mass and stiffness matrices are highly banded. In addition, the convergence rate compares quite well to that exhibited by the normal modes case and the computational cost is less. Therefore as a second choice, the interface restrained assumed modes in the case of the Bernoulli–Euler beam are taken as

$$\overline{\phi} = [\ \overline{V}_i\ ] \tag{3.3.25}$$

where

$$\overline{V}_i = \cos\,(i-1)\frac{\pi x}{L} - \cos\,(i+1)\frac{\pi x}{L}, \quad i = 1, 2, \ldots, n \tag{3.3.26}$$

These functions are admissible since both $\overline{V}_i$ and $\overline{V}_i{}'$ vanish at the boundaries. Using the static constraint modes from Eq. (3.3.5) and the interface restrained assumed modes from Eq. (3.3.25) in the kinetic energy of the Bernoulli–Euler beam element, the mass matrix takes on the form,

$$M = \begin{bmatrix} M_{II} & M_{IN} \\ M_{IN}^T & M_{NN} \end{bmatrix} \tag{3.3.27}$$

The M_{II} partition of the mass matrix is the consistent mass matrix and is again given by Eq. (3.3.18). The M_{NN} partition becomes tridiagonal due to the orthogonality properties of the chosen $\overline{\phi}$,

$$M_{NN} = \frac{\rho AL}{2}\begin{bmatrix} M_1 & 0 \\ 0 & M_2 \end{bmatrix} \tag{3.3.28}$$

where

$$M_{1_{(n_1 \times n_1)}} = \begin{bmatrix} 3 & -1 & 0 & 0 & \cdots \\ -1 & 2 & -1 & 0 & \cdots \\ 0 & -1 & 2 & -1 & \cdots \\ & & \vdots & & \end{bmatrix} \tag{3.3.29}$$

$$M_{2_{(n_2\times n_2)}} = \begin{bmatrix} 2 & -1 & 0 & 0 & \cdots \\ -1 & 2 & -1 & 0 & \cdots \\ 0 & -1 & 2 & -1 & \cdots \\ & & \vdots & & \end{bmatrix} \tag{3.3.30}$$

$$\begin{aligned} n_1 &= \frac{n}{2} \ \text{ and } \ n_2 = \frac{n}{2} \ \text{ for even } n, \\ n_1 &= \frac{n+1}{2} \ \text{ and } \ n_2 = \frac{n-1}{2} \ \text{ for odd } n. \end{aligned} \tag{3.3.31}$$

Furthermore,

$$M_{IN} = [m_{ji}]\,,\ m_{ji} = \rho A \int_0^L \phi_j \overline{\phi}_i dx \tag{3.3.32}$$

$$i = 1, 2, \cdots, \infty,\ j = 1, 2, 3, 4$$

where

$$\begin{aligned} m_{1i} &= \rho AL(c_1 - 3c_3 + 2c_4)_i \\ m_{2i} &= \rho AL^2(c_2 - 2c_3 + c_4)_i \\ m_{3i} &= \rho AL(3c_3 - 2c_4)_i \\ m_{4i} &= \rho AL^2(-c_3 + c_4)_i \end{aligned} \tag{3.3.33}$$

in which,

For $i = 1$,

$$\begin{aligned} c_1 &= 1 \\ c_2 &= 1/2 \\ c_3 &= 1/3 - 1/2\pi^2 \\ c_4 &= 1/4 - 3/4\pi^2 \end{aligned} \tag{3.3.34}$$

For $i = 2, 3, \ldots, n_1$,

$$\begin{aligned} c_1 &= 0 \\ c_2 &= 0 \\ c_3 &= \frac{2}{\pi^2}\left[1/(i_1 - 1)^2 - 1/(i_1 + 1)^2\right] \\ c_4 &= \frac{3}{\pi^2}\left[1/(i_1 - 1)^2 - 1/(i_1 + 1)^2\right] \\ i_1 &= 2i - 1 \end{aligned} \tag{3.3.35}$$

For $i = n_1 + 1, n_1 + 2, \ldots, n,$

$$
\begin{aligned}
c_1 &= 0 \\
c_2 &= -\frac{2}{\pi^2}\left[1/(i_2-1)^2 - 1/(i_2+1)^2\right] \\
c_3 &= -\frac{2}{\pi^2}\left[1/(i_2-1)^2 - 1/(i_2+1)^2\right] \\
c_4 &= -\frac{3}{\pi^2}\left[(1/(i_2-1)^2 - 1/(i_2+1)^2\right] \\
&\quad + \frac{12}{\pi^4}\left[1/(i_2-1)^4 - 1/(i_2+1)^4\right] \\
i_2 &= 2(i - n_1)
\end{aligned}
\tag{3.3.36}
$$

Again using the static constraint modes from Eq. (3.3.5) and the interface restrained assumed modes from Eq. (3.3.25) in the potential energy for the Bernoulli–Euler beam element in Eq. (3.3.23), the stiffness matrix takes on the form,

$$
K = \begin{bmatrix} K_{II} & 0 \\ 0 & K_{NN} \end{bmatrix} \tag{3.3.37}
$$

K_{NN} is tridiagonal because of the orthogonal properties of the chosen $\overline{\phi}$ and K_{II} is the standard finite element stiffness matrix given in Eq. (3.3.24) . Explicitly, K_{NN} becomes,

$$
K_{NN} = \frac{\pi^4 EI}{2L^3}\begin{bmatrix} K_1 & 0 \\ 0 & K_2 \end{bmatrix} \tag{3.3.38}
$$

where

$$
K_{1_{(n_1 \times n_1)}} = \begin{bmatrix} 2^4 & -2^4 & 0 & 0 & \cdots \\ -2^4 & 4^4+2^4 & -4^4 & 0 & \cdots \\ 0 & -4^4 & 6^4+4^4 & -6^4 & \cdots \\ & & \vdots & & \end{bmatrix} \tag{3.3.39}
$$

and,

$$
K_{2_{(n_2 \times n_2)}} = \begin{bmatrix} 3^4+1^4 & -3^4 & 0 & 0 & \cdots \\ -3^4 & 5^4+3^4 & -5^4 & 0 & \cdots \\ 0 & -5^4 & 7^4+5^4 & -7^4 & \cdots \\ & & \vdots & & \end{bmatrix} \tag{3.3.40}
$$

Unlike the normal modes case, no trigonometric functions must actually be evaluated in order to determine the mass and stiffness matrices. In fact, the compuatational effort is quite small and the element is very well–conditioned. This concludes the description of the Bernoulli–Euler beam element.

3.4 Timoshenko Beam

The standard Timoshenko beam theory takes into account both rotary inertia and transverse shear deformation, in addition to the pure bending deformation considered in the Bernoulli–Euler beam theory. These effects cannot be ignored if higher modes of vibration are desired or when the aspect ratio of the beam is not small.

The kinematics of deformation of a Timoshenko beam element is shown in Figure 6. The rotation angle θ is related to the shear angle ψ as follows,

$$\theta = \psi + \frac{\partial v}{\partial x} \tag{3.4.1}$$

where $\partial v/\partial x$ is the slope of the v displacement curve. The two independent displacement functions to be used in the kinetic and strain energy expressions are the transverse displacement $v(x,t)$ and the rotation angle $\theta(x,t)$. The mass and stiffness matrices from Eqs. (2.2.4–2.2.6) and (2.2.11–2.2.13) for a generic finite element E in Section 2.2 can be easily extended for the case of the Timoshenko beam. In fact, M in Eq. (2.2.4) needs only be replaced by

$$M = \int_E \phi^T m \phi \; dm \tag{3.4.2}$$

where the matrix m reflects the mass and geometric properties of the finite element E. Correspondingly, Eq. (2.2.6) becomes,

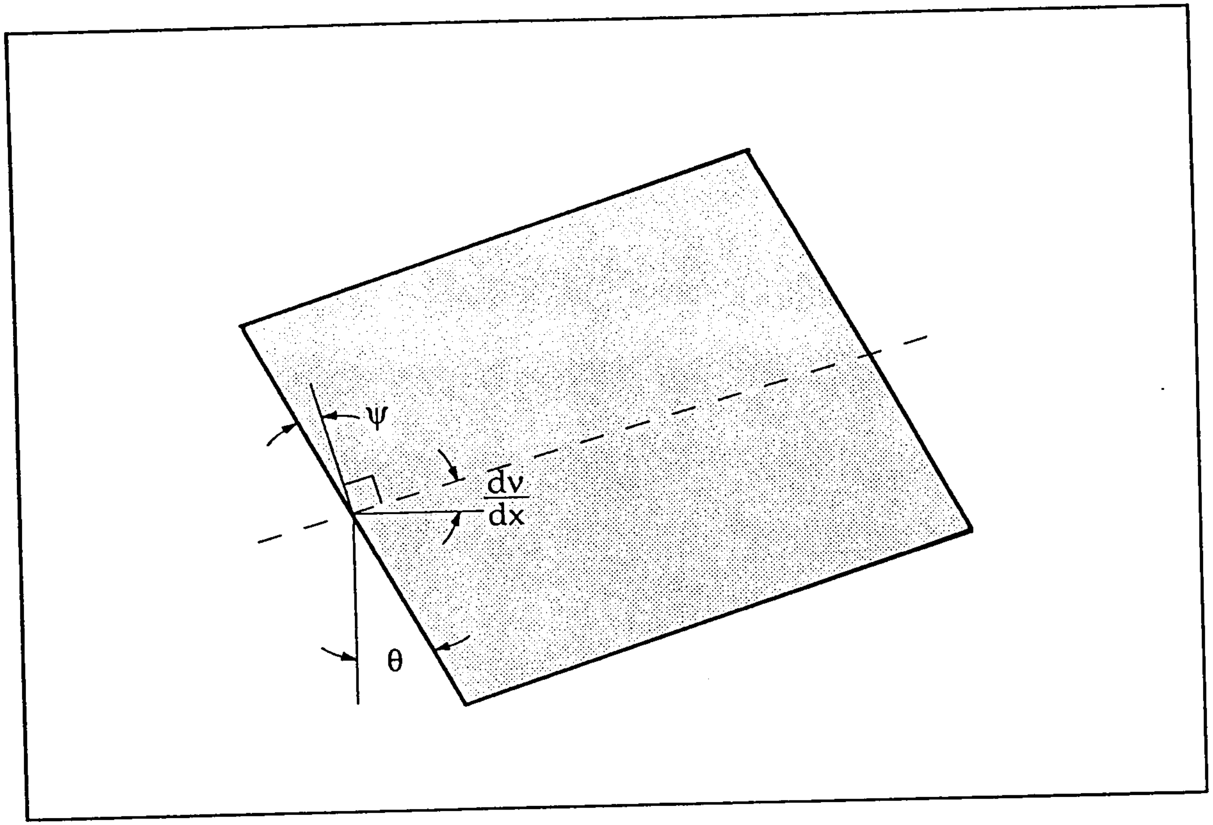

Figure 6. Kinematics of Deformation of a Timoshenko Beam

$$
\begin{aligned}
M_{II} &= \int_E \phi_I^T m \phi_I \, dm \\
M_{IN} &= \int_E \phi_I^T m \overline{\phi} \, dm \\
M_{NN} &= \int_E \overline{\phi}^T m \overline{\phi} \, dm
\end{aligned} \tag{3.4.3}
$$

Furthermore, Eqs. (2.2.11) and (2.2.13) remain formally the same although the matrices B and C may contain different elements.

The interface displacement vector $\boldsymbol{q}_I$ is defined as

$$
\begin{aligned}
\boldsymbol{q}_I &= \lfloor q_1 \ q_2 \ q_3 \ q_4 \rfloor^T \\
&\triangleq \lfloor v(0,t) \ \theta(0,t) \ v(L,t) \ \theta(L,t) \rfloor^T
\end{aligned} \tag{3.4.4}
$$

where L is the length of the beam as shown in Figure 7.

For the Timoshenko beam, the equivalent of Eq. (2.1.7) is

$$
\begin{Bmatrix} v \\ \theta \end{Bmatrix} = \begin{bmatrix} S_v & \overline{V} \\ S_\theta & \overline{\Theta} \end{bmatrix} \begin{Bmatrix} \boldsymbol{q}_I \\ \overline{\boldsymbol{q}} \end{Bmatrix} \tag{3.4.5}
$$

with

$$
\phi_I = \begin{bmatrix} S_v \\ S_\theta \end{bmatrix}, \quad \overline{\phi} = \begin{bmatrix} \overline{V} \\ \overline{\Theta} \end{bmatrix} \tag{3.4.6}
$$

where S_v and S_θ are 1×4 static constraint mode matrices corresponding to v and θ, respectively. Also V and Θ are the corresponding restrained normal mode matrices.

3.4.1 Static Constraint Modes

The static constraint modes can now be computed from the following static equilibrium equations

$$
\begin{aligned}
&EI\frac{\partial^2 \theta}{\partial x^2} + kAG\left(\frac{\partial v}{\partial x} - \theta\right) = 0 \\
&\frac{\partial^2 v}{\partial x^2} - \frac{\partial \theta}{\partial x} = 0
\end{aligned} \tag{3.4.7}
$$

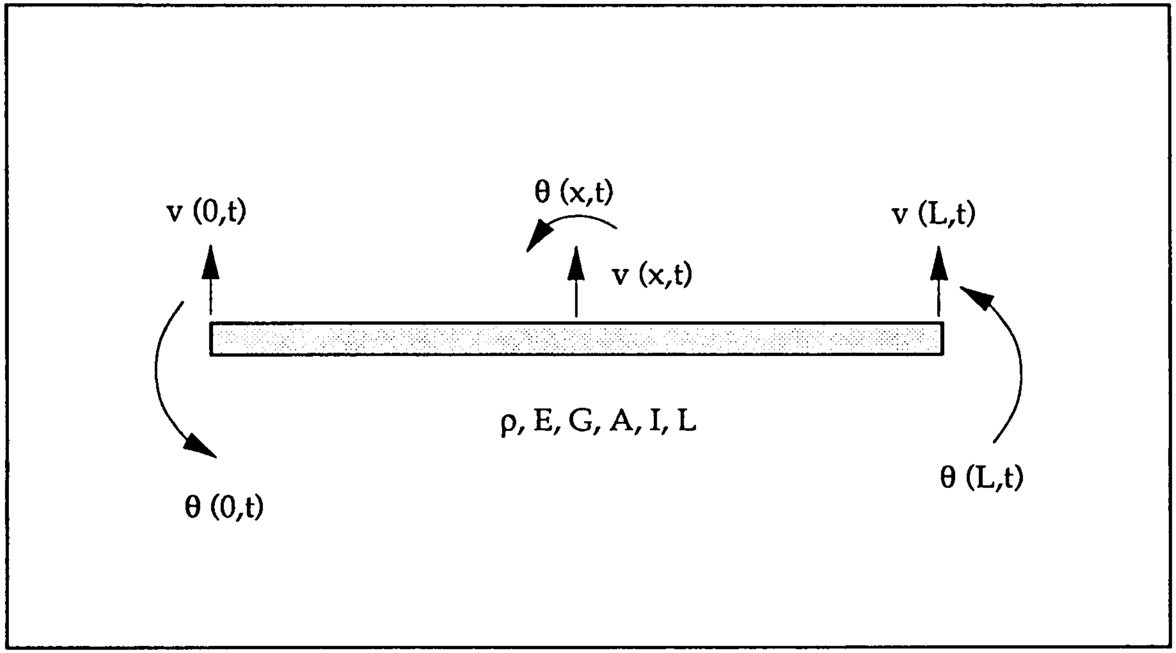

Figure 7. Timoshenko Beam Element

where E is Young's modulus, G the shear modulus, I is the area moment of inertia, A the cross sectional area and k the shear coefficient [29] and the appropriate boundary conditions are

$$\begin{aligned}
&q_1 = 1, \quad q_2 = q_3 = q_4 = 0 \\
&q_1 = 0, \quad q_2 = 1, \quad q_3 = q_4 = 0 \\
&q_1 = q_2 = 0, \quad q_3 = 1, \quad q_4 = 0 \\
&q_1 = q_2 = q_3 = 0, \quad q_4 = 1
\end{aligned} \tag{3.4.8}$$

The results are

$$S_v \triangleq [S_{vq_1} \; S_{vq_2} \; S_{vq_3} \; S_{vq_4}] \tag{3.4.9}$$

where

$$\begin{aligned}
S_{vq_1} &= 1 - \xi + s_2\xi(1-\xi)(1-2\xi) \\
S_{vq_2} &= \frac{L}{2}\left[\xi(1-\xi) + s_2\xi(1-\xi)(1-2\xi)\right] \\
S_{vq_3} &= \xi - s_2\xi(1-\xi)(1-2\xi) \\
S_{vq_4} &= \frac{L}{2}\left[-\xi(1-\xi) + s_2\xi(1-\xi)(1-2\xi)\right]
\end{aligned} \tag{3.4.10}$$

$$S_\theta \triangleq [S_{\theta q_1} \; S_{\theta q_2} \; S_{\theta q_3} \; S_{\theta q_4}] \tag{3.4.11}$$

where

$$\begin{aligned}
S_{\theta q_1} &= -\frac{6}{L}s_2\xi(1-\xi) \\
S_{\theta q_2} &= 1 - \xi - 3s_2\xi(1-\xi) \\
S_{\theta q_3} &= \frac{6}{L}s_2\xi(1-\xi) \\
S_{\theta q_4} &= \xi - 3s_2\xi(1-\xi)
\end{aligned} \tag{3.4.12}$$

and

$$\xi = \frac{x}{L}, \qquad s_1 = \frac{12EI}{kAGL^2}, \qquad s_2 = \frac{1}{1+s_1} \tag{3.4.13}$$

Note that as expected, the static constraint modes are indeed the standard finite element shape functions.

At this point enough information exists to compute M_{II} and K_{II} from Eqs. (3.4.3), (2.2.9) and (2.2.11). Indeed, for the Timoshenko beam, the kinetic and potential energies T and U are given as

$$T = \frac{\rho A}{2}\int_0^L \left(\frac{\partial v}{\partial t}\right)^2 dx + \frac{\rho I}{2}\int_0^L \left(\frac{\partial \theta}{\partial t}\right)^2 dx \tag{3.4.14}$$

and

$$U = \frac{EI}{2}\int_0^L \left(\frac{\partial \theta}{\partial x}\right)^2 dx + \frac{kAG}{2}\int_0^L \psi^2 dx \tag{3.4.15}$$

It can then be seen that in Eqs. (2.2.11) and (2.2.13)

$$m = \begin{bmatrix} \rho A & 0 \\ 0 & \rho I \end{bmatrix} \quad B = \begin{bmatrix} -\dfrac{\partial}{\partial x} & 1 \\ 0 & \dfrac{\partial}{\partial x} \end{bmatrix} \quad C = \begin{bmatrix} kAG & 0 \\ 0 & EI \end{bmatrix} \tag{3.4.16}$$

Next, substituting m from Eq. (3.4.16) and ϕ_I from Eq. (3.4.5), into Eqs. (3.4.14) and (3.4.15) yields

$$M_{II} = \rho A \int_0^L S_v^T S_v dx + \rho I \int_0^L S_\theta^T S_\theta dx \tag{3.4.17}$$

and

$$K_{II} = EI \int_0^L \left(\frac{dS_\theta}{dx}\right)^T \left(\frac{dS_\theta}{dx}\right) dx + kAG \int_0^L \left(S_\theta - \frac{dS_v}{dx}\right)^T \left(S_\theta - \frac{dS_v}{dx}\right) dx \tag{3.4.18}$$

Explicit expressions for M_{II} and K_{II} can be obtained by substituting Eqs. (3.4.10) and (3.4.12) into Eqs. (3.4.17–3.4.18) and are listed below:

$$M_{II} = c_1 \begin{bmatrix} m_1 & m_2 & m_3 & m_4 \\ m_2 & m_5 & -m_4 & m_6 \\ m_3 & -m_4 & m_1 & -m_2 \\ m_4 & m_6 & -m_2 & m_5 \end{bmatrix} + c_2 \begin{bmatrix} m_7 & m_8 & -m_7 & m_8 \\ m_8 & m_9 & -m_8 & m_{10} \\ -m_7 & -m_8 & m_7 & -m_8 \\ m_8 & m_{10} & -m_8 & m_9 \end{bmatrix} \tag{3.4.19}$$

where

$$
\begin{aligned}
s_1 &= \frac{12EI}{kAGL^2}, \quad c_1 = \frac{\rho AL}{(1+s_1)^2}, \quad c_2 = \frac{\rho IL}{L^2(1+s_1)^2} \\
m_1 &= \frac{13}{35} + \frac{7s_1}{10} + \frac{s_1^2}{3}, \quad m_2 = \left(\frac{11}{210} + \frac{11s_1}{120} + \frac{s_1^2}{24}\right)L \\
m_3 &= \frac{9}{70} + \frac{3s_1}{10} + \frac{s_1^2}{6}, \quad m_4 = -\left(\frac{13}{420} + \frac{3s_1}{40} + \frac{s_1^2}{24}\right)L \\
m_5 &= \left(\frac{1}{105} + \frac{s_1}{60} + \frac{s_1^2}{120}\right)L^2, \quad m_6 = -\left(\frac{1}{140} + \frac{s_1}{60} + \frac{s_1^2}{120}\right)L^2 \\
m_7 &= \frac{6}{5}, \quad m_8 = \left(\frac{1}{10} - \frac{s_1}{2}\right)L \\
m_9 &= \left(\frac{2}{15} + \frac{s_1}{6} + \frac{s_1^2}{3}\right)L^2, \quad m_{10} = \left(-\frac{1}{30} - \frac{s_1}{6} + \frac{s_1^2}{6}\right)L^2
\end{aligned}
\tag{3.4.20}
$$

$$
K_{II} = \frac{EI}{L^3(1+s_1)} \begin{bmatrix} 12 & 6L & -12 & 6L \\ 6L & L^2(4+s_1) & -6L & L^2(2-s_1) \\ -12 & -6L & 12 & -6L \\ 6L & L^2(2-s_1) & -6L & L^2(4+s_1) \end{bmatrix} \tag{3.4.21}
$$

These matrices are as expected the consistent mass and stiffness matrices first proposed by McCalley [30–31]. If it is decided that no extra $\bar{q}$ coordinates are to be retained in Eq. (2.1.7), then the procedure can be terminated at this stage. If, on the other hand, it is felt that extra $\bar{q}$ coordinates are needed a set of interface restrained assumed modes must be identified. An entire class of hierarchical models can now be created solely on the basis of choosing the interface restrained assumed modes. In the next section, several possible choices will be investigated.

3.4.2 Normal Modes As Interface Restrained Assumed Modes

A first possible set of interface restrained assumed modes is the set of interface restrained normal modes. These modes are not only admissible, they also satisfy the physical boundary conditions and probably constitute the best choice in terms of convergence rate. It should be noted that this choice for the interface restrained assumed modes represents the Craig/Bampton component mode synthesis technique as applied to a finite element [6].

The interface restrained normal modes and corresponding natural frequencies are obtained by solving the eigenvalue problem implied by the following set of differential equations of motion

$$\begin{aligned} EI\frac{\partial^2\theta}{\partial x^2} + kAG\left(\frac{\partial v}{\partial x} - \theta\right) - \rho I\frac{\partial^2\theta}{\partial t^2} = 0 \\ \rho A\frac{\partial^2 v}{\partial t^2} - kAG\left(\frac{\partial^2 v}{\partial x^2} - \frac{\partial\theta}{\partial x}\right) = 0 \end{aligned} \tag{3.4.22}$$

where ρ is the mass density and clamped-clamped boundary conditions are imposed. Substituting $v = \overline{V}\cos\omega t$ and $\theta = \overline{\Theta}\cos\omega t$ into Eq. (3.4.22) yields

$$\begin{aligned} s^2\overline{\Theta}'' - (1 - b^2r^2s^2)\overline{\Theta} + \overline{V}'/L = 0 \\ \overline{V}'' + b^2s^2\overline{V} - L\overline{\Theta}' = 0 \end{aligned} \tag{3.4.23}$$

where

$$b^2 = \frac{\rho A}{EI}L^4\omega^2, \quad r^2 = \frac{I}{AL^2}, \quad s^2 = \frac{EI}{kAGL^2} \tag{3.4.24}$$

and the primes ($'$) denote differentiation with respect to $\xi = x/L$. Note that the expression for b^2 contains the i–th circular frequency and the index i is omitted for simplicity. The clamped-clamped boundary conditions are

$$\begin{aligned} \overline{V} = 0 \text{ at } \xi = 0 \text{ and } \xi = 1 \\ \overline{\Theta} = 0 \text{ at } \xi = 0 \text{ and } \xi = 1 \end{aligned} \tag{3.4.25}$$

Eqs. (3.4.23) and (3.4.25) lead to two types of modes for the Timoshenko beam [32–33].

The first type corresponds to the case where $\left[(r^2 - s^2)^2 + 4/b^2\right]^{\frac{1}{2}} > (r^2 + s^2)$ and the frequency equation becomes

$$2 - 2\cosh b\alpha_1 \cos b\beta + \frac{b\left[b^2s^2(r^2 - s^2)^2 + 3s^2 - r^2\right]}{(1 - b^2r^2s^2)^{\frac{1}{2}}}\sinh b\alpha_1 \sin b\beta = 0 \tag{3.4.26}$$

where

$$\left\{ \begin{matrix} \alpha_1 \\ \beta \end{matrix} \right\} = \frac{1}{\sqrt{2}} \left\{ \mp (r^2 + s^2) + \left[(r^2 - s^2)^2 + 4/b^2 \right]^{\frac{1}{2}} \right\}^{\frac{1}{2}} \tag{3.4.27}$$

The corresponding restrained normal modes are found as

$$\begin{aligned} \overline{V} &= C \left[\cosh b\alpha_1 \xi - \lambda \zeta \delta \sinh b\alpha_1 \xi - \cos b\beta\xi + \delta \sin b\beta\xi \right] \\ \overline{\Theta} &= C\eta \left[\cosh b\alpha_1 \xi + \frac{\gamma}{\lambda\zeta} \sinh b\alpha_1 \xi - \cos b\beta\xi + \gamma \sin b\beta\xi \right] \end{aligned} \tag{3.4.28}$$

with

$$\begin{aligned} \lambda &= \frac{\alpha_1}{\beta}, \quad \zeta = (\beta^2 - s^2)/(\beta^2 - r^2) \\ \delta &= \frac{-\cosh b\alpha_1 + \cos b\beta}{-\lambda\zeta \sinh b\alpha_1 + \sin b\beta} \\ \gamma &= \frac{-\cosh b\alpha_1 + \cos b\beta}{\dfrac{1}{\lambda\zeta} \sinh b\alpha_1 + \sin b\beta} \\ \eta &= \frac{-\cosh b\alpha_1 + \cos b\beta}{\dfrac{\sinh b\alpha_1}{\dfrac{b}{L}\left(\dfrac{\alpha_1^2 + s^2}{\alpha_1}\right)} - \dfrac{\sin b\beta}{\dfrac{b}{L}\left(\dfrac{\beta^2 - s^2}{\beta}\right)}} \end{aligned} \tag{3.4.29}$$

Note that for $r = s = 0$, Eqs. (3.4.26) and (3.4.28) reduce to the frequency and normal mode equations for the classical Bernoulli–Euler beam.

The second type of modes are obtained when $\left[(r^2 - s^2)^2 + 4/b^2\right]^{\frac{1}{2}} < (r^2 + s^2)$. Eqs. (3.4.26) and (3.4.28) must be modified.i.e., α_1 must be replaced by $j\alpha_2$ and $(1 - b^2 r^2 s^2)^{\frac{1}{2}}$ by $j(b^2 r^2 s^2 - 1)^{\frac{1}{2}}$ where $j = \sqrt{(-1)}$. The modified frequency equation then becomes,

$$2 - 2\cos b\alpha_2 \cos b\beta + \frac{b\left[b^2 s^2 (r^2 - s^2)^2 + 3s^2 - r^2\right]}{(b^2 r^2 s^2 - 1)^{\frac{1}{2}}} \sin b\alpha_2 \sin b\beta = 0 \tag{3.4.30}$$

where

$$\begin{Bmatrix} \alpha_2 \\ \beta \end{Bmatrix} = \frac{1}{\sqrt{2}} \left\{ (r^2 + s^2) \mp \left[(r^2 - s^2)^2 + 4/b^2 \right]^{\frac{1}{2}} \right\}^{\frac{1}{2}} \tag{3.4.31}$$

and the corresponding restrained normal modes are found as

$$\begin{aligned} \overline{V} &= C\left[\cos b\alpha_2\xi + \lambda_2\zeta\delta_2 \sin b\alpha_2\xi \ - \cos b\beta\xi + \delta_2 \sin b\beta\xi\right] \\ \overline{\Theta} &= C\eta_2[\cos b\alpha_2\xi + \frac{\gamma_2}{\lambda_2\zeta} \sin b\alpha_2\xi - \cos b\beta\xi + \gamma_2 \sin b\beta\xi] \end{aligned} \tag{3.4.32}$$

with

$$\begin{aligned} \lambda_2 &= \frac{\alpha_2}{\beta}, \quad \zeta = (\beta^2 - s^2)/(\beta^2 - r^2) \\ \delta_2 &= \frac{-\cos b\alpha_2 + \cos b\beta}{\lambda_2\zeta \sin b\alpha_2 + \sin b\beta} \\ \gamma_2 &= \frac{-\cos b\alpha_2 + \cos b\beta}{\dfrac{1}{\lambda_2\zeta} \sin b\alpha_2 + \sin b\beta} \\ \eta_2 &= \frac{\cos b\alpha_2 - \cos b\beta}{\dfrac{\sin b\alpha_2}{\dfrac{b}{L}\left(\dfrac{s^2 - \alpha_2^2}{\alpha_2}\right)} + \dfrac{\sin b\beta}{\dfrac{b}{L}\left(\dfrac{\beta^2 - s^2}{\beta}\right)}} \end{aligned} \tag{3.4.33}$$

The constant C in Eqs. (3.4.28) and (3.4.32) can be evaluated by requiring mass normalized modes. i.e.,

$$\int_0^L \rho A \overline{V}^2 dx + \int_0^L \rho I \overline{\Theta}^2 dx = 1 \tag{3.4.34}$$

Note that $\overline{V}$ and $\overline{\Theta}$ in Eqs. (3.4.28) and (3.4.32) are typical entries for modes $\overline{V}$ and $\overline{\Theta}$ in Eq. (3.4.34). The evaluation of Eq. (3.4.34) is accomplished in Appendix I. The mass coupling matrix M_{IN} is given in Appendix II. The matrix M_{NN}

becomes unity and K_{NN} becomes a diagonal matrix containing the squares of the circular natural frequencies on its diagonal. These circular natural frequencies can be obtained from Eq. (3.4.26) or Eq. (3.4.30) via a bisection method or a Newton–Raphson scheme.

Although interface restrained normal modes probably represent the optimum set of interface restrained assumed modes in terms of convergence rate, they do have several shortcomings. One disadvantage is the dependence of the frequencies and modeshapes on the structural parameters to the extent that very few one time computations can be identified. In addition, the elements in the corresponding mass and stiffness matrices M and K are quite sensitive to small changes in the computed frequencies, requiring undesirably high computational accuracy [26]. The choice of normal modes, however, is workable, and was used in this dissertation as the standard against which the convergence rate of subsequently derived models will be measured. For problems in which a large number of interface restrained assumed modes are required, use of normal modes is not recommended. However, if the element is to be used in a larger structure, then only a few interface restrained assumed modes are usually required. In such cases, the use of normal modes may still be the best course of action.

This concludes the development of dynamic finite element for Timoshenko beam using interface restrained normal modes. In the next two sections, use of interface restrained assumed modes other than normal modes will be discussed.

3.4.3 Polynomial Functions As Interface Restrained Assumed Modes

As was indicated in Section 3.4.2, normal modes probably represent the optimum choice for the interface restrained assumed modes. However, they cannot be recommended for general practical use due to their numerical instability and their heavy dependence on the structural parameters of the element. Fortunately, only admissible functions for the interface restrained assumed modes are required and therefore, many other choices are possible, so that a slight decrease in convergence rate can be traded for a substantial decrease in computational effort. As a second choice then, the interface restrained assumed modes are taken as a set of admissible polynomials, i.e., polynomials that satisfy the fixed–fixed boundary conditions,

$$\overline{\phi} = \begin{bmatrix} \overline{V} \\ \overline{\Theta} \end{bmatrix} = \left[\begin{array}{c|c|c|c} \overline{V}_{i+2} & 0 & \overline{V}_1 & \overline{V}_2 \\ \overline{V}'_{i+2} & \overline{V}_i & 0 & 0 \end{array} \right] \tag{3.4.35}$$

where

$$\begin{aligned} \overline{V}_i &= \xi^{i_1}(1-\xi)^{i_2}, \quad \xi = \frac{x}{L}, \quad i = 1,2,\ldots \\ \text{and } \; i_1 &= \frac{1+i}{2}, \quad i_2 = \frac{1+i}{2} \;\text{ for }\; i = 1,3,5\ldots \\ i_1 &= \frac{2+i}{2}, \quad i_2 = \frac{i}{2} \;\text{ for }\; i = 2,4,6\ldots \end{aligned} \tag{3.4.36}$$

The first partition in $\overline{\phi}$ in Eq. (3.4.35) is chosen to reflect the Bernoulli–Euler part in the solution, where θ is in fact equal to $\partial v/\partial x$. The index i can be chosen to vary from 1 to n where n is an a priori chosen cut–off point. The second partition is added to account for the shear deformation which is present in the Timoshenko beam element. Here, the index i can run from 1 to m. The third and the fourth partitions represent two extra modes which will account for constant shear at the interfaces in case the element is used with fixed boundary conditions. Note that all chosen $\overline{\phi}_i$ modes satisfy the fixed–fixed boundary conditions.

It is now possible to explicitly obtain the matrices in Eqs. (2.2.6) and (2.2.13). After a series of one time algebraic computations it is seen that

$$\begin{aligned} M_{IN} &= [m_{ji}] \\ i &= 1,2,\cdots,n+m, \; j = 1,2,3,4 \end{aligned} \tag{3.4.37}$$

$$
\begin{aligned}
m_{1i} &= \rho AL\left[c_1 - c_2 + s_2(c_2 - 3c_3 + 2c_4)\right]_i - 6\rho I s_2\left[c_6 - c_7\right]_i \\
m_{2i} &= \frac{\rho AL^2}{2}\left[c_2 - c_3 + s_2(c_2 - 3c_3 + 2c_4)\right]_i + \rho IL\left[c_5 - c_6 - 3s_2(c_6 - c_7)\right]_i \\
m_{3i} &= \rho AL\left[c_2 - s_2(c_2 - 3c_3 + 2c_4)\right]_i + 6\rho I s_2\left[c_6 - c_7\right]_i \\
m_{4i} &= \frac{\rho AL^2}{2}\left[-c_2 + c_3 + s_2(c_2 - 3c_3 + 2c_4)\right]_i + \rho IL\left[c_6 - 3s_2(c_6 - c_7)\right]_i
\end{aligned}
\tag{3.4.38}
$$

For $i = 1, 2, \ldots, n$,

$$
\begin{aligned}
c_1 &= c_{i_1, i_2} \\
c_2 &= c_{i_1+1, i_2} \\
c_3 &= c_{i_1+2, i_2} \\
c_4 &= c_{i_1+3, i_2} \\
c_5 &= (i_1 c_{i_1-1, i_2} - i_2 c_{i_1, i_2-1})/L \\
c_6 &= (i_1 c_{i_1, i_2} - i_2 c_{i_1+1, i_2-1})/L \\
c_7 &= (i_1 c_{i_1+1, i_2} - i_2 c_{i_1+2, i_2-1})/L
\end{aligned}
\tag{3.4.39}
$$

i_1 and i_2 are found from Eq. (3.4.36) by replacing i by $(i+2)$ and,

$$
c_{i,j} = \frac{i!j!}{(i+j+1)!} \tag{3.4.40}
$$

For $i = n+1,\ n+2, \ldots,\ n+m-2$

$$\begin{aligned} c_1 &= c_2 = c_3 = c_4 = 0 \\ c_5 &= c_{i_1,i_2} \\ c_6 &= c_{i_1+1,i_2} \\ c_7 &= c_{i_1+2,i_2} \end{aligned} \tag{3.4.41}$$

i_1 and i_2 are found from Eq. (3.4.36) by replacing i by $(i-n)$.

For $i = n+m-1,\ n+m,$

$$\begin{aligned} c_1 &= c_{i_1,i_2} \\ c_2 &= c_{i_1+1,i_2} \\ c_3 &= c_{i_1+2,i_2} \\ c_4 &= c_{i_1+3,i_2} \\ c_5 &= c_6 = c_7 = 0 \end{aligned}$$

i_1 and i_2 are found from Eq. (3.4.36) by replacing i by $(i-n-m+2)$. (3.4.42)

$$M_{NN} = \begin{bmatrix} M_1 & M_2 & M_3 \\ M_2^T & M_4 & 0 \\ M_3^T & 0 & M_5 \end{bmatrix} \tag{3.4.43}$$

where the elements are given below:

For $i = 1, 2, \ldots, n$ and $j = 1, 2, \ldots, n,$

$$\begin{aligned} M_1(i,j) = \rho ALc_{i_1+j_1,i_2+j_2} + \rho I/L\,(&i_1 j_1 c_{i_1+j_1-2,i_2+j_2} \\ &-(i_2 j_1 + j_2 i_1)c_{i_1+j_1-1,i_1,j_1-1} + i_2 j_2 c_{i_1+j_1,i_2+j_2-2}) \end{aligned} \tag{3.4.44}$$

i_1 and i_2 are found from Eq. (3.4.36) by replacing i by $(i+2)$,

j_1 and j_2 are found from Eq. (3.4.36) by replacing i by $(j+2)$.

For $i = 1, 2, \ldots, n$ and $j = 1, 2, \ldots, m-2$,

$$M_2(i,j) = \rho I(i_1 c_{i_1+j_1-1, i_2+j_2} - i_2 c_{i_1+j_1, i_2+j_2-1})$$

i_1 and i_2 are found from Eq. (3.4.36) by replacing i by $(i+2)$, (3.4.45)

j_1 and j_2 are found from Eq. (3.4.36) by replacing i by j.

For $i = 1, 2, \ldots, n$ and $j = 1, 2$,

$$M_3(i,j) = \rho AL c_{i_1+j_1, i_2+j_2}$$

i_1 and i_2 are found from Eq. (3.4.36) by replacing i by $(i+2)$, (3.4.46)

j_1 and j_2 are found from Eq. (3.4.36) by replacing i by j.

For $i = 1, 2, \ldots, m-2$ and $j = 1, 2, \ldots, m-2$,

$$M_4(i,j) = \rho AL c_{i_1+j_1, i_2+j_2}$$

i_1 and i_2 are found from Eq. (3.4.36), (3.4.47)

j_1 and j_2 are found from Eq. (3.4.36) by replacing i by j.

For $i = 1, 2$ and $j = 1, 2$,

$$M_5(i,j) = \rho AL c_{i_1+j_1, i_2+j_2}$$

i_1 and i_2 are found from Eq. (3.4.36), (3.4.48)

j_1 and j_2 are found from Eq. (3.4.36) by replacing i by j.

$$K_{NN} = \begin{bmatrix} K_1 & K_2 & 0 \\ K_2^T & K_3 & K_4 \\ 0 & K_4^T & K_5 \end{bmatrix} \tag{3.4.49}$$

where the elements are given below:

For $i = 1, 2, \ldots, n$ and $j = 1, 2, \ldots, n$,

$$
\begin{aligned}
K_1(i,j) = \frac{EI}{L^3} [& i_1 j_1 (i_1 - 1)(j_1 - 1) c_{i_1+j_1-4, i_2+j_2} \\
& + i_2 j_2 (i_2 - 1)(j_2 - 1) c_{i_1+j_1, i_2+j_2-4} \\
& - 2(j_1 j_2 i_1 (i_1 - 1) + i_1 i_2 j_1 (j_1 - 1)) c_{i_1+j_1-3, i_2+j_2-1} \\
& - 2(i_1 i_2 j_2 (j_2 - 1) + j_1 j_2 i_2 (i_2 - 1)) c_{i_1+j_1-1, i_2+j_2-3} \\
& + (i_1 j_2 (i_1 - 1)(j_2 - 1) + 4 i_1 i_2 j_1 j_2 \\
& + i_2 j_1 (i_2 - 1)(j_1 - 1)) c_{i_1+j_1-2, i_2+j_2-2}]
\end{aligned}
\tag{3.4.50}
$$

i_1 and i_2 are found from Eq. (3.4.36) by replacing i by $(i + 2)$,

j_1 and j_2 are found from Eq. (3.4.36) by replacing i by $(j + 2)$.

For $i = 1, 2, \ldots, n$ and $j = 1, 2, \ldots, m - 2$,

$$
\begin{aligned}
K_2(i,j) = \frac{EI}{L^2} [& j_1 i_1 (i_1 - 1) c_{i_1+j_1-3, i_2+j_2} - j_2 i_2 (i_2 - 1) c_{i_1+j_1, i_2+j_2-3} \\
& - (2 i_1 i_2 j_1 + j_2 i_1 (i_1 - 1)) c_{i_1+j_1-2, i_2+j_2-1} \\
& + (2 i_1 i_2 j_2 + j_1 i_2 (i_2 - 1)) c_{i_1+j_1-1, i_2+j_2-2} \\
& - j_2 i_2 (i_2 - 1) c_{i_1+j_1, i_2+j_2-3}]
\end{aligned}
$$

i_1 and i_2 are found from Eq. (3.4.36) by replacing i by $(i + 2)$,

j_1 and j_2 are found from Eq. (3.4.36) by replacing i by j. (3.4.51)

For $i = 1, 2, \ldots, m - 2$ and $j = 1, 2, \ldots, m - 2$,

$$
\begin{aligned}
K_3(i,j) = kAGL c_{i_1+j_1, i_2+j_2} + \frac{EI}{L} [& i_1 j_1 c_{i_1+j_1-2, i_2+j_2} \\
& - (i_2 j_1 + j_2 i_1) c_{i_1+j_1-1, i_2+j_2-1} + i_2 j_2 c_{i_1+j_1, i_2+j_2-2}]
\end{aligned}
\tag{3.4.52}
$$

i_1 and i_2 are found from Eq. (3.4.36),

j_1 and j_2 are found from Eq. (3.4.36) by replacing i by j.

For $i = 1, 2, \ldots, m-2$ and $j = 1, 2$,

$$K_4(i,j) = kAG\left[j_2 c_{i_1+j_1, i_2+j_2-1} - j_1 c_{i_1+j_1-1, i_2+j_2}\right]$$

i_1 and i_2 are found from Eq. (3.4.36). (3.4.53)

j_1 and j_2 are found from Eq. (3.4.36) by replacing i by j.

For $i = 1, 2$ and $j = 1, 2$,

$$K_5(i,j) = \frac{kAG}{L}\left[i_1 j_1 c_{i_1+j_1-2, i_2+j_2} + i_2 j_2 c_{i_1+j_1, i_2+j_2-2} - (i_2 j_1 + j_2 i_1) c_{i_1+j_1-1, i_2+j_2-1}\right] \tag{3.4.54}$$

i_1 and i_2 are found from Eq. (3.4.36),

j_1 and j_2 are found from Eq. (3.4.36) by replacing i by j.

In addition, K_{II} and M_{II} are still as mentioned in Section 3.4.1. Note that this time the matrices M_{NN} and K_{NN} are not diagonal, in contrast with the normal modes case. Therefore, before modes can be truncated, the eigenvalue problem corresponding to M_{NN} and K_{NN} must be solved for a limited number of frequencies and modeshapes. This of course represents a disadvantage compared to the normal modes case. It should also be recognized that not all $\bar{q}$ coordinates will be carried over into the overall structural model. Following the Craig/Bampton practice of modal truncation, it is clear that only a limited number of modeshapes corresponding to the M_{NN}, K_{NN} eigenvalue problem need to be retained.

In References [34–35] Lees and Thomas propose another hierarchical Timoshenko beam element based on polynomial expansions. The two independent power series, one for v displacement and the other for the shear angle ψ, are

$$v = \sum_1^n a_i \left(\frac{x}{L}\right)^{i-1}, \quad n \geq 4$$
$$\psi = \sum_1^m \frac{b_i}{L} \left(\frac{x}{L}\right)^{i-1}, \quad m \geq 0 \tag{3.4.55}$$

This element can be seen as an example of the approach proposed in this dissertation by transforming the coefficient vector $q_c = \lfloor a_1\ a_2\ \cdots a_n\ b_1\ b_2 \cdots\ b_m \rfloor^T$ into the generalized coordinate vector q,

$$q = \lfloor q_I\ \overline{q} \rfloor^T = [v(0)\ \theta(0)\ v(L)\ \theta(L)\ a_5\ a_6 \cdots\ a_n\ b_1\ b_2 \cdots b_m]^T \tag{3.4.56}$$

The corresponding interface restrained assumed modes are then found to be,

$$\begin{aligned}
\overline{V}_i &= i\xi^2 - (i+1)\xi^3 + \xi^{i+3}, \quad i = 1, 2, \cdots, n-4 \\
&= -\xi + 3\xi^2 - 2\xi^3, i \quad = n-3 \\
&= \xi^2 - \xi^3, \quad i = n-2, n-1, \cdots, n+m-4 \\
\overline{\Theta}_i &= \frac{1}{L}\left[2i\xi - 3(i+1)\xi^2 + (i+3)\xi^{i+2}\right], \quad i = 1, 2, \cdots, n-4 \\
&= \frac{6}{L}\left[\xi - \xi^2\right], \quad i = n-3 \\
&= \frac{1}{L}\left[2\xi - 3\xi^2 + \xi^{i-n+3}\right], \quad i = n-2, n-1, \cdots, n+m-4
\end{aligned} \tag{3.4.57}$$

in which $\xi = \dfrac{x}{L}$.

It should be noted that the Lees/Thomas element does show ill–conditioning when $i > 10$. This, however, is generally not a severe handicap since i is usually less than ten unless the beam is a significant part of the structure. The element developed from Eq. (3.4.35) starts showing ill–conditioning only when $i > 30$. Also, the Guyan reduction needed in Reference [35] is in fact superfluous if the assumed modes method is used with static constraint modes as in Eq. (3.4.5).

This concludes the description of the Timoshenko beam element with polynomial functions as interface restrained assumed modes.

3.4.4 Trigonometric Functions As Interface Restrained Assumed Modes

In this section trigonometric functions are used as interface restrained assumed modes. The resulting mass and stiffness matrices are much more banded compared to the polynomial case in Section 3.4.3, and are very well–conditioned. In addition, the convergence rate compares quite well to that exhibited by the normal modes case. Therefore as a third choice, the interface restrained assumed modes are taken as

$$\overline{\phi} = \begin{bmatrix} \overline{V} \\ \overline{\Theta} \end{bmatrix} = \left[\begin{array}{c|c|c|c} \overline{V}_i & 0 & \overline{V}_{m-1} & \overline{V}_m \\ \overline{V}_i{}' & \overline{\Theta}_j & 0 & 0 \end{array} \right] \tag{3.4.58}$$

where

$$\begin{aligned} \overline{V}_i &= \cos\,(i-1)\pi\xi - \cos\,(i+1)\pi\xi, \quad i = 1,2,\ldots,n \\ \overline{\Theta}_j &= \sin\; j\pi\xi, \quad j = 1,2,\ldots,m-2 \\ \overline{V}_{m-1} &= \xi(1-\xi), \;\; \overline{V}_m = \xi^2(1-\xi)^2, \;\; \xi = \frac{x}{L} \end{aligned} \tag{3.4.59}$$

and where the philosophy underlying this choice is similar to that of Section 3.4.3. Again, using Eqs. (2.2.6) and (2.2.13) yields explicit expressions for the mass and stiffness matrix partitions which involve a large percentage of one time computations. Firstly,

$$\begin{gathered} M_{IN} = [m_{ji}] \\ i = 1,2,\cdots,n+m, \;\; j = 1,2,3,4 \end{gathered} \tag{3.4.60}$$

$$\begin{aligned} m_{1i} &= \rho AL\,[c_1 - c_2 + s_2(c_2 - 3c_3 + 2c_4)]_i - 6\rho I s_2\,[c_6 - c_7]_i \\ m_{2i} &= \frac{\rho AL^2}{2}\,[c_2 - c_3 + s_2(c_2 - 3c_3 + 2c_4)]_i + \rho IL\,[c_5 - c_6 - 3s_2(c_6 - c_7)]_i \\ m_{3i} &= \rho AL\,[c_2 - s_2(c_2 - 3c_3 + 2c_4)]_i + 6\rho I s_2\,[c_6 - c_7]_i \\ m_{4i} &= \frac{\rho AL^2}{2}\,[-c_2 + c_3 + s_2(c_2 - 3c_3 + 2c_4)]_i + \rho IL\,[c_6 - 3s_2(c_6 - c_7)]_i \end{aligned} \tag{3.4.61}$$

For $i = 1$,

$$\begin{aligned} &c_1 = 1, \;\; c_2 = 1/2, \;\; c_3 = 1/3 - 1/2\pi^2 \\ &c_4 = 1/4 - 3/4\pi^2, \;\; c_5 = 0, \;\; c_6 = -1/L, \;\; c_7 = -1/L \end{aligned} \tag{3.4.62}$$

For $i = 2, 3, \ldots, n$

$$
\begin{aligned}
& c_1 = 0, \quad c_2 = \frac{1}{\pi^2}\left[1/(i-1)^2 - 1/(i+1)^2\right]\left[(-1)^{i-1} - 1\right] \\
& c_3 = \frac{2}{\pi^2}\left[1/(i-1)^2 - 1/(i+1)^2\right](-1)^{i-1} \\
& c_4 = \frac{3}{\pi^2}\left[1/(i-1)^2 - 1/(i+1)^2\right](-1)^{i-1} \\
& \quad + \frac{6}{\pi^4}\left[1/(i-1)^4 - 1/(i+1)^4\right]\left[1 - (-1)^{i-1}\right] \\
& c_5 = 0, \quad c_6 = 0 \\
& c_7 = \frac{2}{\pi^2 L}\left[1/(i-1)^2 - 1/(i+1)^2\right]\left[1 - (-1)^{i-1}\right]
\end{aligned}
\tag{3.4.63}
$$

For $i = n+1,\ n+2, \ldots,\ n+m-2$

$$
\begin{aligned}
& c_1 = c_2 = c_3 = c_4 = 0, \quad c_5 = \left[1 - (-1)^{i-n}\right]/(i-n)\pi \\
& c_6 = \frac{(-1)^{i-n+1}}{(i-n)\pi}, \quad c_7 = \frac{\left[\left\{2 - (i-n)^2\pi^2\right\}(-1)^{i-n} - 2\right]}{(i-n)^3\pi^3}
\end{aligned}
\tag{3.4.64}
$$

For $i = n+m-1$,

$$
\begin{aligned}
& c_1 = 1/6, \quad c_2 = 1/12, \quad c_3 = 1/20 \\
& c_4 = 1/30, \quad c_5 = c_6 = c_7 = 0
\end{aligned}
\tag{3.4.65}
$$

For $i = n+m$,

$$
\begin{aligned}
& c_1 = 1/30, \quad c_2 = 1/60, \quad c_3 = 1/105 \\
& c_4 = 1/168, \quad c_5 = c_6 = c_7 = 0
\end{aligned}
\tag{3.4.66}
$$

Secondly,

$$
M_{NN} = \begin{bmatrix} M_1 & M_2 & M_3 \\ {M_2}^T & M_4 & 0 \\ {M_3}^T & 0 & M_5 \end{bmatrix}
\tag{3.4.67}
$$

where

$$
M_{1_{(n \times n)}} = \frac{\rho A L}{2}\begin{bmatrix}
3 & 0 & -1 & 0 & 0 & 0 & 0 & \cdots\cdots \\
0 & 2 & 0 & -1 & 0 & 0 & 0 & \cdots\cdots \\
-1 & 0 & 2 & 0 & -1 & 0 & 0 & \cdots\cdots \\
0 & -1 & 0 & 2 & 0 & -1 & 0 & \cdots\cdots \\
 & & & \vdots & & & & \\
 & & & \vdots & & & &
\end{bmatrix}
\tag{3.4.68}
$$

$$+\frac{\pi^2\rho I}{2L}\begin{bmatrix} 2^2 & 0 & -2^2 & 0 & 0 & 0 & 0 & \cdots\cdots \\ 0 & 1^2+3^2 & 0 & -3^2 & 0 & 0 & 0 & \cdots\cdots \\ -2^2 & 0 & 2^2+4^2 & 0 & -4^2 & 0 & 0 & \cdots\cdots \\ 0 & -3^2 & 0 & 3^2+5^2 & 0 & -5^2 & 0 & \cdots\cdots \\ & & & \vdots & & & & \\ & & & \vdots & & & & \end{bmatrix}$$

$$M_{2_{(n\times m-2)}} = \frac{\pi\rho I}{2}\begin{bmatrix} 0 & 2 & 0 & 0 & 0 & \cdots\cdots \\ -1 & 0 & 3 & 0 & 0 & \cdots\cdots \\ 0 & -2 & 0 & 4 & 0 & \cdots\cdots \\ & & \vdots & & & \\ & & \vdots & & & \end{bmatrix} \tag{3.4.69}$$

$$M^T_{3_{(2\times n)}} = \frac{\rho AL}{2\pi^2}[\, C_1 \; C_2 \,] \tag{3.4.70}$$

$$C_1 = \begin{bmatrix} \frac{\pi^2}{3}+1 & 0 & \frac{1}{2^2}-\frac{1}{1^2} \\ \frac{3}{\pi^2}\left(\frac{\pi^4}{45}+1\right) & 0 & \frac{3}{\pi^2}\left(\frac{1}{2^4}-\frac{1}{1^4}\right) \end{bmatrix} \tag{3.4.71}$$

$$C_2 = \begin{bmatrix} 0 & \frac{1}{3^2}-\frac{1}{2^2} & 0 & \frac{1}{4^2}-\frac{1}{3^2} & 0 & \cdots \\ 0 & \frac{3}{\pi^2}\left(\frac{1}{3^4}-\frac{1}{2^4}\right) & 0 & \frac{3}{\pi^2}\left(\frac{1}{4^4}-\frac{1}{3^4}\right) & 0 & \cdots \end{bmatrix} \tag{3.4.72}$$

$$M_{4_{(m-2\times m-2)}} = \frac{\rho IL}{2}\begin{bmatrix} 1 & 0 & 0 & 0 & \cdots\cdots \\ 0 & 1 & 0 & 0 & \cdots\cdots \\ 0 & 0 & 1 & 0 & \cdots\cdots \\ & & \vdots & & \\ & & \vdots & & \end{bmatrix} \tag{3.4.73}$$

$$M_{5_{(2\times 2)}} = \rho AL\begin{bmatrix} \frac{1}{30} & \frac{1}{140} \\ \frac{1}{140} & \frac{1}{630} \end{bmatrix} \tag{3.4.74}$$

and finally,

$$K_{NN} = \begin{bmatrix} K_1 & K_2 & 0 \\ {K_2}^T & K_3 & K_4 \\ 0 & {K_4}^T & K_5 \end{bmatrix} \tag{3.4.75}$$

where

$$K_{1_{(n\times n)}} = \frac{\pi^4 EI}{2L^3}\begin{bmatrix} 2^4 & 0 & -2^4 & 0 & 0 & 0 & 0 & \cdots\cdots \\ 0 & 1^4+3^4 & 0 & -3^4 & 0 & 0 & 0 & \cdots\cdots \\ -2^4 & 0 & 2^4+4^4 & 0 & -4^4 & 0 & 0 & \cdots\cdots \\ 0 & -3^4 & 0 & 3^4+5^4 & 0 & -5^4 & 0 & \cdots\cdots \\ & & & \vdots & & & & \\ & & & & & & & \end{bmatrix} \tag{3.4.76}$$

$$K_{2_{(n\times m-2)}} = \frac{\pi^3 EI}{2L^2}\begin{bmatrix} 0 & 2^3 & 0 & 0 & 0 & \cdots\cdots \\ -1^3 & 0 & 3^3 & 0 & 0 & \cdots\cdots \\ 0 & -2^3 & 0 & 4^3 & 0 & \cdots\cdots \\ & & \vdots & & & \\ & & & & & \end{bmatrix} \tag{3.4.77}$$

$$K_{3_{(m-2\times m-2)}} = \frac{\pi^2 EI}{2L}\begin{bmatrix} 1^2 & 0 & 0 & 0 & \cdots\cdots \\ 0 & 2^2 & 0 & 0 & \cdots\cdots \\ 0 & 0 & 3^2 & 0 & \cdots\cdots \\ & & \vdots & & \\ & & & & \end{bmatrix} + \frac{kAGL}{2}\begin{bmatrix} 1 & 0 & 0 & 0 & \cdots\cdots \\ 0 & 1 & 0 & 0 & \cdots\cdots \\ 0 & 0 & 1 & 0 & \cdots\cdots \\ & & \vdots & & \\ & & & & \end{bmatrix} \tag{3.4.78}$$

$$K^T_{4_{(2\times m-2)}} = -\frac{kAG}{\pi}\begin{bmatrix} 0 & 1 & 0 & \frac{1}{2} & 0 & \frac{1}{3} & \cdots\cdots \\ 0 & \frac{3}{\pi^2} & 0 & \frac{3}{2^3\pi^2} & 0 & \frac{3}{3^3\pi^2} & \cdots\cdots \end{bmatrix} \tag{3.4.79}$$

$$K_{5_{(2\times 2)}} = \frac{kAG}{L}\begin{bmatrix} \frac{1}{3} & \frac{1}{15} \\ \frac{1}{15} & \frac{2}{105} \end{bmatrix} \tag{3.4.80}$$

In addition, the matrices M_{II} and K_{II} are again given by Eqs. (3.4.19) and (3.4.21). Note that no trigonometric functions must actually be evaluated in order to determine the elements of the matrices, K_{NN} and M_{NN} and these matrices are well–conditioned and have large portions of simple, one time computations. In fact, the computational effort is much less than the work involved in the polynomial case of section 3.4.3.

This concludes the description of the dynamic finite element for the Timoshenko beam with trigonometric series as interface restrained assumed modes.

CHAPTER 4

METHOD OF SOLUTION

4.1 Element Assembly Process

The element assembly process and its computer implementation is similar to that of the standard finite element method. In particular, it will be shown that the assembled structural unit can be considered as a single larger element.

Following Reference [24], consider the elements E_k and E_ℓ in Figure 8. Element E_k has one interface and element E_ℓ has two distinct interfaces. In order to enforce displacement compatibility, it is necessary to transform the local interface vector $\boldsymbol{q}_I^k$ of element E_k into a global vector $\boldsymbol{Q}_I^k$ using a matrix L_k which contains constant direction cosines of the local system axes with respect to the global reference frame.

$$\boldsymbol{q}_I^k = L_k\, \boldsymbol{Q}_I^k \tag{4.1.1}$$

Similarly for element E_ℓ,

$$\begin{aligned} \boldsymbol{q}_I^\ell &= \begin{Bmatrix} \boldsymbol{q}_{I1}^\ell \\ \boldsymbol{q}_{I2}^\ell \end{Bmatrix} \\ &= \begin{bmatrix} L_{1\ell} & 0 \\ 0 & L_{2\ell} \end{bmatrix} \begin{Bmatrix} \boldsymbol{Q}_{I1}^\ell \\ \boldsymbol{Q}_{I2}^\ell \end{Bmatrix} = L_\ell\, \boldsymbol{Q}_I^\ell \end{aligned} \tag{4.1.2}$$

There exists no need to transform the vectors $\overline{\boldsymbol{q}}_k$ and $\overline{\boldsymbol{q}}_\ell$ because elements only connect through their interfaces.

The first step in the assembly process is to require that,

$$\boldsymbol{Q}_I^k = \boldsymbol{Q}_{I1}^\ell \tag{4.1.3}$$

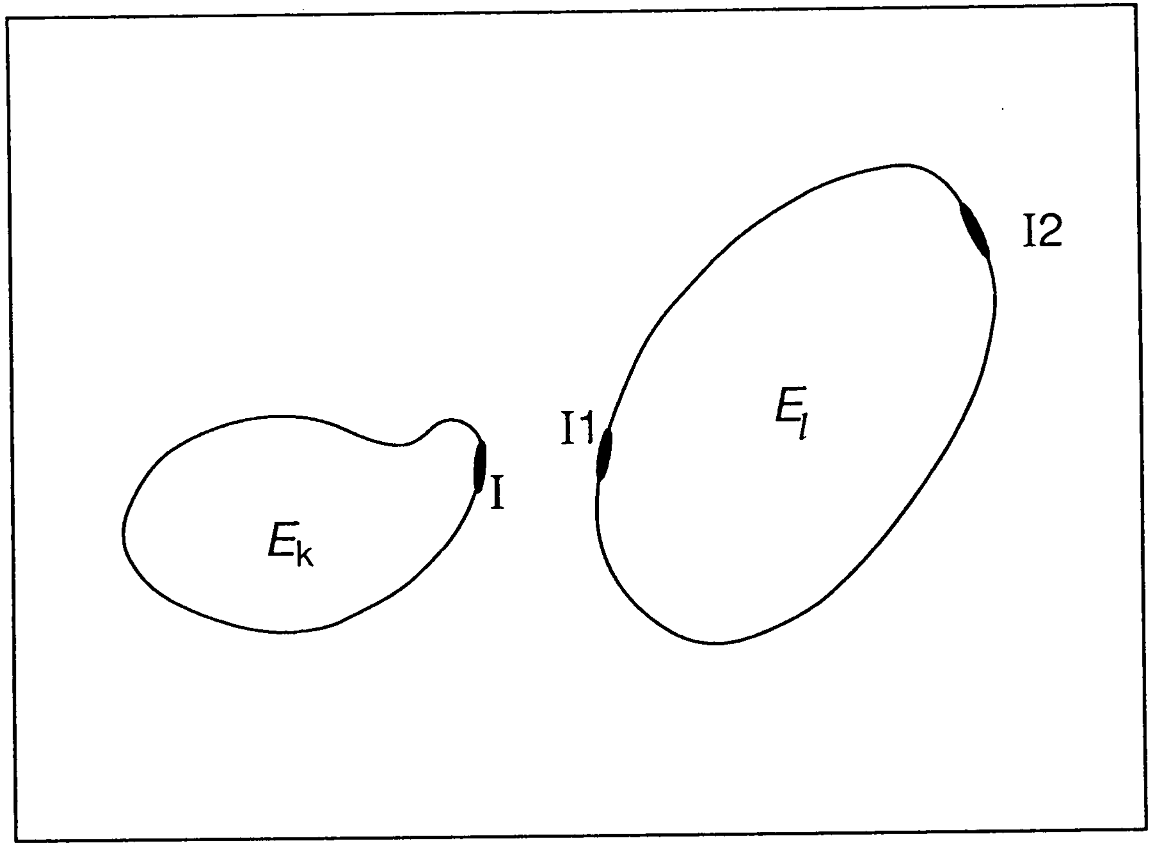

Figure 8. Assembly of Two Elements

i.e., displacement compatibility. The displacement vector for the assembled $k\ell$–element becomes,

$$\boldsymbol{q} = \left\{ \begin{array}{c} \boldsymbol{Q}_{I2}^{\ell} \\ \boldsymbol{Q}_{I}^{k} \\ \overline{\boldsymbol{q}}_{k} \\ \overline{\boldsymbol{q}}_{\ell} \end{array} \right\} \tag{4.1.4}$$

The corresponding stiffness and mass matrices are,

$$K = \begin{bmatrix} k_{22}^{\ell} & k_{12}^{\ell^T} & 0 & 0 \\ k_{12}^{\ell} & k_{11}^{k} + k_{11}^{\ell} & 0 & 0 \\ 0 & 0 & \omega_k^2 & 0 \\ 0 & 0 & 0 & \omega_\ell^2 \end{bmatrix}$$

$$M = \begin{bmatrix} m_{22}^{\ell} & m_{12}^{\ell^T} & 0 & m_{23}^{\ell} \\ m_{12}^{\ell} & m_{11}^{k} + m_{11}^{\ell} & m_{12}^{k} & m_{13}^{\ell} \\ 0 & m_{12}^{k^T} & I & 0 \\ m_{23}^{\ell^T} & m_{13}^{\ell^T} & 0 & I \end{bmatrix} \tag{4.1.5}$$

where

$$\begin{aligned} m_{11}^{k} &= L_k^T\, M_{II}^{k}\, L_k \\ m_{12}^{k} &= L_k^T\, M_{IN}^{k} \\ k_{11}^{k} &= L_k^T\, K_{II}^{k}\, L_k \end{aligned} \tag{4.1.6}$$

and

$$\begin{aligned} \begin{bmatrix} m_{11}^{\ell} & m_{12}^{\ell} \\ m_{12}^{\ell^T} & m_{22}^{\ell} \end{bmatrix} &= L_\ell^T\, M_{II}^{\ell}\, L_\ell \\ \begin{bmatrix} m_{13}^{\ell} \\ m_{23}^{\ell} \end{bmatrix} &= L_\ell^T\, M_{IN}^{\ell} \\ \begin{bmatrix} k_{11}^{\ell} & k_{12}^{\ell} \\ k_{12}^{\ell^T} & k_{22}^{\ell} \end{bmatrix} &= L_\ell^T\, K_{II}^{\ell}\, L_\ell \end{aligned} \tag{4.1.7}$$

The second step in the assembly process is to write the interface vector $\boldsymbol{Q}_I^k$ in terms of a linear combination of static constraint modes ϕ_I and interface restrained normal modes $\overline{\phi}$ similar to Eq. (2.1.7).

$$\boldsymbol{Q}_I^k = [\, \phi_I\ \overline{\phi}\,] \left\{ \begin{array}{c} \boldsymbol{Q}_{I2}^{\ell} \\ \overline{\boldsymbol{q}}_I \end{array} \right\} \tag{4.1.8}$$

where

$$\phi_I = -\left(k_{11}^k + k_{11}^\ell\right)^{-1} k_{12}^\ell \tag{4.1.9}$$

and $\overline{\phi}$ are obtained by solving the interface eigenvalue problem,

$$\omega_I^2 \left[m_{11}^k + m_{11}^\ell\right] \overline{\phi} = \left[k_{11}^k + k_{11}^\ell\right] \overline{\phi} \tag{4.1.10}$$

The modes in $\overline{\phi}$ can be truncated according to the preset system cut–off frequency, if necessary. Using the transformation,

$$\begin{Bmatrix} Q_{I2}^\ell \\ Q_I^k \\ \bar{q}_k \\ \bar{q}_\ell \end{Bmatrix} = \begin{bmatrix} I & 0 & 0 & 0 \\ \phi_I & \overline{\phi} & 0 & 0 \\ 0 & 0 & I & 0 \\ 0 & 0 & 0 & I \end{bmatrix} \begin{Bmatrix} Q_{I2}^\ell \\ \bar{q}_I \\ \bar{q}_k \\ \bar{q}_\ell \end{Bmatrix} \tag{4.1.11}$$

the stiffness and mass matrices in Eq. (4.1.5) become,

$$K_1 = \begin{bmatrix} k_{11} & 0 & 0 & 0 \\ 0 & \omega_I^2 & 0 & 0 \\ 0 & 0 & \omega_k^2 & 0 \\ 0 & 0 & 0 & \omega_\ell^2 \end{bmatrix}$$

$$M_1 = \begin{bmatrix} m_{11} & m_{12} & m_{13} & m_{14} \\ m_{12}^T & I & m_{23} & m_{24} \\ m_{13}^T & m_{23}^T & I & 0 \\ m_{14}^T & m_{24}^T & 0 & I \end{bmatrix} \tag{4.1.12}$$

with

$$\begin{aligned}
m_{11} &= m_{22}^\ell + m_{12}^{\ell^T} \phi_I + \phi_I^T m_{12}^\ell + \phi_I^T \left(m_{11}^k + m_{11}^\ell\right) \phi_I \\
m_{12} &= \left[m_{12}^{\ell^T} + \phi_I^T \left(m_{11}^k + m_{11}^\ell\right)\right] \overline{\phi} \\
m_{13} &= \phi_I^T m_{12}^k \\
m_{14} &= m_{23}^\ell + \phi_I^T m_{13}^\ell \\
m_{23} &= \overline{\phi}^T m_{12}^k \\
m_{24} &= \overline{\phi}^T m_{13}^\ell \\
k_{11} &= k_{22}^\ell + k_{12}^{\ell^T} \phi_I
\end{aligned} \tag{4.1.13}$$

The decomposition of vector Q_I^k in Eq. (4.1.8) allows for stiffness decoupling between Q_{I2}^k and Q_I^k in Eq. (4.1.12). The transformation in Eq. (4.1.11) will allow for frequency and modeshape truncation on the $k\ell$–element level without compromising the accuracy of the quasi–static deformation pattern of the $k\ell$–element.

The last step in the assembly process is to solve for the interface restrained modes of the $k\ell$–element,

$$\omega_{k\ell}^2 \begin{bmatrix} I & m_{23} & m_{24} \\ m_{23}^T & I & 0 \\ m_{24}^T & 0 & I \end{bmatrix} \overline{\phi}_{k\ell} = \begin{bmatrix} \omega_I^2 & 0 & 0 \\ 0 & \omega_k^2 & 0 \\ 0 & 0 & \omega_\ell^2 \end{bmatrix} \overline{\phi}_{k\ell} \tag{4.1.14}$$

Again the modes in $\overline{\phi}_{k\ell}$ can be truncated according to the system cut–off frequency. Using the modal transformation,

$$\begin{Bmatrix} Q_{I2}^\ell \\ \overline{q}_I \\ \overline{q}_k \\ \overline{q}_\ell \end{Bmatrix} = \begin{bmatrix} I & 0 \\ 0 & \overline{\phi}_{k\ell} \end{bmatrix} \begin{Bmatrix} Q_{I2}^\ell \\ \overline{q}_{k\ell} \end{Bmatrix} \tag{4.1.15}$$

the transformed mass and stiffness matrices in Eq. (4.1.12) become,

$$M_2 = \begin{bmatrix} M_{II} & M_{IN} \\ M_{IN}^T & I \end{bmatrix}, \quad K_2 = \begin{bmatrix} K_{II} & 0 \\ 0 & \omega_{k\ell}^2 \end{bmatrix} \tag{4.1.16}$$

where

$$\begin{aligned} M_{II} &= m_{11} \\ M_{IN} &= [m_{12}\ m_{13}\ m_{14}]\overline{\phi}_{k\ell} \\ K_{II} &= k_{11} \end{aligned} \tag{4.1.17}$$

Comparing the mass and stiffness matrices in Eqs. (4.1.17) and the mass and stiffness matrices for a generic element in Eqs. (2.2.5) and (2.2.12) shows that the assembled $k\ell$–element can now be considered as a new single element.

The same assembly procedure can be used when adding the next element E_m to the $E_{k\ell}$ element. The resulting element $E_{k\ell m}$ again has the near minimum number of degrees of freedom necessary to obtain the desired accuracy in the system frequencies and modeshapes of interest. Also, any element chosen by the user can be taken off–line, in order to construct a minimum order model using the same procedure. For example, a model for the bay element in Figure 9 may be constructed by assembling sequentially the axial bars and applying modal truncation at every step. The result is a near minimum order model for the entire bay element. Furthermore, if this bay element is used to build up an entire structure, then the same bay model can be used over again. In fact, multiple bay elements can be constructed from single bay elements, again using the same assembly process. The present technique then is quite suitable to take advantage of spatial periodicity wherever it occurs in the system.

Reanalysis of structures is often required in order to improve the accuracy of previously obtained solutions. Because the proposed approach is hierarchical in nature, more refined models can be easily derived from the existing lower order models. Indeed, no need exists to redefine the old grid as in the case of the h–version of the finite element method. Extra interface restrained assumed modes can be added according to a newly defined cut–off frequency, without disturbing the old grid. In addition, when subspace iteration is used, old intermediate eigenvalue problem solutions can be used profitably as starting vector sets for the new iteration process.

The proposed assembly process allows for the replacement of a large system eigenvalue problem by a series of relatively small eigenvalue problems and is well suited for use with micro computers. Clearly, because the cost of an eigenvalue problem increases roughly with the cube of its dimension, a significant cost reduction can be achieved. It is important to note that even when the elements are small enough so that no interface restrained assumed modes are necessary,

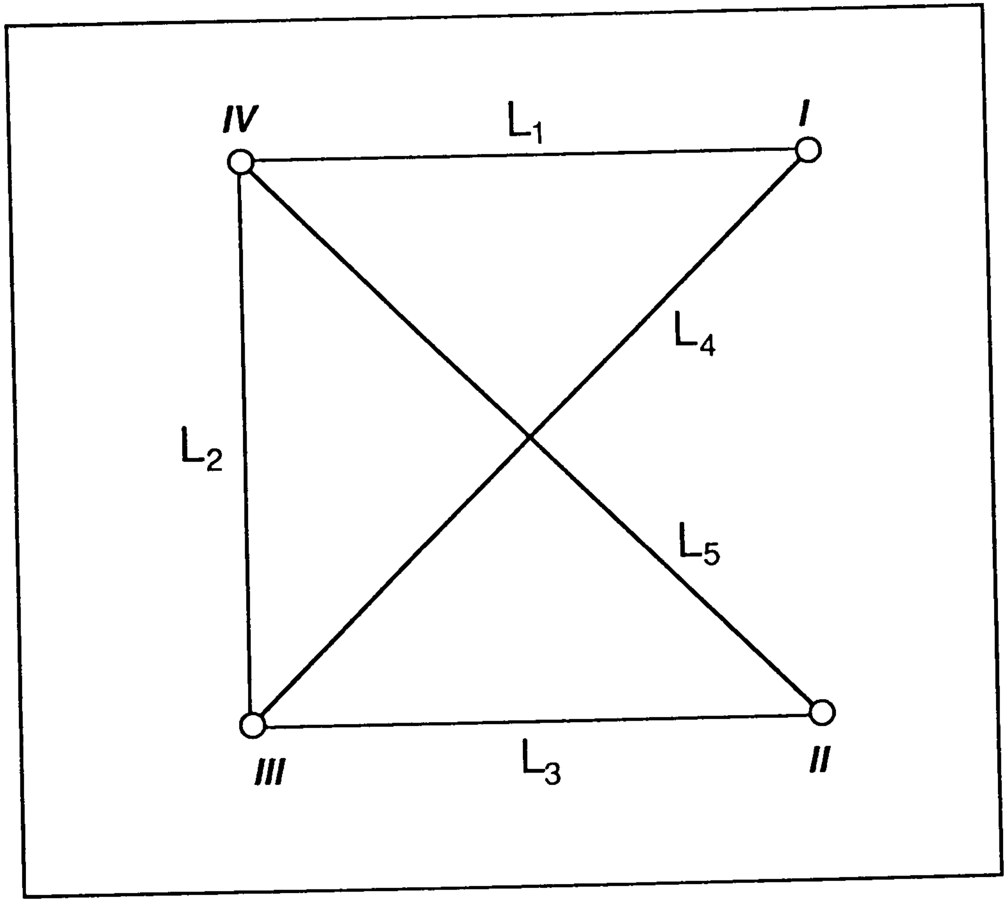

Figure 9. Single Bay of Planar Truss

the sequential nature of the system eigenvalue problem solution still allows for substantial cost reduction. In the following section, a cost–effective algorithm for the eigenvalue problem in Eq. (4.1.14) will be developed.

4.2 System Eigenvalue Problem

The ultimate objective of the analysis process is the determination of a set of low frequency system modes. As was indicated in the previous section, the proposed assembly process allows for the replacement of a large system eigenvalue problem by a series of relatively small and inexpensive eigenvalue problems of the type shown in Eq. (4.1.14).

Of the multitude of existing algorithms, it was judged that the subspace iteration technique would be the most suitable in the present context. Subspace iteration uses Ritz analysis to perform simultaneous inverse iteration on the starting vectors in order to extract the lowest eigenvalue and corresponding eigenvector approximations. These approximations can be further improved iteratively. The basic objective in the subspace iteration method is to solve the following generalized eigenvalue problem of order n,

$$\lambda M \phi = K \phi \tag{4.2.1}$$

for the lowest p ($\leq n$) eigenvalues and eigenvectors. Collecting the p eigenvectors as the columns of Φ and the corresponding eigenvalues as the diagonal entries of matrix Λ, a consequence of Eq. (4.2.1) is that,

$$\Phi^T K \Phi = \Lambda, \quad \Phi^T M \Phi = I \tag{4.2.2}$$

where the eigenvectors are mass normalized.

The underlying philosophy of the subspace iteration solution method is that the eigenvectors Φ form a mass orthonormal basis for the p-dimensional dominant subspace E_∞ of the matrices K and M. The iteration with p linearly independent vectors can therefore be regarded as an iteration with a subspace. The starting iteration vectors, $\overline{X}_1$ span subspace E_1 and iteration continues until E_∞ is spanned to a sufficient degree of accuracy. To this end, the following algorithm is used.

For $k = 1, 2, \cdots$, iterate from E_k to E_{k+1}:

$$KX_{k+1} = M\overline{X}_k \tag{4.2.3}$$

Find the projections of the matrix operators K and M onto E_{k+1}:

$$K_{k+1} = X_{k+1}^T K X_{k+1}, \quad M_{k+1} = X_{k+1}^T M X_{k+1} \tag{4.2.4}$$

Solve for the eigensystem of the projected operators:

$$K_{k+1} Z_{k+1} = M_{k+1} Z_{k+1} \overline{\Lambda}_{k+1} \tag{4.2.5}$$

Find an improved approximation to the eigenvectors:

$$\overline{X}_{k+1} = X_{k+1} Z_{k+1} \tag{4.2.6}$$

Provided that the vectors in $\overline{X}_1$ are not orthogonal to one of the eigenvectors, then $\overline{\Lambda}_{k+1} \longrightarrow \Lambda$ and $\overline{X}_{k+1} \longrightarrow \Phi$ as $k \rightarrow \infty$.

Bathe and Wilson [17] indicate that the number of starting vectors in $\overline{X}_1$ is chosen as $q = \min\,[2p,\ p+8]$ rather than p, in order to achieve faster convergence.

Next, let us rewrite a typical intermediate eigenvalue problem Eq. (4.1.14) in the following more convenient generic form,

$$\lambda \begin{bmatrix} I & m \\ m^T & I \end{bmatrix} \phi = \begin{bmatrix} \mu & 0 \\ 0 & \Omega \end{bmatrix} \phi \tag{4.2.7}$$

The efficiency of the subspace iteration method depends on i) the sparseness of M and K and ii) the starting vectors. From Eq. (4.2.7) it can be seen that the mass and stiffness matrices are indeed quite sparse. In particular, the stiffness matrix is diagonal, and therefore the solution of Eq. (4.2.3) becomes trivial. In addition, the form of the mass matrix is such that further simplifications of Eqs.(4.2.4–4.2.6) can be easily implemented. Such a simplified algorithm was presented in Reference [36].

Furthermore, it is possible to derive an excellent set of starting vectors at relatively little cost. To this end, the q lowest diagonal elements in the stiffness matrix in Eq. (4.2.7) are identified. For each of these values, the following simple eigenvalue problem,

$$\vartheta \begin{bmatrix} 1 & \boldsymbol{m}_i \\ \boldsymbol{m}_i^T & I \end{bmatrix} \begin{Bmatrix} \xi_0 \\ \boldsymbol{q} \end{Bmatrix} = \begin{bmatrix} \mu_i & 0 \\ 0 & \Omega \end{bmatrix} \begin{Bmatrix} \xi_0 \\ \boldsymbol{q} \end{Bmatrix} \tag{4.2.8}$$

is solved for the eigenvalue and corresponding eigenvector which is closest to μ_i, where μ_i is one of the chosen q diagonal elements. It is shown in Reference [37] that the resulting starting set $\overline{X}_1$ is in general, already a very good approximation of the desired q–dimensional dominant subspace of problem (4.2.7).

Next, in order to solve the eigenvalue problem in Eq. (4.2.8) for the eigenvalue ϑ_c closest to μ_i and for the corresponding eigenvector $\lfloor \xi_{0c}\ \boldsymbol{q}_c \rfloor^T$, consider the lower partition of Eq. (4.2.8) and solve for $\boldsymbol{q}$.

$$\boldsymbol{q} = \vartheta[\Omega - \vartheta I]^{-1} \boldsymbol{m}_i^T \xi_0 \tag{4.2.9}$$

The characteristic equation for this problem can then be obtained by substituting Eq. (4.2.9) into the top partition of Eq. (4.2.8).

$$\vartheta - \mu_i + \vartheta^2 \boldsymbol{m}_i [\Omega - \vartheta I]^{-1} \boldsymbol{m}_i^T = 0 \tag{4.2.10}$$

This equation is easily solved for the desired root via the Newton–Raphson iteration method,

$$\vartheta_{r+1} = \vartheta_r - f(\vartheta_r) \left[\frac{df(\vartheta_r)}{d\vartheta} \right]^{-1} \tag{4.2.11}$$

in which r is the iteration index and,

$$
\begin{aligned}
f(\vartheta_r) &= \vartheta_r - \mu_i + \vartheta_r^2 \sum_{j=1}^{n-q} \frac{m_{ij}^2}{\Omega_j - \vartheta_r} \\
\frac{df(\vartheta_r)}{d\vartheta} &= 1 + 2\vartheta_r \sum_{j=1}^{n-q} \frac{m_{ij}^2}{\Omega_j - \vartheta_r} + \vartheta_r^2 \sum_{j=1}^{n-q} \frac{m_{ij}^2}{(\Omega_j - \vartheta_r)^2}
\end{aligned}
\tag{4.2.12}
$$

For $r = 0$, ϑ_0 can be taken to be μ_i. Because the Newton–Raphson method has quadratic convergence and because only a good approximation of the desired root is needed, no more than two iterations are needed in Eq. (4.2.12). In addition because the difference $(\Omega_j - \vartheta_r)$ becomes large with increasing j, all sums in Eq. (4.2.12) can usually be truncated. In practice, the cost to compute the desired root in Eq. (4.2.11) is negligible. The value of ξ_0 is obtained by requiring the eigenvector corresponding to ϑ_c to be M–orthogonal. i.e.,

$$
\begin{Bmatrix} \xi_{0c} \\ \boldsymbol{q}_c \end{Bmatrix}^T \begin{bmatrix} 1 & \boldsymbol{m}_i \\ \boldsymbol{m}_i^T & I \end{bmatrix} \begin{Bmatrix} \xi_{0c} \\ \boldsymbol{q}_c \end{Bmatrix} = 1 \tag{4.2.13}
$$

Substituting Eq. (4.2.9) into Eq. (4.2.13), ξ_{0c} is determined as,

$$
\xi_{0c} = \left[\frac{df(\vartheta_c)}{d\vartheta} \right]^{-\frac{1}{2}} \tag{4.2.14}
$$

where ϑ_c is the converged desired root of Eq. (4.2.11). Note that $\dfrac{df}{d\vartheta}$ is always positive and the vector $\boldsymbol{q}_c$ can be computed using Eqs. (4.2.14) and (4.2.9). Finally, the i–th column of the starting subspace is taken as,

$$
\{\overline{X}_1\}_i = \begin{Bmatrix} \xi_{0c}\boldsymbol{e}_i \\ \boldsymbol{q}_c \end{Bmatrix}, \quad i = 1, 2, \ldots, q \tag{4.2.15}
$$

where $\boldsymbol{e}_i = \lfloor 0\ 0\ \ldots\ 0\ \overset{i}{1}\ 0\ \ldots\ 0 \rfloor^T$ and $\boldsymbol{q}_c$ is computed from Eq. (4.2.9).

CHAPTER 5

DEMONSTRATION EXAMPLES

5.1 Axial Bar

5.1.1 Free–Free Axial Bar

As a first example, consider the simple free–free axial bar. Let $E = 3 \times 10^6\ lb/in^2, \rho g = 0.2839\ lb/in^3, g = 386.4\ in/sec^2, A = 1\ in^2$ and $L = 72\ in.$ The natural frequencies, f_i in Hz of the bar are computed in three different ways:

(1) From the exact theory,

$$f_i = \frac{(i-1)}{2L}\sqrt{\frac{E}{\rho}},\ i = 1, 2, \ldots \tag{5.1.1}$$

(2) Using the standard finite element consistent mass matrix as implemented in MSC-NASTRAN Version 66, DEC (VAX/VMS) Edition.

(3) Using the axial bar model as developed in Section 3.1.1.

Table 5.1.1 lists the results from the standard finite element method (consistent mass matrix approach) using MSC-NASTRAN and Table 5.1.2 gives results corresponding to the dynamic finite element method developed in Section 3.1.1. The number n represents the order of the model and e is the percentage relative error compared to the exact frequencies. In addition, the entries in these tables give the number of natural frequencies with an accuracy of e % or better for a given model order n.

The results indicate that the dynamic finite element method yields consistently better convergence compared to the standard finite element method. Also, the dynamic finite element method does not require explicit subdivision of the bar.

In addition, the mass and stiffness matrices for lower order models form submatrices of the corresponding matrices of a higher order model, i.e., the procedure possesses the hierarchical property.

Table 5.1.1 Converged Frequencies For Free–Free Axial Bar By Standard Finite Element Method

e	n				
	6	16	26	36	51
< 1 %	1	3	4	6	8
< 5 %	2	6	9	13	18
< 10 %	3	8	13	18	26

Table 5.1.2 Converged Frequencies For Free–Free Axial Bar by Dynamic Finite Element Method

e	n				
	6	16	26	36	51
< 1 %	3	12	22	34	49
< 5 %	4	14	24	34	49
< 10 %	4	14	24	34	49

5.1.2 Fixed–Fixed Axial Bar

In order to check out the element assembly process accompanied by modal truncation, an axial bar with fixed–fixed boundary conditions is subdivided into eleven elements. The material and geometric properties are the same as in the example of Section 5.1.2. The theoretical frequencies are given by,

$$f_i = \frac{i}{2L}\sqrt{\frac{E}{\rho}}, \quad i = 1, 2, \ldots \tag{5.1.2}$$

Following Section 4.1, elements are assembled one by one and an eigenvalue problem solved. At each stage, a modal truncation is performed both at the system level and the element level. Table 5.1.3 shows the number of retained modes at each stage for different desired frequency contents. Note that in the present analysis, the frequency content on the element and system levels is taken to be the same. In general, this is not necessary. Tables 5.1.4 through 5.1.6 show the computed frequencies for desired frequency contents of 500 *Hz*, 1000 *Hz* and 2000 *Hz* respectively. The standard finite element model needs a model order of 161 in order to compute the first 25 frequencies to within one percent. This is comparable to the accuracies obtained from Table 5.1.6. Since the maximum size of the dynamic finite element model is only 28, the computational cost is very low when compared to the standard finite element model.

Table 5.1.3 Retained Modes For Different Frequency Contents (ω_c) For Fixed–Fixed Axial Bar At Current System Level (s)

ω_c	s								
	2	3	4	5	6	7	8	9	10
< 500 Hz	1	1	2	3	3	4	5	6	6
< 1000 Hz	2	3	5	6	7	8	10	11	12
< 2000 Hz	5	7	10	12	15	17	20	22	25

Table 5.1.4 Frequency Comparisons For

Fixed–Fixed Axial Bar, $s = 11$ and $\omega_c = 500\ Hz$

Mode Number	Theoretical Frequency (Hz)	Computed Frequency (Hz)	Error %
1	7.139E+01	7.143E+01	-5.802E-02
2	1.428E+02	1.432E+02	-2.804E-02
3	2.142E+02	2.154E+02	-5.749E-01
4	2.855E+02	2.878E+02	-7.794E-01
5	3.569E+02	3.653E+02	-2.348E+00
6	4.283E+02	4.517E+02	-5.453E+00
7	4.997E+02	6.205E+02	-2.418E+01
8	5.711E+02	1.137E+03	-9.903E+01

Table 5.1.5 Frequency Comparisons For

Fixed–Fixed Axial Bar, $s = 11$ and $\omega_c = 1000\ Hz$

Mode Number	Theoretical Frequency (Hz)	Computed Frequency (Hz)	Error %
1	7.139E+01	7.140E+01	-1.266E-02
2	1.428E+02	1.428E+02	-5.002E-02
3	2.142E+02	2.144E+02	-1.117E-01
4	2.855E+02	2.861E+02	-1.815E-01
5	3.569E+02	3.579E+02	-2.763E-01
6	4.283E+02	4.300E+02	-3.961E-01
7	4.997E+02	5.024E+02	-5.384E-01
8	5.711E+02	5.755E+02	-7.775E-01
9	6.425E+02	6.490E+02	-1.022E+00
10	7.139E+02	7.230E+02	-1.277E+00
15	1.071E+03	1.882E+02	-7.575E+01

Table 5.1.6 Frequency Comparisons For

Fixed–Fixed Axial Bar, $s = 11$ and $\omega_c = 2000$ Hz

Mode Number	Theoretical Frequency (Hz)	Computed Frequency (Hz)	Error %
1	7.139E+01	7.139E+01	-1.403E-03
2	1.428E+02	1.428E+02	-5.880E-03
3	2.142E+02	2.142E+02	-1.351E-02
4	2.855E+02	2.856E+02	-2.462E-02
5	3.569E+02	3.571E+02	-4.111E-02
6	4.283E+02	4.286E+02	-6.453E-02
7	4.997E+02	5.002E+02	-9.663E-02
8	5.711E+02	5.719E+02	-1.405E-01
9	6.425E+02	6.437E+02	-1.922E-01
10	7.139E+02	7.156E+02	-2.431E-01
20	1.428E+03	1.439E+03	-7.772E-01
25	1.785E+03	1.816E+03	-1.783E+00

5.1.3 Planar Truss

Figure 10 depicts a planar truss consisting of 16 bays. The relevent geometric and structural properties for a bay (Figure 9) are:

$$L_1 = L_2 = L_3 = 50 \ in$$

$$L_4 = L_5 = 50\sqrt{2} \ in$$

$$A = 1 \ in^2, E = 10 \times 10^6 \ lb/in^2$$

$$\rho g = 0.1 \ lb/in^3, g = 486.4 \ in/sec^2$$

The 'Theoretical' solution was obtained using five interface restrained normal modes for each bar and truncating modes above 3000 Hz at each stage. Table 5.1.7 lists the number of modes retained at each stage and Table 5.1.8 compares these computed frequencies with MSC-NASTRAN results where the pins are taken

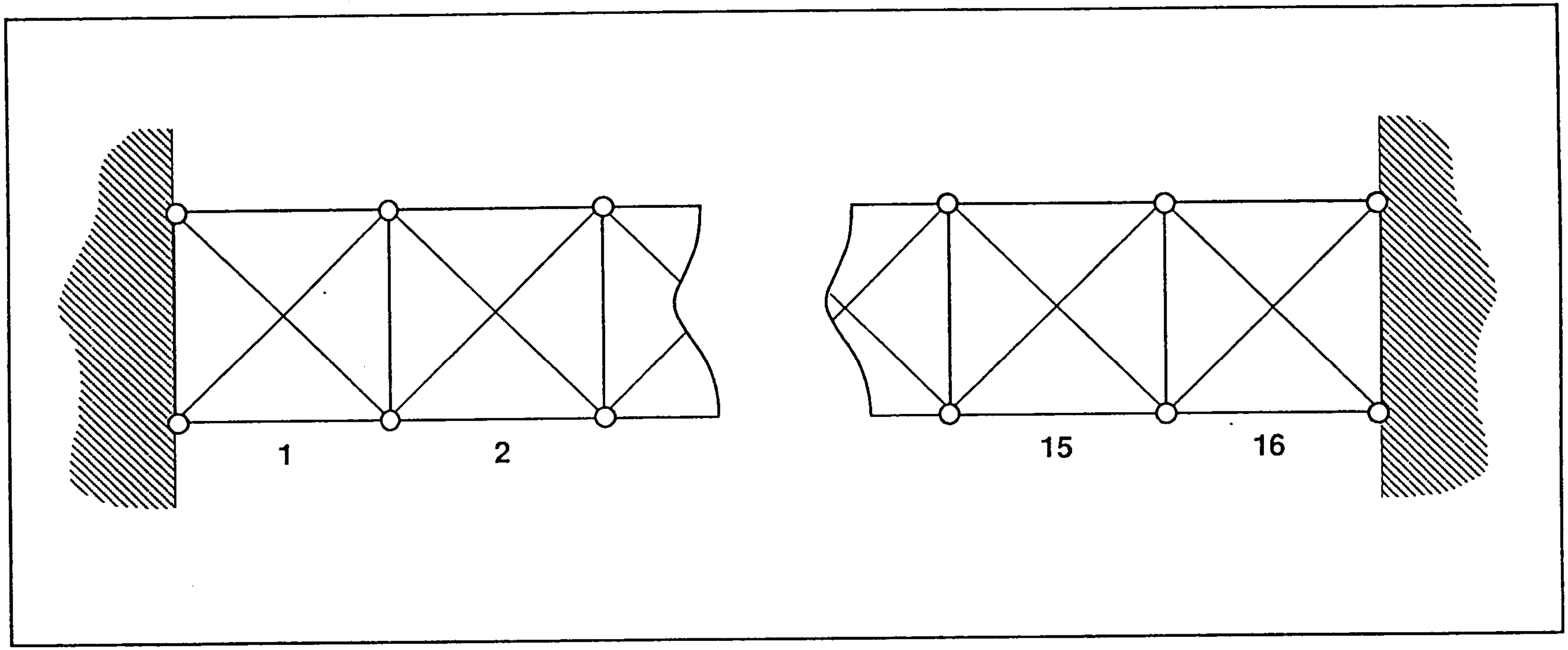

Figure 10. Sixteen–Bay Planar Truss

as nodes and consistent mass matrices are used both for the longitudinal and transverse directions. It is worthwhile to note that in order to obtain results via the standard finite element method, which are identical to those obtained by the dynamic finite element approach, it becomes necessary to further subdivide the individual bars of the truss. Indeed, using MSC–NASTRAN, each bar needed to be divided into four more segments, leading to a 534 degree of freedom model. Only then did the standard finite element method converge to the 'Theoretical' solution. This is an illustration of the advantage of using interface restrained assumed modes which do not require further subdivisions of the element. In addition, far fewer degrees of freedom are required to achieve convergence.

Table 5.1.7 Retained Modes For Frequency Content (ω_c) of 3000 Hz At Current System Level (s) Of 16–Bay Truss

System Level s	Number of Modes n
2	18
3	28
4	38
5	48
6	58
7	68
8	78
9	88
10	98
11	108
12	118
13	128
14	138
15	148

Table 5.1.8 Frequency Comparisons For 16–Bay Truss

Mode Number	Theoretical Frequency (Hz)	Computed Frequency (Hz)	Error %
1	1.513E+01	1.513E+01	-0.212E-02
2	3.928E+01	3.928E+01	-0.178E-01
3	7.208E+01	7.210E+01	-0.453E-01
4	7.951E+01	7.955E+01	-0.643E-01
5	1.112E+02	1.113E+02	-0.125E+00
6	1.551E+02	1.554E+02	-0.221E+00
7	1.592E+02	1.595E+02	-0.287E+00
8	2.028E+02	2.034E+02	-0.313E+00
9	2.391E+02	2.403E+02	-0.503E+00
10	2.533E+02	2.547E+02	-0.568E+00
40	7.881E+02	8.234E+02	-0.452E+01
50	8.509E+02	8.934E+02	-0.507E+01

5.1.4 Large Spatial Truss

Figure 11 simulates a NASA spatial truss consisting of 64 bays and 573 bar elements. The vertical and horizontal bars are 50 *in* long and the structural parameters are the same as for the planar truss. The 'Theoretical' solution was obtained using two interface restrained assumed modes for each bar and the difference between this converged solution to the finite element solution using the consistent mass matrix approach was found to be within 0.01 % for the lowest 100 frequencies. Tables 5.1.9 and 5.1.10 list the size of the eigenvalue problem at each stage of the assembly process for a cut–off frequency of 100 *Hz* and 200 *Hz* respectively and no interface restrained assumed modes for the bar elements are added. Tables 5.1.11 and 5.1.12 compare the corresponding frequencies to the converged solution.

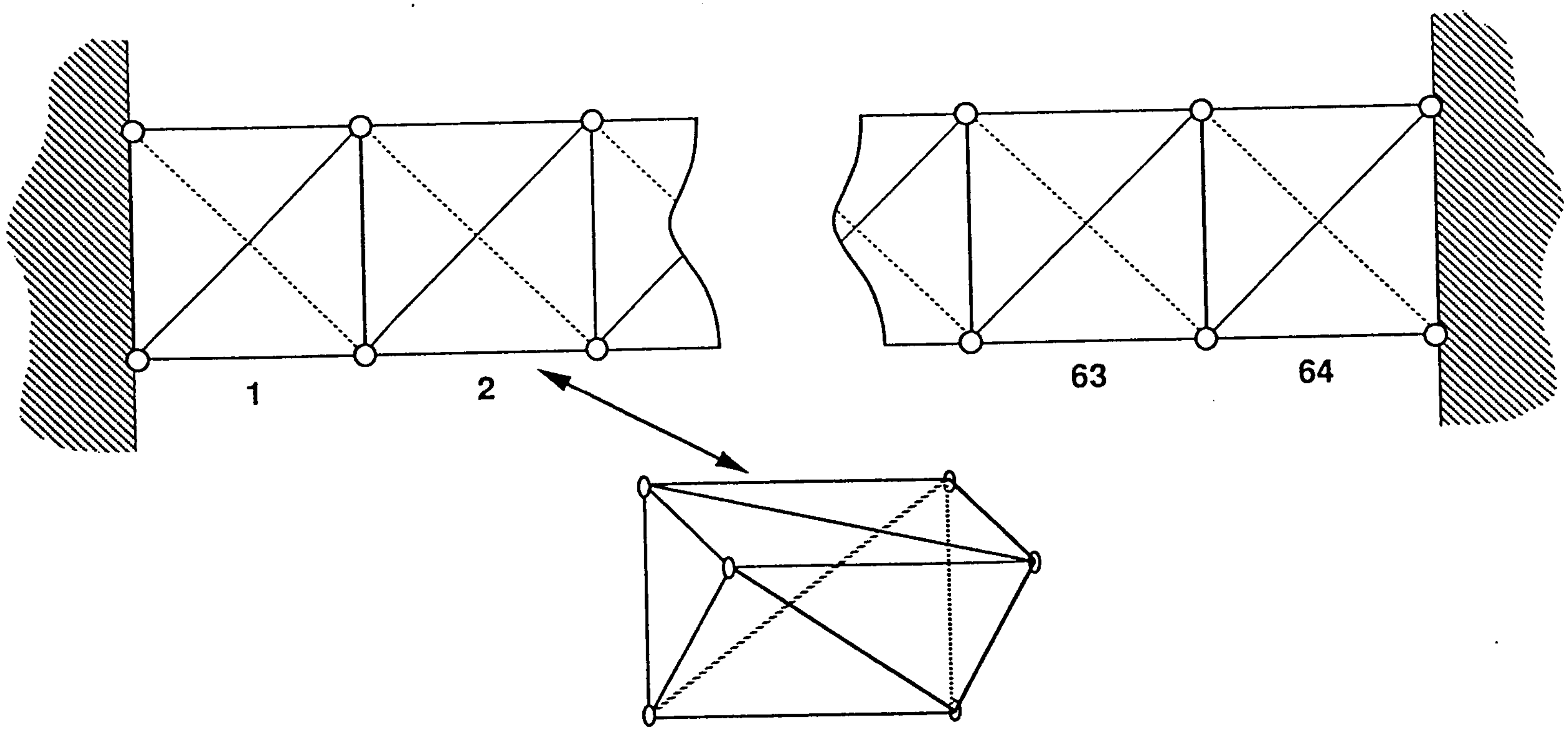

Figure 11. Large Spatial Truss

Table 5.1.9 Size of Eigenvalue Problem n

For Frequency Content (ω_c) of 100 Hz

At Current System Level (s) Of 64–Bay Truss

s	n
2	9
4	10
8	15
16	21
32	35
64	67

Table 5.1.10 Size of Eigenvalue Problem n

For Frequency Content (ω_c) of 200 Hz

At Current System Level (s) Of 64–Bay Truss

s	n
2	9
4	11
8	17
16	33
32	63
64	123

Table 5.1.11 Frequency Comparisons For 64–Bay Truss

For Frequency Content Of 100 Hz

Mode Number	Theoretical Frequency (Hz)	Computed Frequency (Hz)	Error %
1	7.494E-01	7.494E-01	-0.712E-04
5	3.972E+00	3.972E+00	-0.687E-02
10	9.350E+00	9.361E+00	-1.176E-01
20	2.152E+01	2.160E+01	-3.717E-01
30	3.687E+01	3.729E+01	-1.139E+00
40	5.461E+01	5.630E+01	-3.095E+00
50	6.948E+01	7.460E+01	-7.369E+00
60	8.751E+01	1.009E+02	-1.530E+01

Table 5.1.12 Frequency Comparisons For 64–Bay Truss

For Frequency Content Of 200 Hz

Mode Number	Theoretical Frequency (Hz)	Computed Frequency (Hz)	Error %
1	7.494E-01	7.494E-01	-0.273E-05
5	3.972E+00	3.972E+00	-7.253E-03
10	9.350E+00	9.351E+00	-1.070E-02
20	2.152E+01	2.159E+01	-3.253E-01
30	3.687E+01	3.724E+01	-1.004E+00
50	6.948E+01	6.950E+01	-2.879E-02
70	1.052E+02	1.085E+02	-3.137E+00
100	1.590E+02	1.662E+02	-4.528+E00

5.2 Bernoulli–Euler Beam

5.2.1 Simply Supported Beam

This example concerns a simply supported beam, ie., the displacement and bending moment are zero at both ends. The beam parameters used are $E = 30 \times 10^6\ lb/in^2, \rho g = 0.2839\ lb/in^3, A = 1\ in^2, I = \frac{1}{12}\ in^4$ and $L = 72\ in$.

The exact frequency formula for the simply supported Bernoulli–Euler beam is given by

$$f_i = \frac{i^2\pi}{2L^2}\sqrt{\frac{EI}{\rho A}},\ i = 1, 2, \ldots \tag{5.2.1}$$

Tables 5.2.1 through 5.2.3 show the number of converged frequencies to within a given percentage relative error when compared to the theoretical frequency in Eq. (5.2.1). These frequencies are computed in three different ways.

(1) Using the standard finite element method (consistent mass matrix approach) as implemented in MSC-NASTRAN.

(2) Using the dynamic finite element method with static constraint modes and interface restrained normal modes as developed in Section 3.3.1.

(3) Using the dynamic finite element method with static constraint modes and trigonometric functions as interface restrained assumed modes as developed in Section 3.3.2.

Figures 12 and 13 show that the dynamic finite element models consistently perform better than the corresponding standard finite element models.

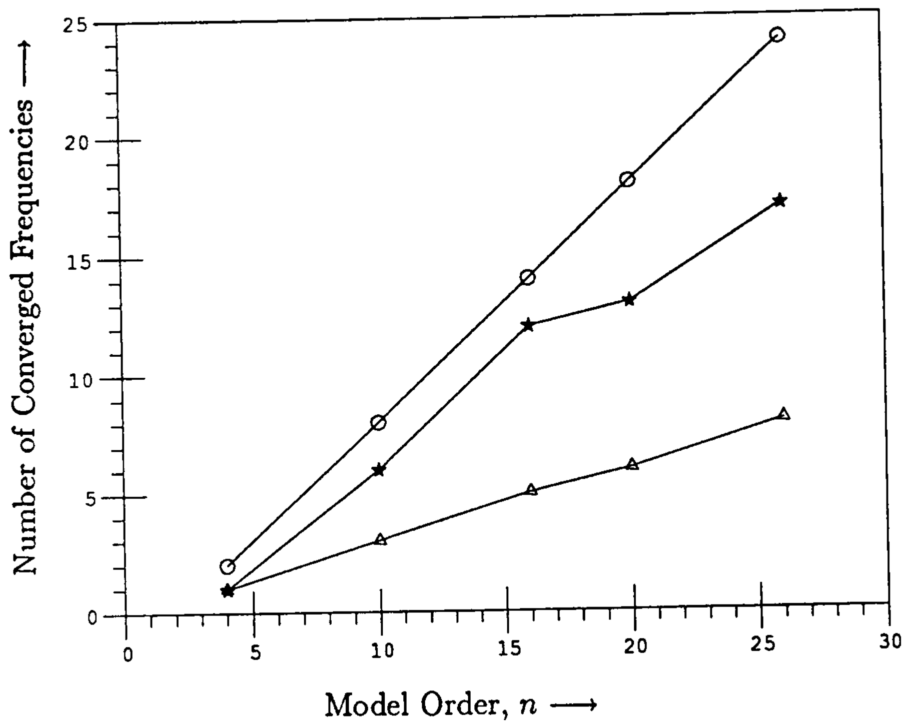

△ — Standard Finite Element Method

o — Normal Modes As Interface Restrained Modes

⋆ — Trigonometric Functions As Interface Restrained Modes

Fig. 12. Number of Frequencies Converged to within 1 %

Simply Supported Beam (Bernoulli–Euler Theory)

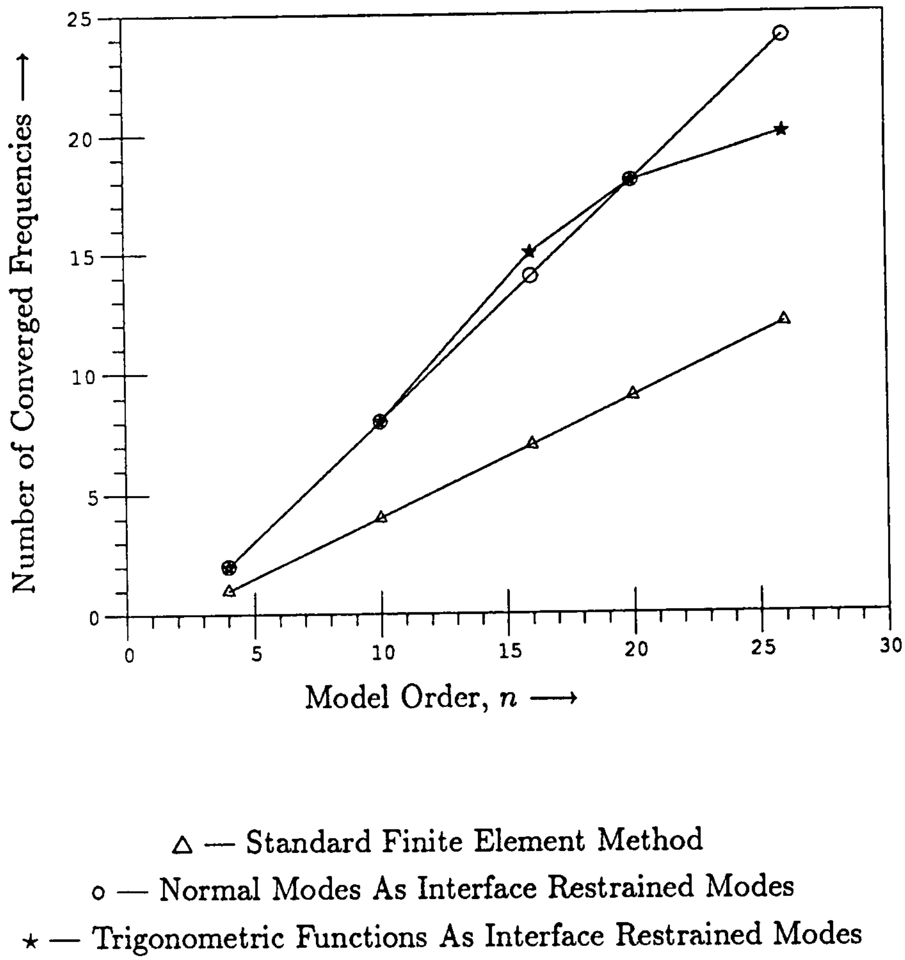

Fig. 13. Number of Frequencies Converged to within 5 %

Simply Supported Beam (Bernoulli–Euler Theory)

Table 5.2.1 Standard Finite Element Method

For Simply Supported Beam (Bernoulli–Euler Theory)

e	n				
	4	10	16	20	26
< 1 %	1	3	5	6	8
< 5 %	1	4	7	9	12
< 10 %	1	4	7	9	12

Table 5.2.2 Normal Modes As Interface Restrained Modes

For Simply Supported Beam (Bernoulli–Euler Theory)

e	n				
	4	10	16	20	26
< 1 %	2	8	14	18	24
< 5 %	2	8	14	18	24
< 10 %	2	8	14	18	24

Table 5.2.3 Trigonometric Functions As Interface Restrained Modes

For Simply Supported Beam (Bernoulli–Euler Theory)

e	n				
	4	10	16	20	26
< 1 %	1	6	12	13	17
< 5 %	2	8	15	18	20
< 10 %	2	8	15	19	26

5.2.2 Four–Bay Frame

Next, consider the cantilevered planar frame with four bays as shown in Figure 14. The frame element is obtained by superposition of the axial bar and the Bernoulli–Euler beam elements. The frame parameters are the same as for the axial bar in Section 5.1.1 and the Bernoulli–Euler beam in Section 5.2.1. The length, $L = 72\ in$ is for the vertical and horizontal members and the diagonal member is therefore $72\sqrt{2}\ in$ long. This time no closed form solution for the frequencies exists. A reference solution is obtained by constructing two models one with 600 degrees of freedom and another with 900 degrees of freedom. These models were then solved for the first 216 frequencies. Because these frequencies differ by less than 0.4 %, it is assumed that convergence has been reached.

Tables 5.2.4 through 5.2.6 list the number of natural frequencies with an accuracy of e percent or better compared to the converged solution for different model orders, n. These tables are generated using the standard finite element method (consistent mass matrix approach) as well as the dynamic finite element approaches developed in Sections 3.3.1 and 3.3.2. Figures 15 and 16 show the performance of the standard finite element method and the two dynamic finite elements.

Table 5.2.4 Standard Finite Element Method For Four–Bay Frame (Bernoulli–Euler Theory)

e	n				
	24	72	120	168	216
< 1 %	0	3	17	29	37
< 5 %	0	16	34	46	77
< 10 %	0	16	35	57	105

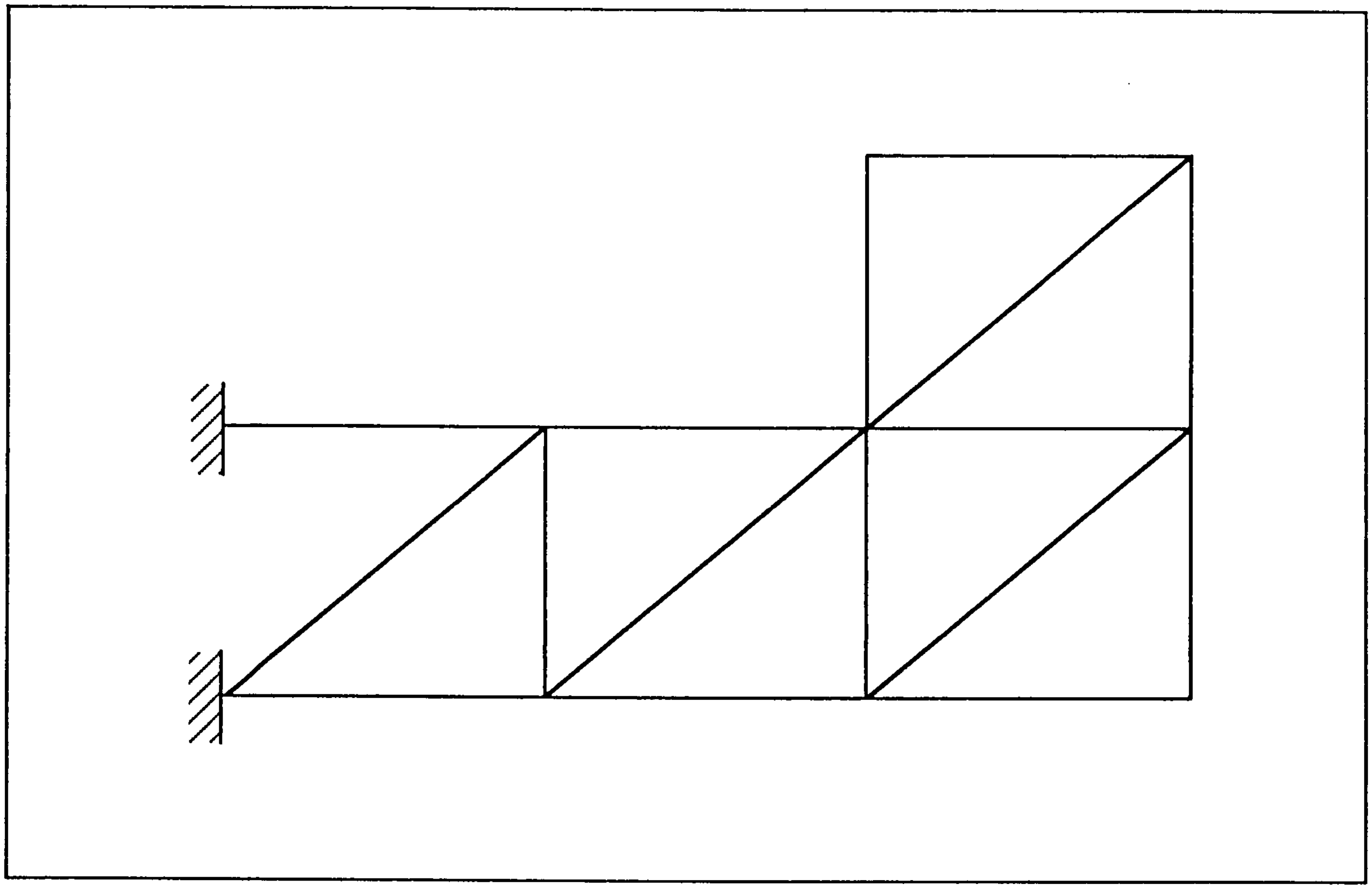

Figure 14. Four–Bay Frame

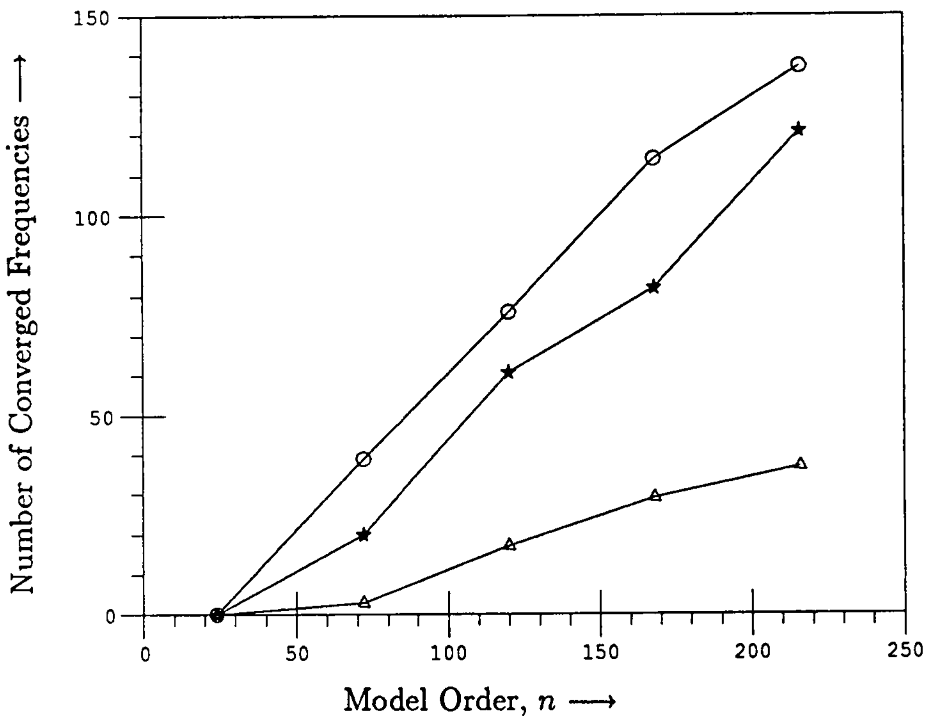

△ — Standard Finite Element Method

○ — Normal Modes As Interface Restrained Modes

⋆ — Trigonometric Functions As Interface Restrained Modes

Fig. 15. Number of Frequencies Converged to within 1 %

Four–Bay Frame (Bernoulli–Euler Theory)

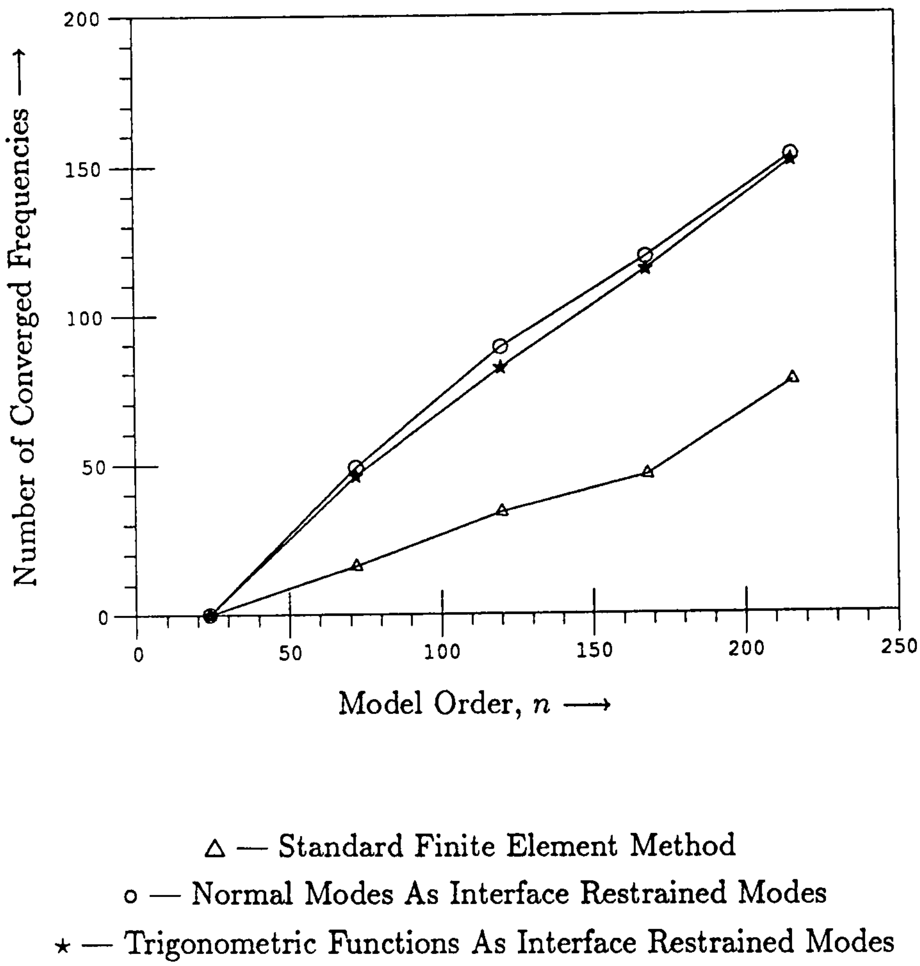

Fig. 16. Number of Frequencies Converged to within 5 %

Four–Bay Frame (Bernoulli–Euler Theory)

Table 5.2.5 Normal Modes As Interface Restrained Modes For Four–Bay Frame (Bernoulli–Euler Theory)

e	n				
	24	72	120	168	216
< 1 %	0	39	76	114	137
< 5 %	0	49	89	119	153
< 10 %	0	51	90	129	163

Table 5.2.6 Trigonometric Functions As Interface Restrained Modes For Four–Bay Frame (Bernoulli–Euler Theory)

e	n				
	24	72	120	168	216
< 1 %	0	20	61	82	121
< 5 %	0	46	82	115	151
< 10 %	0	51	90	125	162

5.3 Timoshenko Beam

5.3.1 Simply Supported Beam

This example is concerned with a simply supported Timoshenko beam. The relevent parameters are the same as in the Bernoulli–Euler beam example of Section 5.2.1. The additional relations needed are $G = E/2(1+\nu)$ and $k = 10(1+\nu)/(12+11\nu)$ where the Poisson's ratio is taken as 0.3.

The exact frequency is found numerically from the characteristic equation for the simply supported Timoshenko beam which is

$$\begin{aligned} \sinh b\alpha_1 \sin b\beta = 0 \quad &\text{for} \quad \left[(r^2 - s^2)^2 + 4/b^2\right]^{\frac{1}{2}} > (r^2 + s^2) \\ \sin b\alpha_2 \sin b\beta = 0 \quad &\text{for} \quad \left[(r^2 - s^2)^2 + 4/b^2\right]^{\frac{1}{2}} < (r^2 + s^2) \end{aligned} \qquad (5.3.1)$$

The variables r, s, b, α_1, α_2, β are the same as in Section 3.4.2. Tables 5.3.1

through 5.3.4 show the number of converged frequencies to within a given percentage relative error when compared to the theoretical frequencies from Eq. (5.3.1). This data is presented graphically in Figures 17 and 18. The frequencies are computed in four different ways.

(1) Using standard finite element method (consistent mass matrix approach) as implemented in MSC-NASTRAN.

(2) Using the dynamic finite element method with static constraint modes and interface restrained normal modes as developed in Sections 3.4.1 and 3.4.2.

(3) Using the dynamic finite element method with static constraint modes and polynomial functions as interface restrained assumed modes as developed in Section 3.4.3.

(4) Using the dynamic finite element method with static constraint modes and trigonometric functions as interface restrained assumed modes as developed in Section 3.4.4.

In order to produce the data for the Tables 5.3.3 and 5.3.4, a certain number of the two types of interface restrained assumed modes must be selected. The number of Bernoulli–Euler beam type modes is taken as n_1 and is kept the same as in the example of Section 5.3.1. Furthermore, the optimum number of shear type modes is found to be $n_1 - 2$. After solving the Timoshenko beam element eigenvalue problem, the lowest n_1 modes are retained to form the simply supported beam model. The number n_1 for the retained modes is chosen so that comparison with the example in Section 5.3.1 becomes possible. In general, however, the number of interface restrained assumed modes kept depends on the chosen cut–off frequency.

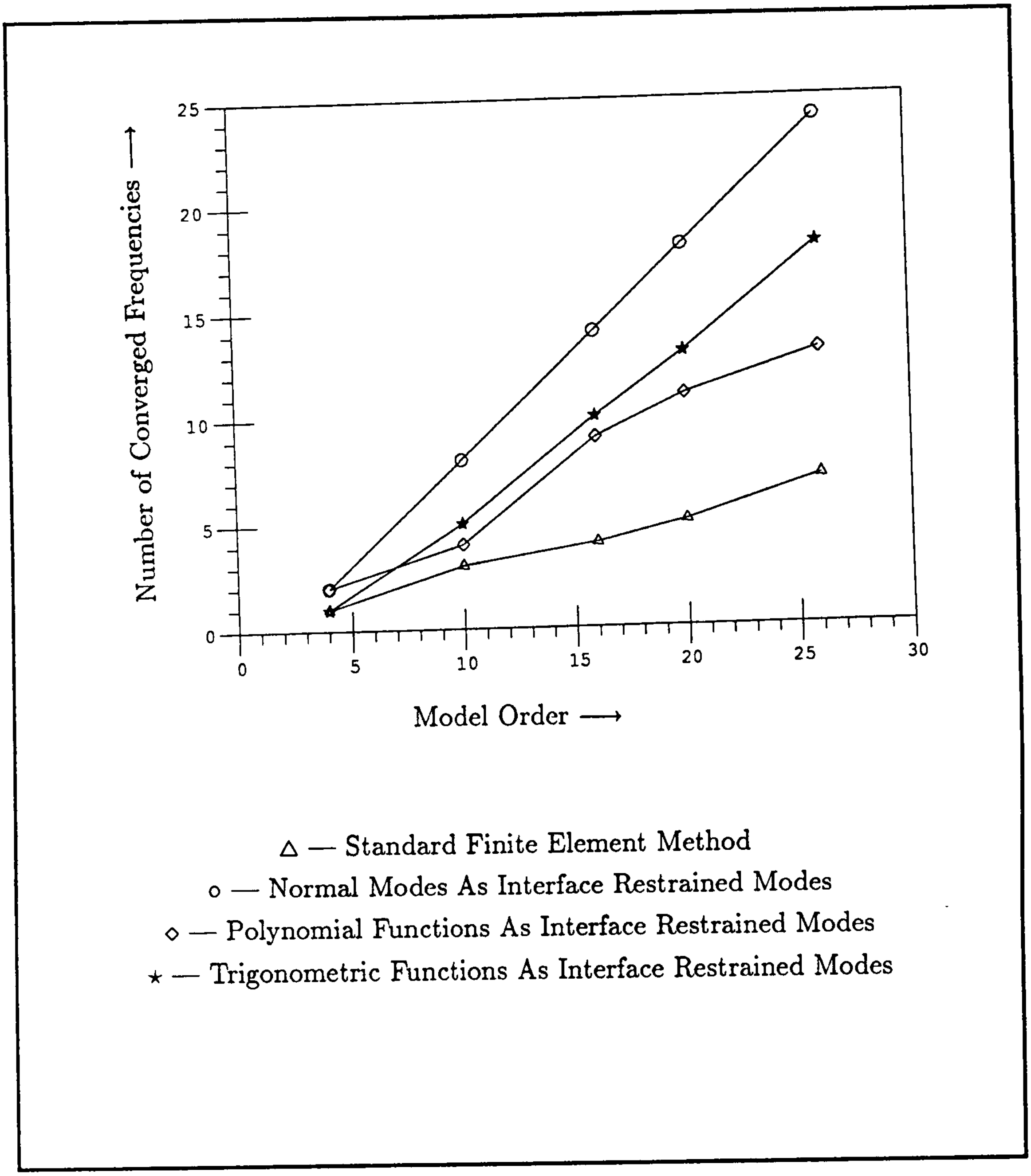

Figure 17. Number of Frequencies Converged to within 1 %
For Simply Supported Beam (Timoshenko Theory)

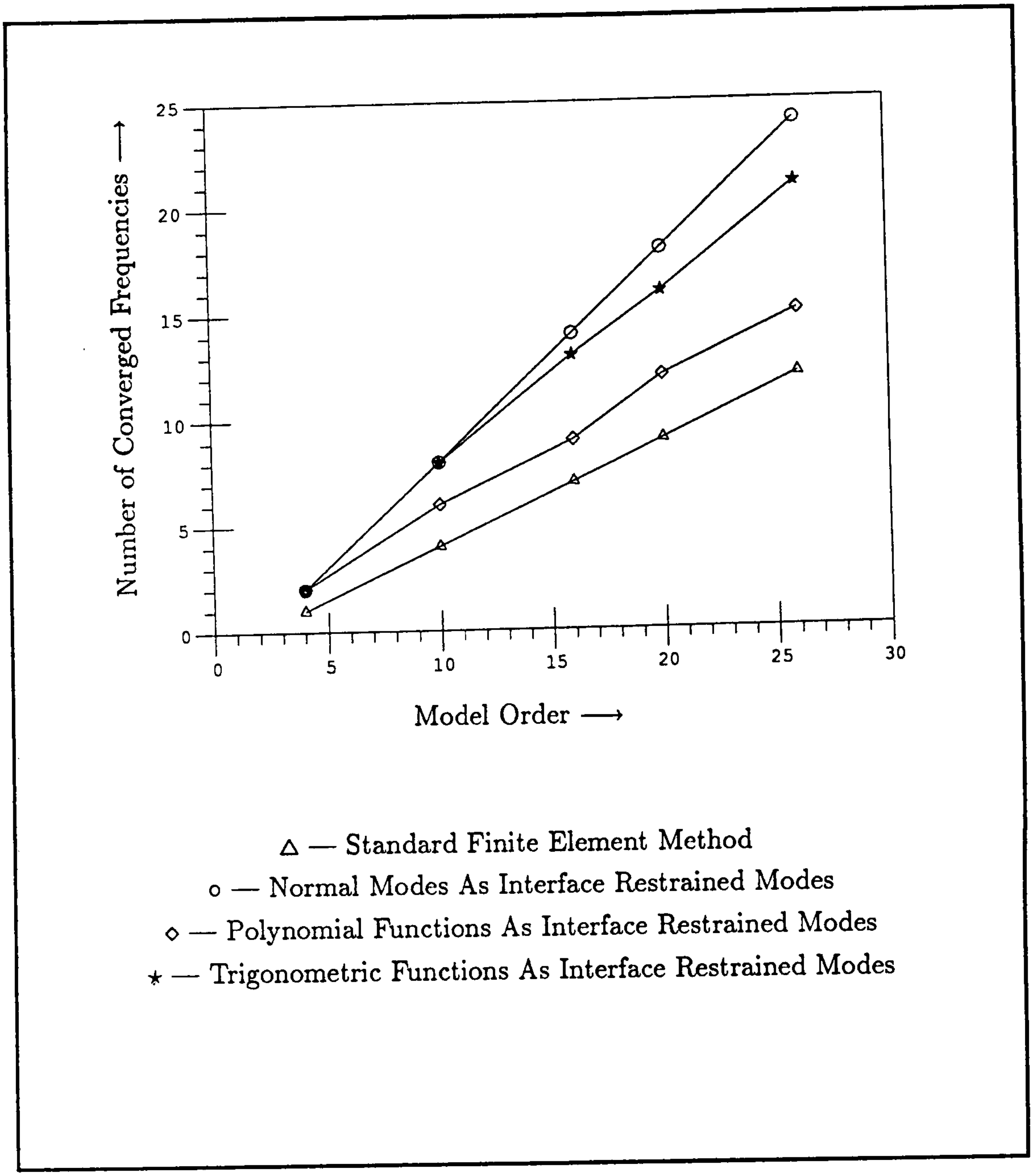

Figure 18. Number of Frequencies Converged to within 5 % For Simply Supported Beam (Timoshenko Theory)

Table 5.3.1 Standard Finite Element Method

For Simply Supported Beam (Timoshenko Theory)

e	n				
	4	10	16	20	26
$< 1\ \%$	1	3	4	5	7
$< 5\ \%$	1	4	7	9	12
$< 10\ \%$	1	4	7	9	12

Table 5.3.2 Normal Modes As Interface Restrained Modes

For Simply Supported Beam (Timoshenko Theory)

e	n				
	4	10	16	20	26
$< 1\ \%$	2	8	14	18	24
$< 5\ \%$	2	8	14	18	24
$< 10\ \%$	2	8	14	18	24

Table 5.3.3 Polynomial Functions As Interface Restrained Modes

For Simply Supported Beam (Timoshenko Theory)

e	n				
	4	10	16	20	26
$< 1\ \%$	2	4	9	11	13
$< 5\ \%$	2	6	9	12	15
$< 10\ \%$	2	6	10	13	16

Table 5.3.4 Trigonometric Functions As Interface Restrained Modes For Simply Supported Beam (Timoshenko Theory)

e	n				
	4	10	16	20	26
< 1 %	1	5	10	13	18
< 5 %	2	8	13	16	21
< 10 %	2	8	14	18	23

5.3.2 Four–Bay Frame

Next, consider the cantilevered planar frame with four bays as shown in Figure 14. The frame element is obtained by superposition of the axial bar and the Timoshenko beam elements. The frame parameters are the same as for the axial bar in Section 5.1.1 and the Timoshenko beam in Section 5.3.1. The length, $L = 72\ in$ is for the vertical and horizontal members and the diagonal member is therefore $72\sqrt{2}\ in$ long. No 'exact' frequency formula exists in this case. A reference solution is obtained by constructing two models one with 600 degrees of freedom and another with 900 degrees of freedom. These models were then solved for the first 216 frequencies. Because these frequencies differ by less than 0.4 %, it is assumed that convergence has been reached.

Tables 5.3.5 through 5.3.8 list the number of natural frequencies with an accuracy of e percent or better compared to the converged solution for different model orders, n. These tables are generated using standard finite element method (consistent mass matrix approach) as well as the dynamic finite elements developed in Sections 3.4.1 through 3.4.4. Figures 19 and 20 show the performance of the standard finite element method and the three dynamic finite elements.

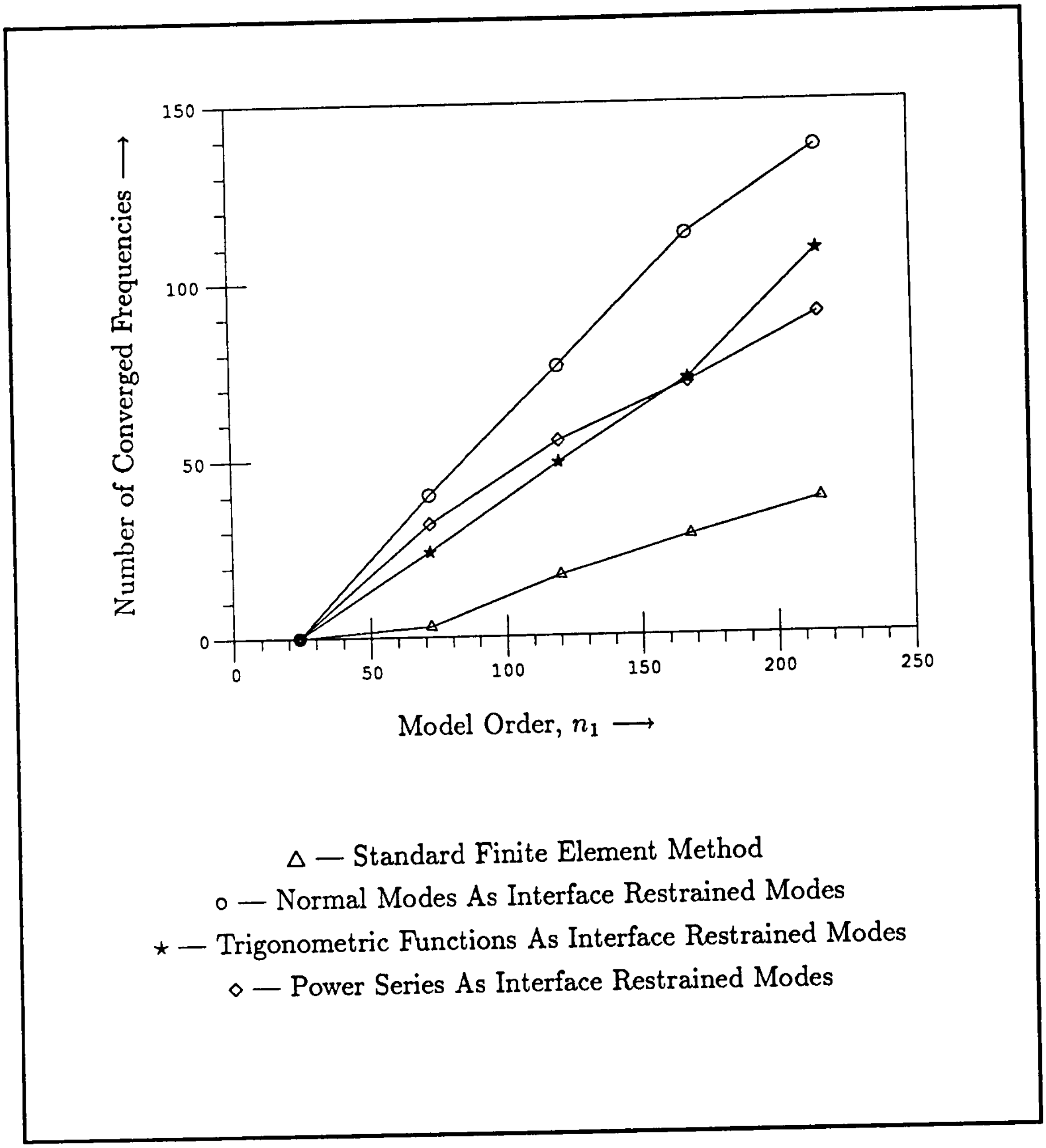

Figure 19. Number of Frequencies Converged to within 1 %

For Four–Bay Frame (Timoshenko Theory)

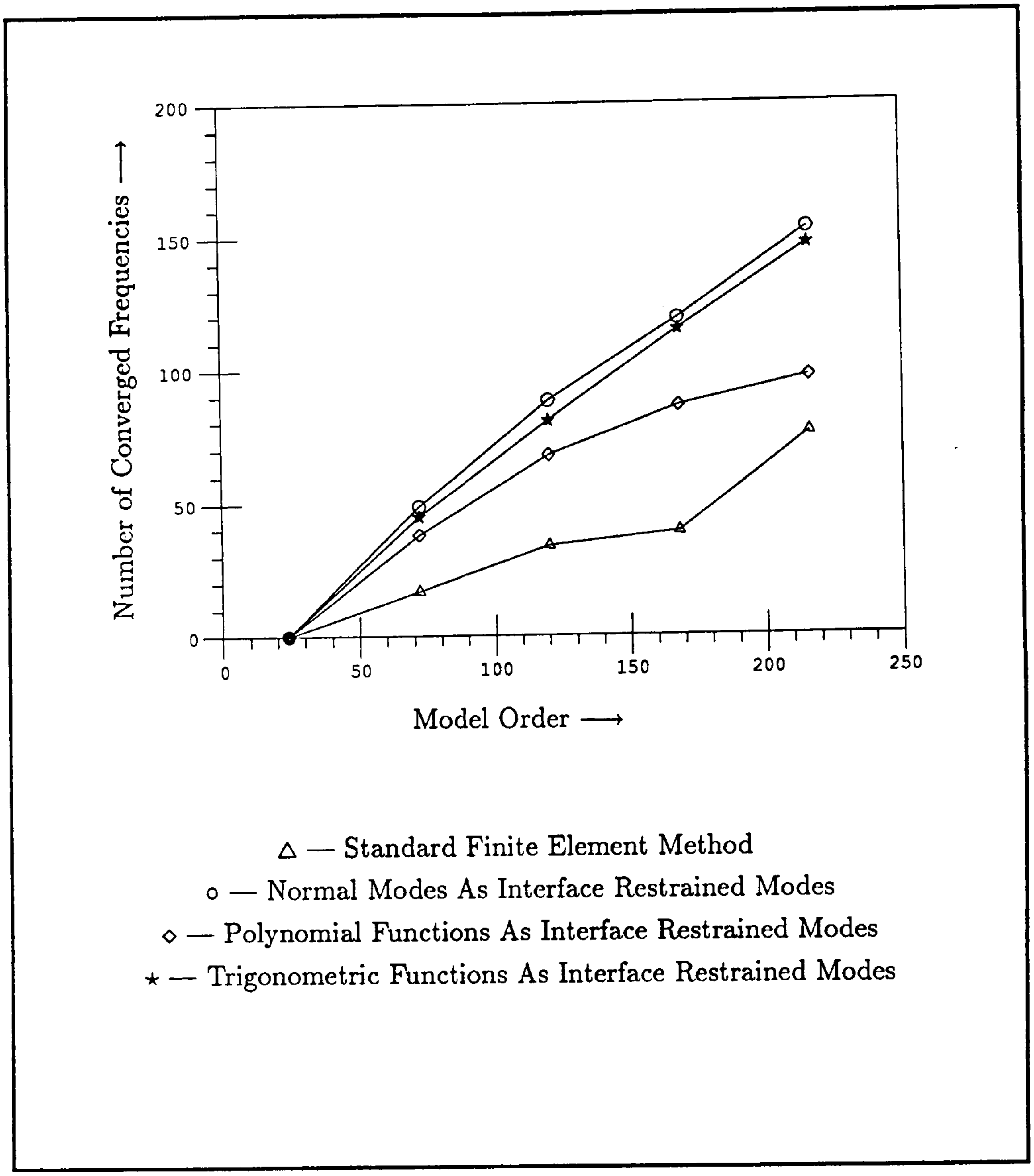

Figure 20. Number of Frequencies Converged to within 5 % For Four–Bay Frame (Timoshenko Theory)

To improve the accuracy of the frequencies computed, reanalysis of structures are often desired with higher order models. Using the dynamic finite elements, it is easier to refine the elements by increasing the number of interface restrained modes. Here the number of dynamic finite elements is fixed by geometry rather than the requirements of precision in frequency and as a result, substantial reduction in the data preparation effort for the finite element codes is achieved. Also, the mass and stiffness matrices of higher order models can be obtained by bordering the lower order model matrices with a few additional rows and columns corresponding to the newly added interface restrained modes. Stiffness and mass matrices corresponding to a given approximation are embedded in the stiffness and mass matrices of all higher order approximations. In other words, the presented models possess the hierarchical property. Using the solution corresponding to the lower order models, the mass and stiffness matrices of the higher order models can be put in the form of Eq. (4.2.7) and hence the computation of improved approximations can be achieved using the same procedure as outlined in Section 4.2.

Table 5.3.5 Standard Finite Element Method

For Four–Bay Frame (Timoshenko Theory)

e	n				
	24	72	120	168	216
< 1 %	0	3	17	28	38
< 5 %	0	17	34	39	76
< 10 %	0	17	35	56	110

Table 5.3.6 Normal Modes As Interface Restrained Modes

For Four–Bay Frame (Timoshenko Theory)

e	n				
	24	72	120	168	216
< 1 %	0	40	76	113	137
< 5 %	0	49	88	119	153
< 10 %	0	51	91	128	162

Table 5.3.7 Polynomial Functions As Interface Restrained Modes

For Four–Bay Frame (Timoshenko Theory)

e	n				
	24	72	120	168	216
< 1 %	0	32	55	71	90
< 5 %	0	38	68	86	97
< 10 %	0	47	70	101	122

Table 5.3.8 Trigonometric Functions As Interface Restrained Modes

For Four–Bay Frame (Timoshenko Theory)

e	n				
	24	72	120	168	216
< 1 %	0	24	49	72	108
< 5 %	0	45	81	115	147
< 10 %	0	51	90	124	155

CHAPTER 6

CONCLUSIONS AND RECOMMENDATIONS

A method to dynamically model generic structural elements has been presented. The approach is based on the assumed modes method with static constraint modes and interface restrained assumed modes and is reminiscent of known component mode synthesis techniques such as the Craig/Bampton method. However, basic structural members are dealt with and near continuum solutions are obtained with relatively few degrees of freedom. The proposed models are hierarchical, so that different levels of approximation can be obtained with little additional data preparation effort and without the need for further physical subdivisions of the basic structural members. Furthermore, at each stage of the assembly process, the current structural component can be treated as a single larger element. The presented assembly technique can exploit spatial periodicity. Also included is a special algorithm for solving the eigenvalue problem at each stage of the assembly process. In particular, it is concluded that

- dynamic finite element models need about 40 % fewer degrees of freedom than those constructed with the consistent mass matrix approach, in order to achieve comparable covergence in the natural frequencies.
- because the element assembly process employs modal truncation at every stage, a near minimum order model for the overall structure is obtained.
- for very large frame structures, no interface restrained assumed modes may be necessary and even truncating all the interface restrained normal modes at early stages of the assembly process is feasible, resulting in a smaller model than required by the standard finite element approach.

- dynamic finite element models with interface restrained normal modes yield the best convergence compared to all the other models considered, both for the Bernoulli–Euler and the Timoshenko beams.
- for the case of the Timoshenko beam, the dynamic finite elements using trigonometric functions as interface restrained assumed modes are more cost effective.

Future efforts can be directed towards developing dynamic finite elements for axial bars, torsional shafts and flexural beams with tapered cross sections as well as two dimensional dynamic finite elements for membrane, plate or shell structures and three dimensional brick elements. Interface restrained normal modes in terms of Bessel functions and static constraint modes can be obtained for the case of tapered line elements.

The main difficulty in forming two or three dimensional dynamic finite elements lies in finding a set of static constraint modes because the interfaces of such elements are collections of displacement functions of one or more spatial variables. The assembly process as presented in Chapter 4, on the other hand, is still valid even when the structure consists of many different types of elements.

Another area of potential research concerns the determination of an optimum cut–off frequency. The cut–off frequency on the element level usually does not exceed twice the preset cut–off frequency at the system level. But the proper criterion for the cut–off frequency at the element level is still a matter of research. The fast growing field of adaptive finite elements may be useful in answering these questions of practical importance.

BIBLIOGRAPHY

BIBLIOGRAPHY

1. O. C. Zienkiewicz and J. P. de S. R. Gago, D. W. Kelly, 1983 *Computers and Structures* **16**, 53–65. The hierarchical concept in finite element analysis.

2. A. Peano, A. Pasini, R. Riccioni and L. Sardella, 1979 *Computers and Structures* **10**, 333–342. Adaptive approximations in finite element structural analysis.

3. I. Babuska, B. A. Szabo and I. N. Katz, 1981 *Society of Industrial and Applied Mathematics Journal of Numerical Analysis*, **18** 515–545. The p-version of the finite element method.

4. J. K. Bennighof and L. Meirovitch, 1986 *International Journal for Numerical Methods in Engineering* **23**, 2153–2165. Eigenvalue convergence in the finite element method.

5. W. C. Hurty, 1960 *Proceedings of the American Society of Civil Engineers, Journal of the Engineering Mechanics Division* **86**, 51–69. Vibrations of structural systems by component mode synthesis.

6. R. R. Craig and M. C. C. Bampton, 1968 *American Institute of Aeronautics and Astronautics Journal* **6**, 1313–1319. Coupling of substructures for dynamic analysis.

7. W. A. Benfield and R. F. Hruda, 1971 *American Institute of Aeronautics and Astronautics Journal* **9**, 1255–1261. Vibration analysis of structures by component mode substitution.

8. E. J. Kuhar and C. V. Stahle, 1974 *American Institute of Aeronautics and Astronautics Journal* **12**, 672–8. Dynamic transformation method for modal synthesis.

9. R. M. Hintz, 1975 *American Institute of Aeronautics and Astronautics Journal* **13**, 1007–1016. Analytical methods in component modal synthesis.

10. R. Bamford, B. K. Wada, J. A. Garba and J. Chisholm, 1971 *Synthesis of Vibrating Systems, ASME Booklet* 57–71. Dynamic analysis of large structural systems.

11. R. H. MacNeal, 1971 *Computers and Structures* **1**, 581–601. A hybrid method of component mode synthesis.

12. S. Rubin, 1975 *American Institute of Aeronautics and Astronautics Journal* **13**, 995–1006. Improved component mode representation for structural dynamic analysis.

13. R. J. Guyan, 1965 *American Institute of Aeronautics and Astronautics Journal* **3**, 380. Reduction of stiffness and mass matrices.

14. M. Geradin, 1971 *Journal of Sound and Vibration* **19**, 111–132. Error bounds for eigenvalue analysis by elimination of variables.

15. D. L. Thomas, 1982 *Internatinal Journal for Numerical Methods in Engineering* **18**, 1521–1527. Errors in natural frequency calculations using eigenvalue economization.

16. R. L. Kidder, 1973 *American Institute of Aeronautics and Astronautics Journal* **11**, 892. Reduction of structural frequency equations.

17. A. H. Flax, 1975 *American Institute of Aeronautics and Astronautics Journal* **13**, 701–702. Comment on 'Reduction of structural frequency equations'.

18. R. D. Henshell and J. H. Ong, 1975 *Earthquake Engineering and Structural Dynamics* **3**, 375–383. Automatic masters for eigenvalue economization.

19. V. N. Shah and M. Raymund, 1982 *International Journal for Numerical Methods in Engineering* **18**, 89–98. Analytical selection of masters for the reduced eigenvalue problem.

20. A. Jennings, 1985 *Sparsity and its Applications, Edited by D. J. Evans* 153–183, Solution of sparse eigenvalue problems, Cambrige University Press.

21. B. Nour–Omid, B. N. Parlett and R. L. Taylor, 1983 *International Journal for Numerical Methods in Engineering* **19**, 859–871. Lanczos versus subspace iteration for solution of eigenvalue problems.

22. A. Jennings, 1973 *International Journal for Numerical Methods in Engineering* **6**, 543–552. Mass condensation and simultaneous iteration for vibration problems.

23. T. C. Cheu, C. P. . Johnson and R. R. Craig, Jr., 1987 *International Journal for Numerical Methods in Engineering* **24**, 1841–1848. Computer algorithms for calculating effiecient initial vectors for subspace iteration method.

24. R. C. Engels, 1990 *Proceedings of The 31st AIAA/ASME/ASCE/AHS/ASC Structures, Structural Dynamics and Materials Conference, Long Beach, CA., Paper No. 90–1038*, 1922–1931. The assumed modes method with static constraint modes.

25. R. C. Engels, 1986 *Final Report for Air Force Weapons Laboratory, Kirtland, New Mexico.* Reduced order structural modeling techniques for high energy laser systems.

26. T. C. Chang and R. R. Craig, Jr., 1969 *Proceedings of the American Society of Civil Engineers, Journal of the Engineering Mechanics Division* **95**, 1027–1031. Normal modes of uniform beams.

27. J. R. Gartner and N. Olgac, 1982 *Journal of Sound and Vibration* **84**, 481–489. Improved numerical computation of uniform beam characteristic values and characteristic functions.

28. J. Dugundji, 1988 *American Institute of Aeronautics and Astronautics Journal* **26**, 1013–1014, Simple expressions for higher vibration modes of uniform Euler beams.

29. G. R. Cowper, 1966 *Journal of Applied Mechanics* **33**, 335–340. The shear coefficient in Timoshenko beam theory.

30. R. B. McCalley 1963 *General Electric Knolls Atomic Power Laboratory, Schenectady, New York, Report DIG/SA 63–68.* Mass lumping for beams.

31. R. B. McCalley 1963 *General Electric Knolls Atomic Power Laboratory, Schenectady, New York, Report DIG/SA 63–73.* Rotary inertia correction for mass matrices.

32. T. C. Huang, 1961 *Journal of Applied Mechanics* **28**, 579–584. The effects of rotary inertia and of shear deformation on the frequency and normal mode equations of uniform beams with simple end conditions.

33. M. Levinson and D. W. Cooke, 1982 *Journal of Sound and Vibration* **84**, 319–326. On the two frequency spectra of Timoshenko beams.

34. A. W. Lees, and D. L. Thomas, 1982 *Journal of Sound and Vibration* **80**, 355–366. Unified Timoshenko beam finite element.

35. A. W. Lees, and D. L. Thomas, 1985 *Journal of Sound and Vibration* **99**, 455–461. Modal hierarchical Timoshenko beam finite elements.

36. R. C. Engels, 1990 *Paper to be Published,* 7 p. A convergence improvement scheme for component mode synthesis techniques.

37. R. C. Engels, 1990 *Proceedings of The 1990 ASME International Computers in Engineering Conference, Boston, MA.*, **1**, 493–503. Dynamic finite element modeling of some basic structural members.

38. N. Ganesan and R. C. Engels, 1990 *AIAA Space Programs and Technologies Conference, September 25–28, 1990, Huntsville, AL., Paper No. 90–3547.* A dynamic finite element model for the Timoshenko beam.

39. D. L. Thomas, J. M. Wilson and R. R. Wilson, 1973 *Journal of Sound and Vibration* **31**, 315–330. Timoshenko beam finite elements.

40. G. R. Heppler and J. S. Hansen, 1988 *American Institute of Aeronautics and Astronautics Journal* **26**, 1378–1386. Timoshenko beam finite elements using trigonometric shape functions.

41. A. Tessler and S. B. Dong, 1981 *Computers and Structures* **14**, 335–344. On a hierarchy of conforming Timoshenko beam elements.

42. S. H. Chen and H. H. Pan, 1988 *Communications in Applied Numerical Methods* **4**, 549–556. Guyan reduction.

43. P. C. Hughes, 1987 *Institution of Electrical and Electronics Engineers Control Systems Magazine* **7**, 22–28, Space structure vibration modes: how many exist ? which ones are important ?

44. B. G. Prakash and M. S. S.Prabhu, 1986 *Computers and Structures* **22**, 539–552. Reduction techniques in dynamic substructures for large problems.

45. Y. Xuegang, 1985 *Proceedings of the Third International Modal Analysis Conference, Orlando, FL.*, **2**, 1245–1249. Dynamic finite element method of a frame.

46. X. Lu, 1988 *Computers and Structures* **30** 851–854. Simplified dynamic condensation in multi–substructure systems.

47. D. C. Zhu, 1982 Structures, Structural Dynamics and Materials Conference, Twenty Third, New Orleans, LA., **1**, 206–211. Hierarchical finite elements and their application to structural natural vibration problems.

48. A. Curnier, 1983 *Journal of Sound and Vibration* **90**, 527–540. On three modal synthesis variants.

49. T. C. Huang and X. L. Huang, 1988 *International Journal of Analytical and Experimental Modal Analysis* **3**, 6–11. Fixed interface substructural modal perturbation method.

50. A. Peano, 1976 *Computers and Mathematics with Applications* **2**, 211–224. Hierarchies of conforming finite elements for plane elasticity and plate bending.

51. M. P. Rossow and I. N. Katz, 1978 *International Journal for Numerical Methods in Engineering* **12**, 977–999. Hierarchical finite elements and precomputed arrays.

52. G. Prathap and G. R. Bhashyam, 1982 *International Journal for Numerical Methods in Engineering* **18**, 195–210. Reduced integration and the shear flexible beam element.

53. I. Babuska and B. A. Szabo, 1982 *International Journal for Numerical Methods in Engineering* **18**, 323–341. On the rates of convergence of the finite element method.

54. I. Babuska, O. C. Zinkiewicz, J. Gago and E. R. de A. Oliveira, 1986 *Accuracy estimates and adaptive refinements in finite element computations*, John Wiley and Sons.

55. O. C. Zienkiewicz and K. Morgan, 1983 *Finite Elements and Approximations*, John Wiley and Sons.

56. B. N. Parlett, 1989 *State–Of–The–Art Surveys on Computational Mechanics, Edited by A. K. Noor and J. T. Oden*, 201–218, The state of the art in extracting eigenvalues and eigenvectors in structural mechanics.

57. J. Krahula and J. Polhemus, 1968 *American Institute of Aeronautics and Astronautics Journal* **6**, 726–728. Use of Fourier series in the finite element method.

58. J. S. Archer, 1963 *Proceedings of the American Society of Civil Engineers, Journal of the Structural Division* **89**, 161–178. Consistent mass matrix for distributed mass systems.

59. W. L. Craver, Jr. and D. M. Egle, 1972 *Journal of Sound and Vibration* **22**, 133–142. A method for selection of significant terms in the assumed solution in a Rayleigh–Ritz analysis.

60. W. C. Hurty, 1965 *American Institute of Aeronautics and Astronautics Journal* **3**, 678–685. Dynamic analysis of structural systems using component modes.

61. R. R. Craig, Jr. and C. J. Chang, 1976 *Advances in Engineering Science, NASA CP-2001*, 393–408. A review of substructure coupling methods for dynamic analysis.

APPENDICES

APPENDIX I

Normalization of Interface Restrained Normal Modes of the Timoshenko Beam Element

The constant C for the hyperbolic mode in Eq. (3.4.28) is determined using Eq. (3.4.34) as follows:

$$C = \frac{1}{\Omega^{\frac{1}{2}}}$$

where

$$\begin{aligned}\Omega =& \rho AL(c_1 + (\lambda\zeta\delta)^2 c_3 + c_2 + \delta^2 c_4 - 2\lambda\zeta\delta c_5 - 2c_{10} + 2\delta c_9 \\ & + 2\lambda\zeta\delta c_8 - 2\lambda\zeta\delta^2 c_7 - 2\delta c_6) + \rho IL\eta^2 \left(c_1 + \left(\frac{\gamma}{\lambda\zeta}\right)^2 c_3 \right. \\ & \left. + c_2 + \gamma^2 c_4 + \frac{2\gamma}{\lambda\zeta} c_5 - 2c_{10} + 2\gamma c_9 - \frac{2\gamma}{\lambda\zeta} c_8 + \frac{2\gamma^2}{\lambda\zeta} c_7 - 2\gamma c_6 \right)\end{aligned}$$

$$c_1 = \int_0^1 \cosh^2 b\alpha_1\xi \; d\xi = \frac{\sinh 2b\alpha_1}{4b\alpha_1} + \frac{1}{2}$$

$$c_2 = \int_0^1 \cos^2 b\beta\xi \; d\xi = \frac{\sin 2b\beta}{4b\beta} + \frac{1}{2}$$

$$c_3 = \int_0^1 \sinh^2 b\alpha_1\xi \; d\xi = \frac{\sinh 2b\alpha_1}{4b\alpha_1} - \frac{1}{2}$$

$$c_4 = \int_0^1 \sin^2 b\beta\xi \; d\xi = \frac{1}{2} - \frac{\sin 2b\beta}{4b\beta}$$

$$c_5 = \int_0^1 \sinh b\alpha_1\xi \cosh b\alpha_1\xi \; d\xi = \frac{(\cosh 2b\alpha_1 - 1)}{4b\alpha_1}$$

$$c_6 = \int_0^1 \sin b\beta\xi \cos b\beta\xi \; d\xi = \frac{(1 - \cos 2b\beta)}{4b\beta}$$

$$c_7 = \int_0^1 \sinh b\alpha_1\xi \sin b\beta\xi \; d\xi = \frac{\alpha_1 \cosh b\alpha_1 \sin b\beta - \beta \sinh b\alpha_1 \cos b\beta}{b(\alpha_1^2 + \beta^2)}$$

$$c_8 = \int_0^1 \sinh b\alpha_1\xi \cos b\beta\xi \; d\xi = \frac{\alpha_1 \cosh b\alpha_1 \cos b\beta + \beta \sinh \alpha_1 \sin b\beta - \alpha_1}{b(\alpha_1^2 + \beta^2)}$$

$$c_9 = \int_0^1 \cosh b\alpha_1\xi \sin b\beta\xi \; d\xi = \frac{\alpha_1 \sinh b\alpha_1 \sin b\beta - \beta \cosh b\beta\alpha_1 cos b\beta + \beta}{b(\alpha_1^2 + \beta^2)}$$

$$c_{10} = \int_0^1 \cosh b\alpha_1\xi \cos b\beta\xi \; d\xi = \frac{\alpha_1 \sinh b\alpha_1 \cos b\beta + \beta \cosh b\alpha_1 \sin b\beta}{b(\alpha_1^2 + \beta^2)}$$

Using a similar procedure, the normalization constant C for the trignometric mode in Eq. (3.4.32) can also be determined from Eq. (3.4.34). All the other parameters, not defined here, are given in Sections 3.4.1 and 3.4.2.

APPENDIX II

The Mass Coupling Matrix M_{IN} of the Timoshenko Beam Element

From Eqs. (3.4.3) and (3.4.28), the mass coupling matrix M_{IN} for the hyperbolic mode is found explicitly as follows:

$$M_{IN} = [m_{ji}]\,,\ m_{ji} = \rho A \int_0^L S_{vq_j} V_i dx + \rho I \int_0^L S_{\theta q_j} \Theta_i dx$$

$$i = 1, 2, \cdots, \infty,\ j = 1, 2, 3, 4$$

where

$$m_{1i} = \rho AL\,[c_1 - c_2 + s_2(c_2 - 3c_3 + 2c_4)]_i - 6\rho I s_2\,[c_6 - c_7]_i$$

$$m_{2i} = \frac{\rho AL^2}{2}\,[c_2 - c_3 + s_2(c_2 - 3c_3 + 2c_4)]_i + \rho IL\,[c_5 - c_6 - 3s_2(c_6 - c_7)]_i$$

$$m_{3i} = \rho AL\,[c_2 - s_2(c_2 - 3c_3 + 2c_4)]_i + 6\rho I s_2\,[c_6 - c_7]_i$$

$$m_{4i} = \frac{\rho AL^2}{2}\,[-c_2 + c_3 + s_2(c_2 - 3c_3 + 2c_4)]_i + \rho IL\,[c_6 - 3s_2(c_6 - c_7)]_i$$

$$c_1 = \int_0^1 V d\xi = C\,(c_{18} - \lambda\zeta\delta c_{14} - c_{26} + \delta c_{22})$$

$$c_2 = \int_0^1 \xi V d\xi = C\,(c_{19} - \lambda\zeta\delta c_{15} - c_{27} + \delta c_{23})$$

$$c_3 = \int_0^1 \xi^2 V d\xi = C\,(c_{20} - \lambda\zeta\delta c_{16} - c_{28} + \delta c_{24})$$

$$c_4 = \int_0^1 \xi^3 V d\xi = C\,(c_{21} - \lambda\zeta\delta c_{17} - c_{29} + \delta c_{25})$$

$$c_5 = \int_0^1 \Theta d\xi = C\eta \left(c_{18} + \frac{\gamma}{\lambda\zeta} c_{14} - c_{26} + \gamma c_{22} \right)$$

$$c_6 = \int_0^1 \xi\Theta d\xi = C\eta \left(c_{19} + \frac{\gamma}{\lambda\zeta} c_{15} - c_{27} + \gamma c_{23} \right)$$

$$c_7 = \int_0^1 \xi^2\Theta d\xi = C\eta \left(c_{20} + \frac{\gamma}{\lambda\zeta} c_{16} - c_{28} + \gamma c_{24} \right)$$

$$c_{14} = \int_0^1 \sinh b\alpha_1\xi \; d\xi = \frac{\cosh b\alpha_1 - 1}{b\alpha_1}$$

$$c_{15} = \int_0^1 \xi \sinh b\alpha_1\xi \; d\xi = \frac{\cosh b\alpha_1}{b\alpha_1} - \frac{\sinh b\alpha_1}{b^2\alpha_1^2}$$

$$c_{16} = \int_0^1 \xi^2 \sinh b\alpha_1\xi \; d\xi = \frac{b^2\alpha_1^2 + 2}{b^3\alpha_1^3} \cosh b\alpha_1 - \frac{2}{b^2\alpha_1^2} \sinh b\alpha_1 - \frac{2}{b^3\alpha_1^3}$$

$$c_{17} = \int_0^1 \xi^3 \sinh b\alpha_1\xi \; d\xi = \frac{b^2\alpha_1^2 + 6}{b^3\alpha_1^3} \cosh b\alpha_1 - \frac{3b^2\alpha_1^2 + 6}{b^4\alpha_1^4} \sinh b\alpha_1$$

$$c_{18} = \int_0^1 \cosh b\alpha_1\xi \; d\xi = \frac{\sinh b\alpha_1}{b\alpha_1}$$

$$c_{19} = \int_0^1 \xi \cosh b\alpha_1\xi \; d\xi = \frac{\sinh b\alpha_1}{b\alpha_1} - \frac{\cosh b\alpha_1}{b^2\alpha_1^2} + \frac{1}{b^2\alpha_1^2}$$

$$c_{20} = \int_0^1 \xi^2 \cosh b\alpha_1\xi \; d\xi = \frac{b^2\alpha_1^2 + 2}{b^3\alpha_1^3} \sinh b\alpha_1 - \frac{2}{b^2\alpha_1^2} \cosh b\alpha_1$$

$$c_{21} = \int_0^1 \xi^3 \cosh b\alpha_1\xi \; d\xi = \frac{b^2\alpha_1^2 + 6}{b^3\alpha_1^3} \sinh b\alpha_1 - \frac{3b^2\alpha_1^2 + 6}{b^4\alpha_1^4} \cosh b\alpha_1 + \frac{6}{b^4\alpha_1^4}$$

$$c_{22} = \int_0^1 \sin b\beta\xi \; d\xi = \frac{1 - \cos b\beta}{b\beta}$$

$$c_{23} = \int_0^1 \xi \sin b\beta\xi \; d\xi = \frac{\sin b\beta}{b^2\beta^2} - \frac{\cos b\beta}{b\beta}$$

$$c_{24} = \int_0^1 \xi^2 \sin b\beta\xi \; d\xi = \frac{2}{b^2\beta^2}\sin b\beta - \frac{b^2\beta^2 - 2}{b^3\beta^3}\cos b\beta - \frac{2}{b^3\beta^3}$$

$$c_{25} = \int_0^1 \xi^3 \sin b\beta\xi \; d\xi = \frac{3b^2\beta^2 - 6}{b^4\beta^4}\sin b\beta - \frac{b^2\beta^2 - 6}{b^3\beta^3}\cos b\beta$$

$$c_{26} = \int_0^1 \cos b\beta\xi \; d\xi = \frac{\sin b\beta}{b\beta}$$

$$c_{27} = \int_0^1 \xi \cos b\beta\xi \; d\xi = \frac{\cos b\beta}{b^2\beta^2} + \frac{\sin b\beta}{b\beta} - \frac{1}{b^2\beta^2}$$

$$c_{28} = \int_0^1 \xi^2 \cos b\beta\xi \; d\xi = \frac{2}{b^2\beta^2}\cos b\beta + \frac{b^2\beta^2 - 2}{b^3\beta^3}\sin b\beta$$

$$c_{29} = \int_0^1 \xi^3 \cos b\beta\xi \; d\xi = \frac{3b^2\beta^2 - 6}{b^4\beta^4}\cos b\beta + \frac{b^2\beta^2 - 6}{b^3\beta^3}\sin b\beta + \frac{6}{b^4\beta^4}$$

Using a similar procedure, the mass coupling matrix M_{IN} for the trigonometric mode can be found fron Eqs. (3.4.3) and (3.4.32). All the other parameters, not defined here, are given in Sections 3.4.1 and 3.4.2.

VITA

N. Ganesan was born in Zamin Kaliapuram, Coimbatore District, India. He received his early education at the Pollachi High School in Tamil Nadu and graduated in 1975, second in a class of 150. After completing one year of a Pre–University Program, he entered the College of Engineering, Guindy, Madras and in 1981 received his Bachelor of Engineering degree in Mechanical Engineering with honors. Later, he obtained a Master of Engineering degree in Mechanical Engineering from the Indian Institute of Science, Bangalore in 1983. In 1984, Ganesan also obtained a Master of Science degree in Mechanical Engineering from the Pennsylvania State University, University Park. He came to the University of Tennessee Space Institute in the Summer of 1985 to pursue a Doctor of Philosophy degree and was awarded the same in January 1991.

He is married to Sowmyalakshmi Thangavel Ganesan and they have a lovely little daughter, Narmadha.